Some magnetic effects of clustering in iron doped magnesium oxide

Williams, Charles D.H.

SOME MAGNETIC EFFECTS OF CLUSTERING IN IRON DOPED MAGNESIUM OXIDE

Charles D.H. Williams, B.Sc.

(Graduate Society)

Thesis submitted to the University of Durham in candidature for the degree of Doctor of Philosophy

February 1987

Department of Physics,
Science Laboratories,
Durham.

Charles D.H. Williams, Ph.D. Thesis, February, 1987.

Some magnetic effects of clustering in iron doped magnesium oxide

Abstract

The growth of a magnesioferrite precipitate in iron doped (~10000ppm wt.) magnesium oxide crystals, heat treated at 973K in oxygen, is studied with torque, magnetisation and magnetic resonance measurements. The torque and magnetisation results are in agreement with a model which assumes that the precipitate grows by diffusion limited Ostwald ripening. The effects of the particle size distribution and cubic magnetocrystalline anisotropy of the orientated octahedral precipitate particles on the magnetisation and torque curves are calculated. A magnetometric demagnetisation tensor is defined for assemblies of orientated dipoles, its variation with the assembly size is investigated and used to calculate the longitudinal demagnetisation factors of octahedra.

The ferromagnetic resonance spectra obtained were not in agreement with the generally used theory of de Biasi and Devezas (J. Appl. Phys. (1978) 49, 2466). A new theory, based on a spin Hamiltonian, of the FMR response of an anisotropic superparamagnet is proposed and compared with some of the experimental spectra.

To all the

"Men far beyond a merely local need -"

CONTENTS

List of figures

List of tables

List of abbreviations

Ch - Chapter

eqn - Equation

ESR - Electron spin resonance

fig - Figure

FMR - Ferro/ferrimagnetic resonance

LSW - Lifshitz, Slezov and Wagner

ppm - Parts per million

PSD - Particle size distribution

ref - Reference

sec - Section

SPM - Superparamagnetic/superparamagnetism

VSM - Vibrating sample magnetometer

wt - Weight

CHAPTER 1

Introduction

Novel magnetic liquids have been made and characterised at Durham for several years. The present method of magnetic assessment involves measurements of liquids' magnetisation, audio-frequency susceptibility and, after freezing in a high magnetic field, anisotropy. Ferromagnetic resonance (FMR) spectra at microwave frequencies were obtained by us as part of an attempt to improve the characterisation procedures. These spectra reflected aspects of a liquid's age and history as well as its magnetic properties but it seemed that a detailed, quantitative analysis of the results could be extremely complicated. It would have been sensible to attempt such an analysis only when the factors influencing the FMR behaviour of a similar, but simpler, magnetic system had been identified and thoroughly understood.

Microscopic (typically 10nm diameter) particles of strongly magnetic material, usually magnetite but sometimes metals or other oxides, are responsible for the interesting properties of magnetic liquids. The fine* particles are

---

*The term "fine" applied to a magnetic particle in this work implies that it has only a single magnetic domain. Some authors use the term, rather less rigidly, to mean small.

coated in surfactant and dispersed in a "carrier" liquid, water or toluene for example, forming a colloid. A concentrated system might have over 15% of its volume occupied by strongly magnetic material, less than 1% magnetic material would be considered weak. Brownian motion and the surfactant disperse the particles, gravity tends to segregate particles from the carrier liquid, and magnetic attraction can cause aggregation. The possibility of aggregation greatly complicates the detailed behaviour of a magnetic liquid; an assumption, which could render calculation of its properties tractable, that it comprises many individual particles interacting only weakly with each other cannot be justified. Comprehensive bibliographies of the literature relevant to magnetic fluids are published triannually (M. Zahn and K.E. Shenton. IEEE Trans. Magn. (1980) MAG-16, 387; S.W. Charles and R.E. Rosenweig. J. Magn. Magn. Mater. (1983) 39, 190).

Fine particle effects are important in several other types of magnetic systems, for example:

(a) Recording media. Magnetic discs and tapes are normally made from orientated acicular particles of γ-Fe_2O_3 which are large enough for thermal effects to be negligible and closely packed so that there is a large interaction between particles.

(b) Permanent magnets. These are also usually made from

elongated particles. The improvement in properties can, depending on the material, either be due to the large shape anisotropy or prevention of domain wall motion.

(c) Geomagnetism. Many rocks contain a small proportion of magnetic material, largely mixed titanium iron oxides. In some cases this is in fine particle form.

(d) Catalysts. Iron and nickel are both important industrial catalysts. The area available for reaction is maximised by preparing them as microscopic particles supported on alumina or silica. They are extremely reactive and must be kept stable by inert atmospheres. The crystallographic orientation of the metal particles is unpredictable.

(e) Living organisms. Magnetotactic bacteria contain chains of single domain octahedral particles of magnetite, they precess in the earth's field whilst swimming.

(f) Quenched alloy systems. Several metal alloys form ferromagnetic fine particle systems in magnetically inert matrices if suitably heat treated. The Cu-Co system has been particularly popular for many years. Unfortunately FMR investigations of these samples are limited by the penetration depth of the microwaves (about 1μm) and surface effects dominate results.

(g) Quenched metal oxide systems. These are good insulators, relatively inert and have been extensively investigated. The limited solubility of iron oxides in alkaline oxides can be exploited to produce a well dispersed

precipitate of orientated ferrimagnetic particles in a diamagnetic host with negligible interparticle interactions. The iron magnesium oxide (Fe/MgO) system was selected as a suitable model to study fine particle behaviour under FMR conditions.

There has been interest in MgO for many years; it is a good electrical insulation material at temperatures up to about 1100K and an understanding of the reactions between iron and MgO is needed also for the design of steel production processes. This thesis describes a magnetic study of the early stages of growth of magnesioferrite ($MgFe_2O_4$) precipitates in a MgO host, its objective is: to develop a simple quantitative description of its magnetisation, anisotropy and FMR response over a range of temperatures. A summary of the work follows.

At temperatures above about 1500K iron oxide dissolves in MgO forming a solid solution. The oxidation state of the iron depends on the ambient atmosphere. If its temperature is reduced rapidly, the solution supersaturates. The iron in the now metastable system can be investigated using electron spin resonance spectroscopy (chapter 2). At temperatures above about 600K diffusion occurs at a perceptible rate allowing a slow approach to equilibrium by precipitation. These processes, the possible resultant particle size distributions and the Fe/MgO chemistry are discussed in chapter 3. Under the conditions of low iron concentration and an oxidising atmosphere used for this work

the precipitate comprises fine octahedral particles of the ferrimagnet magnesioferrite. Even well below room temperature the magnetic behaviour of the precipitate is dominated by thermal fluctuations and it exhibits superparamagnetic effects (chapter 4). The magnetostatic behaviour of uniformly magnetised octahedra is investigated in chapter 5 and the conclusions do not invalidate the use of a classical theory of superparamagnetic behaviour. Experimental details and some representative results comprise chapter 6. Finally the experimental results are discussed with reference to the theory described in earlier chapters and some general conclusions are drawn (chapter 7). Detailed reviews of the relevant literature are contained within each chapter.

CHAPTER 2

Electron spin resonance

1. Introduction

Magnetic resonance spectroscopy examines transitions between energy levels whose separation is affected by a static magnetic field (1). Electron spin resonance (ESR) is the branch of the subject concerning systems in which s the total spin quantum number is not zero: these could be atoms, molecules or "centres" in solids. This interpretation of ESR requires that the states of the system are eigenfunctions of S^2 (to a good approximation) and are characterised by the spin quantum numbers s and m_s. Atoms or defects trapped in inert lattices often (compared with the majority of molecules which exist in singlet states) have ground, or accessible, states with $s \neq 0$.

A typical ESR investigation of a sample involves measurement of the position, width and intensity of absorption lines with the sample at several orientations in the magnetic field, and often at several temperatures. It is usually most convenient to irradiate a sample with a constant frequency microwave source and sweep the magnetic field whilst recording the "spectrum" - the derivative of radiation absorption as a function of field. If the spectrum is well resolved: line positions give information

about an atom's static environment; line widths relate to its dynamic interaction with this environment; and the line intensity is proportional to the concentration of absorbing atoms for a sufficiently dilute sample.

Al'tshuler and Kozyrev (2) give a history of ESR to 1945. By about 1950 it had become a standard spectroscopic technique. Poole (3) has comprehensively reviewed experimental ESR and Harriman discusses the rigorous theory and calculation of line positions (4). Existing theoretical treatments of relaxation are satisfactory in some cases and useful in others but a unified a priori theory has not yet emerged (5,6).

2. Line position

Dirac's theory of the electron describes the behaviour of an electron in an electromagnetic field using a Lorentz invariant formulation of quantum mechanics (7,8). In a uniform magnetic field the solution of Dirac's equation associates intrinsic angular momentum and a magnetic moment with the electron. Electrons interact with the field and with each other (9,10). Zeeman and magnetic hyperfine interactions in the Dirac hydrogen-like ion can be treated by perturbation theory (4). ESR is therefore, an essentially relativistic phenomenon but to calculate the energies of states sufficiently accurately to get at small differences by subtraction would be practically impossible for the many-electron systems of interest. Rather, the

relativistic theory has been used as a guide to the spin-dependent corrections to a spinless Hamiltonian which can be treated by perturbation methods. This treatment and the resultant Hamiltonian (which has thirty-five terms) are discussed by Harriman (4).

Even after its reduction to a non-relativistic problem the calculation of the energy levels of the magnetic electrons of an ion in a crystalline field is difficult; a considerable knowledge of atomic spectroscopy complicated by the crystalline fields is necessary. It is convenient to describe experimental results by an effective spin Hamiltonian. This is a Hermitian operator containing only spin operators and parameters, it operates within an electron spin space whose dimension corresponds to the number of experimentally observed electronic energy levels. An effective spin quantum number can be defined by requiring that $2s'+1$ equals the number of electronic states. s' is not necessarily the same as the s quantum number, if it exists. The spin Hamiltonian parameters may be functions of sample orientation Ω and external field B but contain no operators. This definition is sufficient to reproduce any observed set of energy levels with a spin Hamiltonian. For a set of experimental energies $\{E_i(\Omega,B)\}$ and any orthornormal basis set in the appropriate spin space $\{|i\rangle\}$ the spin Hamiltonian is (4)

$$H = \sum_i E_i(\Omega,B)\,|i\rangle\langle i| \qquad (1)$$

The E_i fit the definition of parameters and the projection operators $|i\rangle\langle i|$ can be written as linear combinations of spin operator products. Other features of an experimental spectrum, such as relative line intensities, can be reproduced by a suitable choice of $\{|i\rangle\}$. Equation 1 will not usually uniquely prescribe a spin Hamiltonian for an experimental spectrum. Uniqueness is usually achieved by restricting its form on the basis of convenience and the presumed derivability of the restricted form from the full quantum mechanical treatment. A common choice is

$$H = \sum_{ij} U^i M^{ij} U^j \qquad (2)$$

where U is an axial vector - one of the spin operators $\underline{S}$' or $\underline{I}$ (nuclear spin) or the magnetic field $\underline{B}$. M is a matrix depending on sample orientation.

Most reference books concerned with ESR derive spin Hamiltonians with varying degrees of rigour, clarity and generality (e.g. 1-4,11,12). The spectroscopy of isolated ions and atoms has been extensively studied and is discussed in the text by Condon and Shortley (13) and the papers of Racah (14-16). The dominant interaction within an atom is Coulombic: between the nucleus and the N electrons and between the electrons themselves. In non-relativistic approximation

$$H_C = \sum_{k=1}^{N} \left(\frac{p_k^2}{2m} - \frac{Ze^2}{4\pi\varepsilon_0 r_k} + \sum_{j>k}^{N} \frac{e^2}{4\pi\varepsilon_0 r_{jk}} \right) \qquad (3)$$

Here $\underline{p}_k$ is the linear momentum of the k electron, $\underline{r}_k$ is its

radius from the nucleus and m its mass, Ze is the nuclear charge. There is an interaction between the electron spins $\underline{s}_k$ and their orbital momentum

$$H_{LS} = \sum_{jk} \left(a_{jk} \underset{\sim}{l}_j . \underset{\sim}{s}_k + b_{jk} \underset{\sim}{l}_j . \underset{\sim}{l}_k + c_{jk} \underset{\sim}{s}_j . \underset{\sim}{s}_k \right) \qquad (4)$$

this term is of relativistic origin, the a_{jk}, b_{jk}, c_{jk} are constants. For the iron transition group of interest Russell-Saunders coupling (17) is a good approximation and H_{LS} can be written $\lambda \underline{L}.\underline{S}$ where λ is a constant for a given ion. A much weaker mutual interaction between the electron dipole moments was described by Pryce (18)

$$H_{SS} = \frac{\mu_0}{4\pi} \left(\frac{eg}{2m} \right)^2 \sum_{jk} \left[\frac{\underline{s}_j . \underline{s}_k}{r_{jk}^3} - \frac{3 (\underline{r}_{jk} . \underline{s}_j)(\underline{r}_{jk} . \underline{s}_k)}{r_{jk}^5} \right] \qquad (5)$$

g is the electron's gyromagnetic ratio.

These three terms dominate the free ion. If the nucleus has spin $\underline{I}$ and quadrupole moment Q there are two additional contributions

$$H_N = \frac{\mu_0 e^2 g_N}{16\pi m m_p} \sum_k \left(\frac{(2\underline{l}_k - g\underline{s}_k).\underline{I}}{r_k^3} + \frac{3g(\underline{r}_k . \underline{s}_k)(\underline{r}_k . \underline{I})}{r_k^5} + \frac{8\pi g}{3} \delta(\underline{r}_k)(\underline{s}_k . \underline{I}) \right) \qquad (6)$$

$$H_Q = \frac{e^2 Q}{4\pi\varepsilon_0 2I(I+1)} \sum_k \left(\frac{\underline{I}(\underline{I}+1)}{r_k^3} - \frac{3(\underline{r}_k . \underline{I})^2}{\hbar^2 r_k^5} \right) \qquad (7)$$

g_N is the gyromagnetic ratio of the nucleus, m_p is the proton mass. An external magnetic field contributes

$$H_B = \underset{\sim}{B} . \left[\frac{e}{2m} \sum_k \left(\underline{l}_k + g\underline{s}_k \right) - \frac{g_N e}{2m_p} . \underline{I} \right] \qquad (8)$$

and the general Hamiltonian of the free ion is

$$H = H_C + H_{LS} + H_{SS} + H_N + H_Q + H_B \qquad (9)$$

The magnitude of these interactions has been estimated from experimental spectra and for the iron transition group $H_c \sim 10^5 cm^{-1}, H_{LS} \sim 10^2 cm^{-1}, H_{SS} \sim cm^{-1}, H_N \sim 10^{-1}-10^{-3} cm^{-1}, H_Q 10^{-3} cm^{-1}$ (19). The ground state of these ions is well known theoretically and experimentally although the calculations can be extremely involved.

The electrons in an ion are strongly affected by a crystalline environment's electric field. The paramagnetic ion is surrounded by a nearly continuous charge distribution which overlaps the electronic density of the paramagnetic ion to some extent. Attempts to calculate directly the effect on the ion's energy levels have not generally been successful (12). The simplification which facilitates understanding of many ESR spectra is Kramers's crystal or ligand field approximation (20-22). Surrounding ions are treated as point charges or dipoles at approximate lattice points. The paramagnetic ion is influenced via the static electric field. The problem is now to find the energy levels in the field, its symmetry fixed by the static charges. The solution is usually perturbative (23) with optical spectra providing the necessary information about the aproximate magnitude of the splittings. The surrounding charges are passive and do not overlap the paramagnetic ion so the electrostatic potential satisfies Laplace's equation

$$\nabla^2 V = 0 \qquad (10)$$

and can be expanded in terms of spherical harmonics (24). It is usually necessary to retain only a few terms in the expansion

$$V=\sum_{mn} A_n^m r^n Y_n^m(\theta,\phi) \qquad (11)$$

and it has been shown that for d-shell electron wavefunctions only the n=2 and n=4 terms yield non-vanishing elements in the perturbation matrix (25). Further simplification occurs because the crystal field symmetry restricts contributing values of m (2). There are some extremely elegant methods for evaluating the matrix elements based on Stevens's equivalent operators (25-27). It is possible to determine the Stark splitting of a term in a crystal field without detailed calculations by using group theory (28,29 and references therein).

Experiments are performed generally at room temperature or colder ($kT \lesssim 200 cm^{-1}$) so only levels within a few hundred wavenumbers of the lowest need to be examined. If the lowest level of H_c is degenerate it is sufficient to treat the ion as being in one of the lowest energy eigenstates. If the lowest level is not degenerate (an S-state for example, e.g. Fe^{3+} or Mn^{2+}) then the crystal field acts with the spin-orbit coupling to split the spin degeneracy; other eigenstates of H_c are admixed as a higher order perturbation term (19). The complexity of the splitting of S-states makes direct calculations difficult; the spin Hamiltonians used to interpret experimental spectra are derived from

symmetry properties of the crystal. Several workers have attempted to calculate the simplest case of cubic symmetry (30-33). In low symmetry Pryce pointed out that the electrons' spin-spin interaction (equation 5) can lead to significant splittings (18). Leushin (34,35) developed Watanabe's work (30) by a semi-empirical calculation and obtained reasonable agreement with experiment. Recent work (36 and references therein) has produced an eighth order perturbation formula which agrees well with experiment for Mn^{2+} in a cubic field. For S-state iron transition series ions the crystal field approximation is inadequate (37) but the effects of electron-ligand overlap can be included and corrections to the splittings obtained. Naturally the spectroscopic splitting factor g for S-state ions differs only slightly from the free electron value. Deviations from this value arise from slight admixing of excited states with non-zero orbital angular momenta (35). Fortunately it is possible to derive the form of the spin Hamiltonian using symmetry methods and results for S-state ions in all 32 point groups have been tabulated (2). For Fe^{3+} in an octahedral environment the appropriate form is (38,39)

$$\mathcal{H}_S = \left(\frac{e\underset{\sim}{g}}{2m}\right) \underset{\sim}{B}\cdot\underset{\sim}{S} + \frac{a}{6\hbar^4}\left[S_x^4 + S_y^4 + S_z^4 - \frac{1}{5}\underset{\sim}{S}^2\left(3\underset{\sim}{S}^2 - 1\right)\right] \qquad (12)$$

Only 2.17% of naturally occurring iron has non-zero nuclear spin (^{57}Fe, $I=\frac{1}{2}$) (40) so terms in $\underset{\sim}{I}$ have been ignored. Exact solutions to equation (12) are obtained by substituting combinations of spin step operators for S_x and

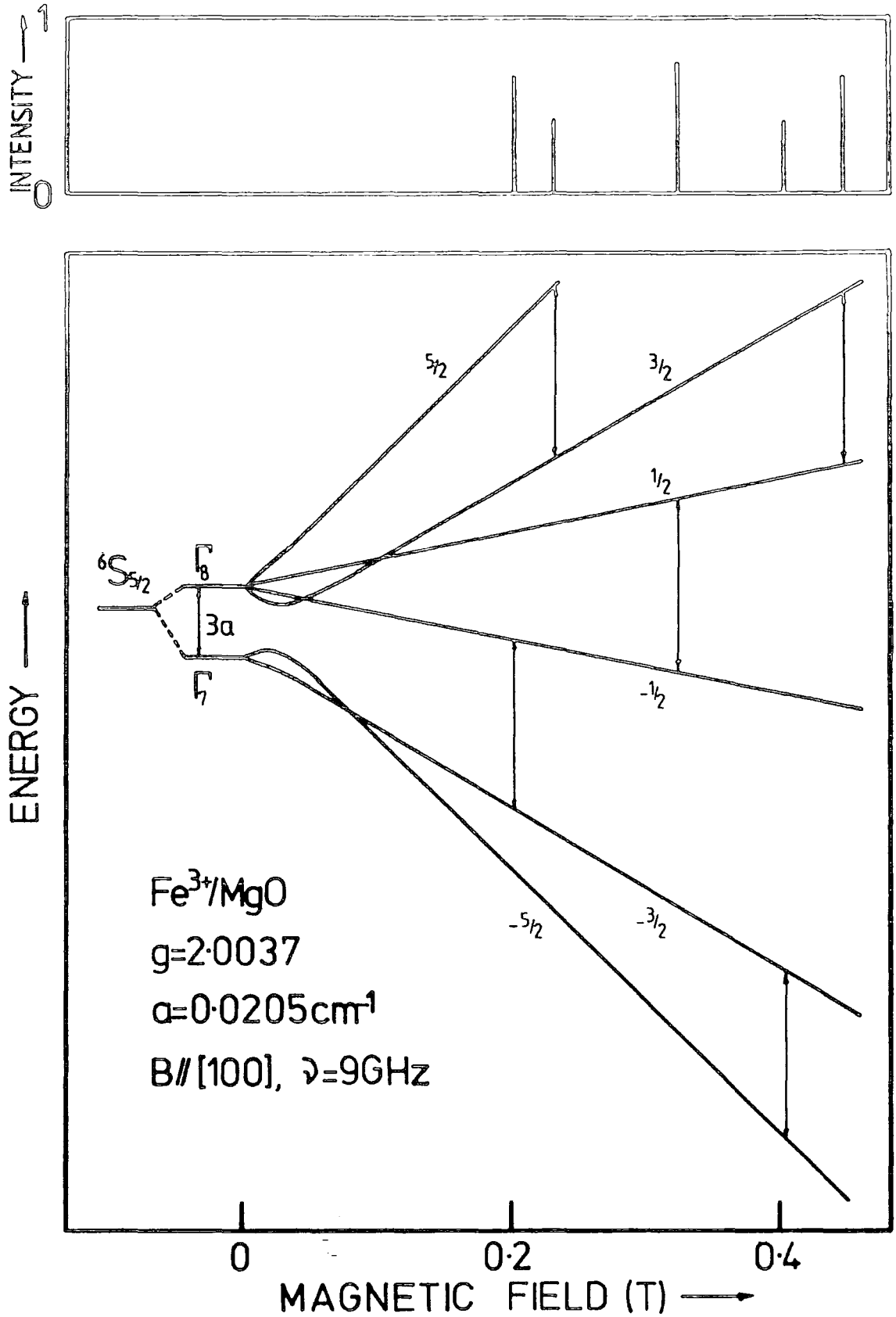

Fig 1. Calculated energy levels of Fe^{3+} in MgO. $\Delta m=1$ ESR transitions have been indicated, their relative intensities are on the upper 'spectrum'. Levels have been labelled by the m_s value of the pure state that they most resemble.

S_y, and solving the resultant 6x6 eigenvalue problem using matrix techniques (for example 41) and the $|5/2,m_s>$ manifold as a basis. This method was used to construct figure 1* which shows the energy levels of Fe^{3+} in MgO, and to check the accuracy of the series expansions (42) used to anlayse experimental data. The octahedral crystal field splits the $^6S_{5/2}$ level into a four-fold degenerate level (Γ_8) and a two-fold degenerate level (Γ_7). The magnetic field splits these levels as illustrated (figure 1). The $\Delta m_s=1$ transitions for a 9GHz spectrometer have been indicated and the relative intensities of these lines would be expected to be 8:5:9:5:8 (39). The $\Delta m_s>2$ transitions are somewhat weaker but can be observed under favourable circumstances (41,43-45); similar remarks apply to the hyperfine structure (45).

3. Line intensity and static susceptibility

An oscillating magnetic field of the correct frequency ν and magnetic polarisation transverse to the static field can induce transitions between the energy levels of Figure 1. If the spins interact weakly amongst themselves and, via crystal field modulation, (46-48) with a phonon "heat reservoir" the assembly is amenable to thermodynamic calculations (49). Spontaneous processes are negligible at

---

* Some minor errors in the tables of Kolopus and Holroyd (41) were found in the process.

radio frequencies, net absorption of energy is due to an excess of $\Delta m_s=1$ (up) over $\Delta m_s=-1$ (down) induced transitions; these are equally probable so the absorption is due to population differences between the states. For a two level system with induced transition rate $w_{12}=w_{21}$ the absorbed power will be

$$\frac{dU}{dt} = w_{12} h\nu (n_1 - n_2) \qquad (13)$$

where n_1, n_2 are the instantaneous populations. The spin temperature T_s is defined by

$$\frac{n_2}{n_1} = \exp\left(\frac{-h\nu}{kT_s}\right) \qquad (14)$$

The separation of the levels is small ($h\nu << kT$) so the occupation of states is accurately represented by the Boltzmann distribution. At equilibrium

$$\frac{N_1}{N_2} = \exp\left(\frac{-h\nu}{kT_o}\right) \qquad (15)$$

with T_o the ambient temperature and N_1, N_2 the equilibrium populations. For a simple two level system the interaction of the spins with the lattice is described by a parameter t_1 known as the spin-lattice relaxation time defined by

$$\frac{d}{dt}(n_1 - n_2) = \frac{1}{t_1}\left[(N_1 - N_2) - (n_1 - n_2)\right] \qquad (16)$$

The steady state solution when the oscillating field is causing transitions at a rate w gives the absorbed power

$$\frac{dU}{dt} = \frac{(N_1 - N_2) h\nu w}{1 + 2wt_1} \qquad (17)$$

For high oscillator powers absorption is limited only by t_1 and the spin system is said to be saturated.

The static magnetic initial susceptibility of an assembly of S-state ions in cubic fields is isotropic and approximately (50)

$$\chi_o = \frac{N\mu_o\mu_B^2 g^2 S(S+1)}{3kT} \qquad (18)$$

when there are N ions per unit volume interacting weakly. Correction terms proportional to T^{-2} vanish because of the cubic symmetry and higher order corrections are negligible.

4. Line shape and width

The shape f(B) of an absorption line as a function of field B can be described by specifying its moments

$$M_n = \int_o^\infty (B - B_o)^n f(B)\, dB \qquad (19)$$

M_o the integrated intensity is made unity by normalising f(B) and B_o is determined by requiring $M_1 = 0$. Most theoretical treatments yield expectation values for these moments directly using Van Vleck's method (51). Experimental determinations of moments in the presence of instrumental effects and comparisons of line shapes with known distributions have been discussed by many authors (reviewed in chapter 12 of (3)); much of the literature is redundant because of the readily available computing resources of the present.

4.1 Instrumental broadening

The instrument used to record a spectrum can contribute to the measured width of a line in a variety of ways, most important for the Varian V4502 instrument used in this work are (3,52):

(a) Static field homogeneity across the sample, $\Delta B \lesssim 1 \mu T$.

(b) Field modulation frequency, $\Delta B \sim 5 \mu T$.

(c) Field modulation amplitude. To obtain a true first derivative spectrum the modulation amplitude must be kept much less than the width of the line being recorded.

(d) Sweep rate. To record an undistorted first derivative spectrum the rate of change of the static field must be much less than the product of the line width and instrument bandwidth.

(e) Saturation broadening occurs if the oscillator power is too high (i.e. in the terms of equation 18 if $2wt_1 > 1$).

(f) Detector non-linearity. The crystal detector used to measure the absorption is non-linear and if the absorption is extremely large (comparable with the detector bias level) the recorded line will be distorted.

The first two effects (a and b) represent unavoidable limitations to the spectrometer performance, the remainder can usually be avoided with care and their presence or absence established by recording spectra under several

combinations of conditions.

4.2 Inhomogeneous broadening

The expression inhomogeneously broadened describes a recorded "line" that is in fact an envelope of unresolved components. These could be hyperfine lines, lines from differing ionic species or sites with nearly coincident resonances. If the line of interest is anisotropic and the sample comprises misorientated grains or in the extreme case is a powder or polycrystalline this can also contribute to the measured line width. Treatments of this form of broadening tend to be limited to rather special cases (for a review see chapter 13 of (3)) (55,56).

4.3 Spin-lattice broadening

In the microwave frequency range the thermal electromagnetic radiation bath has an energy density far too small to account for the observed t_1 values. However, the energy density of the phonon bath is greater by a factor of about $(c/v)^3 \sim 10^{15}$ with v the velocity of sound $\sim 3 \times 10^3 ms^{-1}$. This easily compensates for the weak spin-phonon coupling (11). There are many possible complications but in the majority of cases (47-49)

$$\frac{1}{t_1} = a \coth\left(\frac{h\nu}{2kT}\right) + b T_0^n + \frac{c}{\exp(\Delta/kT_0)-1} \qquad (20)$$

The processes contributing to the relaxation rate are:

(a) Direct process, involves phonons of energy hν the

resonance quantum.

(b) Raman process, (so called because of its similarity to the electromagnetic interaction) a two phonon effect in which all phonons can participate. Typical values for n are in the range 5-9.

(c) Orbach process, a phonon is absorbed by a direct process to excite the spin system to an energy Δ above the ground multiplet followed by an emission of another phonon of slightly differing energy resulting in an indirect transfer from one level to the other of the ground multiplet.

The implicit assumption that phonons are in thermal equilibrium with the bath temperature T_o is not always correct. There are considerably fewer phonons with the correct energy for direct processes than spins and sometimes it is the transfer of energy from these few phonons "on speaking terms with the spin system" to the bath that determines the energy absorption rate. This phonon bottle-neck (53,54) can be the cause of various interesting effects (11) not apparent in the Fe^{3+}/MgO system. When the line shape is dominated by the spin-lattice interaction the appropriate shape function is the collision broadening formula of Van Vleck and Weisskopf (57). When the resonant field is much greater than the width of the absorption this is approximately

$$\frac{dU}{dt} \propto \frac{B\Delta B}{(B-B_o)^2+(\Delta B)^2} \quad ; \quad \Delta B = \frac{\hbar}{g\mu_B t_1} \qquad (21)$$

with the derivative peak to peak separation ΔB_{pp}

$$\Delta B_{pp} = \frac{2\hbar}{\sqrt{3} g \mu_B t_1} \qquad (22)$$

4.4 Strain broadening

The samples used to gather experimental data inevitably contain defects and attendant strains which distort the lattice from its idealised form. The strains can result in a distribution of spin Hamiltonian parameters throughout the crystal and may cause inhomogeneous broadening of the ESR spectrum. Feher (58) investigsated the effect of uniaxial stress on $^6S_{5/2}$ ions in MgO and found that a correction to the spin Hamiltonian was in agreement with experiment:

$$H_{nc} = \sum_{ij} S^i D^{ij} S^j \qquad (23)$$

where D^{ij} is a traceless symmetric matrix which for crystals of cubic symmetry has elements determined by only two constants C_{11} and C_{44} called stress coefficients. the linearity of this description is justified when the strains are small and to first order the $-\frac{1}{2} \rightarrow \frac{1}{2}$ transition is unaffected by the strain. By assuming that the elements of the stress tensor are uncorrelated and described by a Gaussian probability distribution of width to be experimentally determined (symmetry dictates that there are only two such parameters α and β) it is possible to calculate the second moment of the broadened lines. For the

transition $M-\frac{1}{2} \rightarrow M+\frac{1}{2}$ $(M=-2,-1,0,1,2)$ (59)

$$\langle \delta B^2 \rangle = \frac{3M^2}{4}\left[\left(\frac{3}{2}C_{11}\right)^2\left(\frac{\alpha}{2}\right)^2(1-3F)+3C_{44}^2\beta^2F\right]\left(\frac{hc}{g\beta}\right)^2 \qquad (24a)$$

$$F = l^2m^2 + m^2n^2 + n^2l^2 \qquad (24b)$$

and l,m,n are the direction cosines of the static magnetic field in the coordinate system [100], [010], [001] of crystal axes. Feher (58) found that $C_{11}=+2.6\times10^{-5}N^{-1}m$ and $C_{44}=-5.5\times10^{-6}N^{-1}m$ for Fe^{3+} in MgO (cubic sites), she was able to fit the behaviour of the Mn^{2+} spectra to within experimental errors by a suitable choice of α and β. For iron, although the width of the fine structure lines was reasonably predicted by the theory, unidentified broadening mechanisms affected the $-\frac{1}{2} \rightarrow \frac{1}{2}$ transition. Later treatments (60,61) recognised that a single defect contributes to more than one strain component and an additional parameter γ is necessary to describe the broadening fully.

4.5 Interacting ions

To this point the ions have been isolated from each other. The treatment must usually be extended to include interactions between ions if reasonable agreement with experiment is desired. The Hamiltonian for an assembly of N interacting ions is formally

$$H = \sum_{i=1}^{N} H_i + \sum_{\substack{j>i \\ i=1}}^{N} H_{ij} \qquad (25)$$

where H_i is the single ion spin Hamiltonian. Contributions to H_{ij} have been discussed in detail by, amongst others,

Abragam and Bleaney (11). Three cases are of special interest:

(a) N small, H_{ij} strong - Pair and small cluster spectra; such investigations are almost the only source of quantitative measurements of the spin-spin interaction. Examples in MgO are mentioned in chapter 7.

(b) N large, H_{ij} strong - Strong magnetism and superparamagnetism are discussed in chapter 4.

(c) N large, H_{ij} weak - Essentially single ion spectra with line shapes modified by interaction with other ions.

Dilute systems of paramagnetic ions in inert hosts have been used in many studies in the hope that the third case (c) would dominate results. For a disperse system the most promising candidate for H_{ij} is the weak, but long range, magnetic dipole coupling (c.f. equation 5). In practice a proportion of the paramagnetic ions are close enough to each other (chapter 3) to experience significant wavefunction overlap: the short range, but strong, exchange interaction.

4.6 Dipolar broadening and exchange narrowing

Exchange and dipolar coupling described by the Hamiltonian

$$H_{ED} = \sum_{\substack{j>i \\ i=1}}^{N} \underline{S}_i \cdot A_{ij} \cdot \underline{S}_j + \frac{\mu}{4\pi}\left(\frac{eg}{2m}\right)^2 \sum_{\substack{j>i \\ i=1}}^{N} \left[\frac{\underline{S}_i \cdot \underline{S}_j}{r_{ij}^3} - \frac{3(\underline{r}_{ij}\cdot\underline{S}_i)(\underline{r}_{ij}\cdot\underline{S}_j)}{r_{ij}^5} \right] \qquad (26)$$

has been studied by several groups (51,62-64). Van Vleck (51) tackled the problem by using step operators and

retaining only terms contributing to $\Delta m_s = \pm 1$ transitions*. Van Vleck's assumptions were: the ions are in pure S-states; the Zeeman energy is larger than the dipole-dipole interaction; the temperature is high enough to populate the Zeeman levels equally. He obtained expressions for the second and fourth moments of the absorption lines and found an almost Gaussian line shape if exchange was absent. When present, exchange increased the fourth moment but left the second moment unaffected apparently "narrowing" the line. An intuitive explanation of dipolar broadening describes two mechanisms of about equal magnitude: a static effect caused by the variation of local field due to surrounding moments at random orientations; a dynamic effect when moments precessing in the external field cause transitions between magnetic sublevels - the total energy and angular momentum of interacting moments cannot change as a result of such transitions. The Anderson and Weiss interpretation of exchange effects is based on such a picture (62). Contributions to the Hamiltonian of dipolar and exchange terms do not commute with each other and the dipole configuration evolves with time. The system temperature is high and there are many accessible mirostates so, it is

---

*Other transitions are extremely faint but if they were not disgarded would contribute significantly to the calculated moments of $\Delta m_s = \pm 1$ lines.

asserted, the time variation is random and characterised by a frequency $V_e \sim H_{Exchange}/\hbar$. The precession frequency without exchange is $V_o + V'$ determined by the external field and the internal local fields which impart a Gaussian distribution to V'. The precession of each moment is subject to random frequency changes. The frequency modulation narrows the line when $V_e >> V_p$; $V_p^2 = \overline{V'^2}$. Statistical treatment yields an explicit expression for the shape function and the frequencies V_p and V_e which are free parameters of the Anderson and Weiss treatment are fixed by reference to Van Vlecks results for the second and fourth moments because (2)

$$V_p^2 = M_2 \qquad (27a)$$

$$2M_4 = 6V_p^4 + \pi V_p^2 V_e^2 \qquad (27b)$$

It is found that the line shape function is Lorentzian near the centre of the absorption and Gaussian in its wings. If the exchange energy is extremely large so that $V_e > V_o$ then equation 27a becomes

$$3V_p^2 = 10M_2 \qquad (28)$$

because the truncation of the Hamiltonian used to obtain equation 27a is no longer valid in this case. The general theory of resonance line shape has been treated in detail by Kubo and Tomita (65,55). So far the theories described are directly applicable only to regular lattices of paramagnetic ions. Kittel and Abrahams modified the theory of dipolar broadening in the absence of exchange so that it could be applied to systems where a candidate site has a probability f

of being occupied by a paramagnetic ion and found that the line shape was described by a truncated Lorentzian function (63). De Biasi and Fernandes (64) concluded that the Kittel and Abrahams formula overestimated the line widths - the relatively few ions in close proximity to one another made a large contribution to the line width which in a real system would be much reduced by exchange coupling. The problem with de Biasi and Fernandes's treatment is that two free parameters enable it to fit a very wide range of behavours when clustering is a potential effect (67). Henner and co-workers came to similar conclusions (68,69).

Since all the spin-spin broadening theories described are derived from Van Vleck's treatment they must be subject to its restrictions: the effect of the crystal field must be negligible (51); any hyperfine splitting must be resolved (70). They must therefore be applied with caution to the Fe^{3+}/MgO system.

5. References

1. Slichter, C.P. (1963) "Principles of magnetic resonance" Harper and Row, New York.

2. Al'tshuler, S.A. and B.M. Kozyrev (1972) "Electron paramagnetic resonance in compounds of transition elements" 2nd edn. (Translation 1974) John Wiley, New York.

3. Poole, C.P. (1983) "Electron spin resonance" 2nd edn., John Wiley, New York.

4. Harriman, J.E. (1978) "Theoretical foundations of electron spin resonance" Academic Press, New York.

5. Poole Jr., C.P. and H.A. Farach (1971) "Relaxation in magnetic resonance" Academic Press, New York.

6. Muus, L.T. and P.W. Atkins, Eds. (1972) "Electron spin relaxation in liquids" Academic Press, New York.

7. Dirac, P.A.M. (1958) "The principles of quantum mechanics" 4th edn. Oxford Univ. Press, Oxford.

8. Dirac, P.A.M. The quantum theory of the electron. Proc. Roy. Soc. Lond. (1958) A117, 610.

9. Duff, L.D. The motion of a Dirac electron in a magnetic field. Phys. Rev. (1931) 38, 501.

10. Johnson, M.H. and B.A. Lipman. Motion in a constant magnetic field. Phys. Rev. (1949) 76, 828.

11. Abragam, A. and B. Bleaney (1970) "Electron paramagnetic resonance of transition ions" Oxford Univ. Press, London.

12. Low, W. (1969) "Paramagnetic resonance in solids" Sol. Stat. Phys. Suppl. 2 Academic Press, New York.

13. Condon, E.U. and G.H. Shortley (1935) "Theory of atomic spectra" Cambridge Univ. Press, London.

14. Racah, G. Theory of complex spectra I. Phys. Rev. (1942) 61, 186.

15. Racah, G. Theory of complex spectra II. Phys. Rev. (1942) 62, 438.

16. Racah, G. Theory of complex spectra III. Phys. Rev. (1943) 63, 367.

17. Russell, H.N. and F.A. Saunders. New regularities in the spectra of the alkaline earths. Astrophys. J. (1925) 61, 38.

18. Pryce, M.H.L. Spin-spin interaction within paramagnetic ions. Phys. Rev. (1950) 80, 1107.

19. Abragam, A. and. M.H.L. Pryce. Theory of the nuclear hyerfine structure of paramagnetic resonance spectra in crystals. Proc. Roy. Soc. Lond. (1951) A205, 135.

20. Van Vleck, J.H. Theory of the variations in anisotropy among different salts of the iron group. Phys. Rev. (1932) 41, 208.

21. Penney, W.G. and R. Schlapp. The influence of crystalline fields on the susceptibilities of salts of paramagnetic ions I. The rare earths, especially Pr and Nd. Phys. Rev. (1932) 41, 194.

22. Schlapp, R. and W.G. Penney. The influence of crystalline fields on the susceptibilities of salts of paramagnetic ions II. The iron group, especially Ni, Cr and Co. Phys. Rev. (1932) 42, 666.

23. Schiff, L.I. (1968) "Quantum mechanics" 3rd edn., McGraw-Hill International, Auckland.

24. Arfken, G. (1970) "Mathematical methods for physicists" 2nd edn., Academic Press, London.

25. Stevens, K.W.H. Matrix elements and operator equivalents connected with the magnetic properties of rare earth ions. Proc. Phys. Soc. (1952) A65, 209.

26. Elliott, R.J. and K.W.H. Stevens. The theory of magnetic resonance experiments on salts of the rare earths. Proc. Roy. Soc. Lond. (1953) A218, 553.

27. Judd, B.R. Operator equivalents and matrix elements for the excited states of rare earth ions. Proc. Roy. Soc. Lond. (1955) A227, 552.

28. Bethe, H.A. Termaufspaltung in Kristallen. Annln. Phys. (1929) 3, 133.

29. Elliott, J.P. and P.G. Dawber (1979) "Symmetry in physics" pp.156-212, Macmillan, London.

30. Watanabe, H. On the ground level splitting of Mn^{++} and Fe^{+++} in nearly cubic crystalline field. Prog. Theor. Phys. (1957) 18, 405.

31. Powell, M.J.D., J.R. Gabriel and D.F. Johnson Ground state splitting for d^5 ^6S ions in a cubic field. Phys. Rev. Lett. (1960) 5, 145.

32. Gabriel, J.R., D.F. Johnson and M.J.D. Powell. A calculation of the ground-state splitting for Mn^{2+} ions in a cubic field. Proc. Roy. Soc. Lond. (1961) A264, 503.

33. Low, W. and G. Rosengarten. The optical spectrum and ground-state splitting of Mn^{2+} and Fe^{3+} ions in the crystal field of cubic symmetry. J. Molec. Spectrosc. (1964) 12, 319.

34. Leushin, A.M. Splitting of the ground-state of Mn^{2+} and Fe^{3+} in low symmetry crystal fields. Fiz. Tverd. Tela (1963) 5, 2352.

35. Leushin, A.M. g-Factors of ions in the S-state in crystals. Fiz. Tverd. Tela (1963) 5, 3373.

36. Du M-L, and M-G Zhao. The eighth-order perturbation formula for the EPR cubic zero-field splitting parameter parameter of $d^5(^6S)$ ion and its applications to $MgO:Mn^{2+}$ and $MnCl_2.2H_2O$. J. Phys. C. (1985) 18, 3241.

37. Sharma, R.R., T.P. Das and R. Orbach. Zero-field splitting of S-state ions II. Overlap and covalency model. Phys. Rev. (1967) 155, 338.

38. Bleaney, B. and K.W.H. Stevens. Paramagnetic resonance. Rep. Prog. Phys. (1953) 16, 108.

39. Low, W. The paramagnetic resonance spectrum of Fe^{3+} in the cubic field of MgO. Proc. Phys. Soc. Lond. (1956) B69, 1169.

40. Kaye, G.W.C. and T.H. Laby (1973) "Tables of physical and chemical constants" 14th edn., Longman, London.

41. Kolopus, J.L. and L.V. Holroyd. Higher order transitions in the EPR spectrum of MgO. Phys. Stat. Sol. (1965) 8, 711.

42. Kronig, R. de L. and C.J. Bouwkamp. Spin levels and paramagnetic dispersion in iron-ammonium-alum. Physica (1939) 6, 290.

43. Griffiths, J.H.E. and J.W. Orton. Some weak lines in the paramagnetic resonance spectra of impure MgO crystals. Proc. Phys. Soc. (1959) 73, 948.

44. de Biasi, R.S. Forbidden $\Delta m_S=2$ transitions in the EPR spectrum of Fe^{3+} in MgO. Phys. Stat. Sol. (1978) 87, K29.

45. Henderson, B., J.E. Wertz, T.P.P. Hall and R.D. Dowsing. An EPR study of vacancy-impurity association in MgO. J. Phys. C. (1971) 4, 107.

46. Van Vleck, J.H. Paramagnetic relaxation times for titanium and chrome alum. Phys. Rev. (1940) 57, 426.

47. Orbach, R. Spin-lattice relaxation in rare-earth salts. Proc. Roy. Soc. Lond. (1961) A264, 458.

48. Orbach, R. Spin-lattice relaxation in rare-earth salts: field dependence of the two phonon process. Proc. Roy. Soc. Lond. (1961) A264, 485.

49. Bowler, M.G. (1982) "Lectures on statistical mechanics" Pergamon, Oxford.

50. Van Vleck, J.H. and W.G. Penny. The theory of the paramagnetic rotation and susceptibility in manganous and ferric salts. Phil. Mag. (1934) 17, 961.

51. Van Vleck, J.H. The dipolar broadening of magnetic resonance lines in crystals. Phys. Rev. (1948) 74, 1168.

52. Varian Associates, Palo Alto. EPR Operational techniques. Publn. 87-114-402.

53. Van Vleck, J.H. Paramagnetic relaxation and the equilibrium of lattice oscillators. Phys. Rev. (1941) 59, 724.

54. Van Vleck, J.H. Calculations of energy exchange between lattice oscillators. Phys. Rev. (1941) 59, 730.

55. Cullis, P.R. Electron paramagnetic resonance in inhomogeneously broadened systems: a spin temperature approach. J. Magn. Reson. (1976) 21, 397.

56. Stoneham, A.M. Shapes of inhomogeneously broadened lines in solids. Rev. Mod. Phys. (1969) 41, 82.

57. Van Vleck, J.H. and V.F. Weisskopf. On the shape of collision-broadened lines. Rev. Mod. Phys. (1945) 17, 227.

58. Feher, E.R. Effect of uniaxial stresses on the paramagnetic spectra of Mn^{++} and Fe^{+++} in MgO. Phys. Rev. (1964) 136, A146.

59. Feher, E.R. and M. Weger. Internal strains and the linewidth of Mn^{++} and Fe^{+++} in MgO. Bull. Amer. Phys. Soc. (1962) 7, 613.

60. Stoneham, A.M. The theory of the strain broadened lineshapes of spin resonance and optical zero phonon lines. Proc. Phys. Soc. Lond. (1966) 89, 909.

61. Clare, J.F. and S.D. Devine. The determination of intrinsic strain in a crystal from EPR linewidths and the spin-strain coupling tensor. J. Phys. C. (1984) 17, 2801.

62. Anderson, P.W. and P.R. Weiss. Exchange narrowing in paramagnetic resonance. Rev. Mod. Phys. (1953) 25, 269.

63. Kittel, C. and E. Abrahams. Dipolar broadening of magnetic resonance lines in magnetically diluted crystals. Phys. Rev. (1953) 90, 238.

64. de Biasi, R.S. and A.A.R. Fernandes. The ESR linewidth of dilute solid solutions. J. Phys. C. (1983) 16, 5481.

65. Kubo, R. and K.J. Tomita. A general theory of magnetic resonance absorption. J. Phys. Soc. Japan (1954) 9, 888.

66. Kubo, R. Note on the stochastic theory of resonance absorption. J. Phys. Soc. Japan (1954) 9, 935.

67. de Biasi, R.S. Evidence for clustering in Fe^{3+} doped MgO. Magn. Lett. (1978) 1, 103.

68. Henner, E., I. Shaposhnikov, B. Bonis and R. Sardos. EPR concentration dependence in magnetically diluted crystals with strong spin-spin interaction. J. Magn. Reson. (1978) 32, 107.

69. Henner, E.K. and I.G. Shaposhnikov. Clustering of magnetic ions in diluted solid paramagnets. Phys. Stat. Sol. (1979) A55, 315.

70. Pryce, M.H.L. and K.W.H. Stevens. The theory of magnetic resonance-line widths in crystals. Proc. Phys. Soc. Lond. (1950) 63, 36.

CHAPTER 3

Precipitation and the Fe-Mg-O system

1. Introduction

Two types of point defects in crystals may be identified: impurities and thermally activated point defects. Impurities may be present either as a result of deliberate doping or because it is impracticable to make and keep solids perfectly pure. At non-zero temperatures thermally activated point defects are present in the equilibrium structures of crystals. The mobility of point defects provides a mechanism for the intermixing of atoms in solids. The degree of mobility is strongly temperature dependent. A crystal's equilibrium structure at a high temperature has a higher defect* density than at lower temperatures, so if a crystal is cooled it must lose defects to regain equilibrium, possibly by precipitation. The rate at which this can happen is governed by the defects' mobility and reactions at the precipitate surfaces. The discussion here begins by mentioning the possibility of defects distributed at random in a lattice forming clusters by chance.

---

*The term defect will refer to a point defect for the rest of this Chapter.

2. Random clusters

If the probability p of a defect occupying a particular site in a crystal of N atoms is independent of surrounding defects then it is possible to calculate the expected numbers of particular arrangements of atoms. Tables are available for various lattices (1). If the lattice is cubic then the number of defects without another as a nearest neighbour is $Np(1-p)^6$. Crocker's group has developed a formalism to describe clusters of more than one defect type which considerably simplifies statistical calculations (2,3 and refs. therein).

3. Diffusion

It is not yet possible to examine the mechanisms of atomic jumps between sites in a solid in microscopic detail experimentally. A particle migrating in a solid tends to linger at each site long enough for any dynamical effects of its earlier jumps to dissipate. Prediction of probable migration paths can realistically proceed by assuming that jump paths are independent of time (4). Provided the jumps are over short distances the diffusion is isotropic and obeys a diffusion equation

$$\frac{\partial C}{\partial t} = \underset{\sim}{\nabla}.\tilde{D}.\underset{\sim}{\nabla}C \qquad (1)$$

with $C=C(\underline{r})$ the concentration per unit volume at $\underline{r}$ and time t, and $\tilde{D}$ a second rank tensor, symmetric if the lattice is perfect. If the lattice is cubic and the system is

unstressed the description

$$\frac{\partial C}{\partial t} = D \nabla^2 C \qquad (2)$$

with D a scalar suffices. Measurement of $\tilde{D}$ is relatively straightforward (using radioactive tracers for example) but it is difficult to attribute values to a particular jump mechanism.

The calculation of $\tilde{D}$ from first principles has three parts:

(i) The statistical mechanics relating jump frequency to the potential energy surfaces within the solid, usually involving the method of Rice (5) or Vineyard (6).

(ii) The calculation of energy surfaces. Sangster and Stoneham performed the calculations for MgO using a standard computer package (7).

(iii) The inclusion of dynamic behaviour of the lattice during the jump.

Sangster and Stoneham (8) have performed such calculations for the diffusion of Fe^{3+} and Mg^{2+} in MgO using a "supercell" of 64 atoms to represent the lattice in the jump's immediate vicinity. Their results are in excellent agreement with recent experimental measurements for Mg^{2+} diffusion and assume that the Mg^{2+} ion exchanges sites with a recent neighbour cation vacancy. When the mobile ion is Fe^{3+} the calculated diffusion rates are about four orders of

magnitude lower than radioactive tracer experiments (9) indicate and it must be concluded that other mechanisms are responsible for the transport of iron in MgO.

The temperature dependence of the diffusion constant for Fe^{3+} in MgO at high temperatures is

$$D = D_o \exp\left(\frac{-E_A}{kT}\right) \qquad (3)$$

with the tracer experiments of Blank and Pask (9) giving the activation energy $E_A = (4.3 \pm 0.4) \times 10^{-19}$ J and the prefactor $D_o = (1.8 \div 5.6) \times 10^{-3}\ m^2 s^{-1}$ *†

4. Precipitation

A system might have to change phase to regain equilibrium after one of its state variables is changed. The phase transformation can sometimes happen extremely slowly because the system may initially have to pass through states with higher values of Gibbs function to form nuclei of the new phase. The effects known as supercooling and supersaturation are examples of this. After nucleation the new phase grows by diffusive processes.

---

*Blank and Pask quote values $D_o = 8.83 \times 10^{-4}\ m^2 s^{-1}$ and $E_A = 5.18 \times 10^{-19}$ J but these are not consistent with their figure 9. The values quoted above were recalculated from that figure.

† That is $\log_e D_o = -6.32 \pm 5.2$

4.1 Nucleation

If the Gibbs free energy G of a binary system varies with composition C so that there exists a region where at temperature T and pressure P

$$\left(\frac{\partial^2 G}{\partial C^2}\right)_{TP} < 0 \qquad (4)$$

then it is possible for "spinodal" decomposition to occur in this region (4). Spinodal decomposition starts as an infinitesimal composition fluctuation over the crystal and proceeds because some of the (Fourier) components of the composition wave grow preferentially. In a cubic crystal, depending on the elastic constants, this eventually gives rise to a network of {100} rods or cubes of alternately enriched and depleted material along the {100} directions (10). The relatively long range periodic variations in lattice parameter associated with spinodal decomposition can be recognised by the presence of satellite lines in X-ray diffraction patterns (11).

Homogeneous nucleation occurs in all unstable systems and can be important when spinodal decomposition does not occur; random fluctuations in the homogeneous (on average) composition result in a random spatial distribution of precipitates. Homogeneous nucleation has been observed in transitions from vapours or liquids but in solids the alternative of heterogeneous nucleation is far more common; nucleation occurs at dislocations, grain boundaries or

around impurities (4).

4.2 Diffusive growth

If nucleation occurs rapidly the precipitate particle size distribution remains narrow until the degree of supersaturation has become small. At this point the smaller particles begin to dissolve and the larger particles grow. This process, known as Ostwald ripening, proceeds because the solute concentration near small particles is greater than, and in the vicinity of large particles is less than the average supersaturation. Jain and Hughes have recently reviewed the subject (12). The theory of Ostwald ripening was formulated by Greenwood (13) and following the extensions of Wagner (14) and Lifshitz and Slezov (15-17) it has become known as LSW theory. More recently the effects of the finite volume occupied by the precipitate (18) and pair correlations (19) have been investigated. The traditional treatments (14-17) and more recent work (20) have shown that the precipitate particle size distribution assumes a unique form in the late stages; the shape of the distribution is independent of material and sample history, the amplitude depends only on a few material constants and the average particle radius scales with time. Analytic expressions for the particle radius distribution (12) have been transformed to volume distributions which are more convenient for magnetic studies, they are shown in figure 1. The three idealised cases shown correspond to systems where

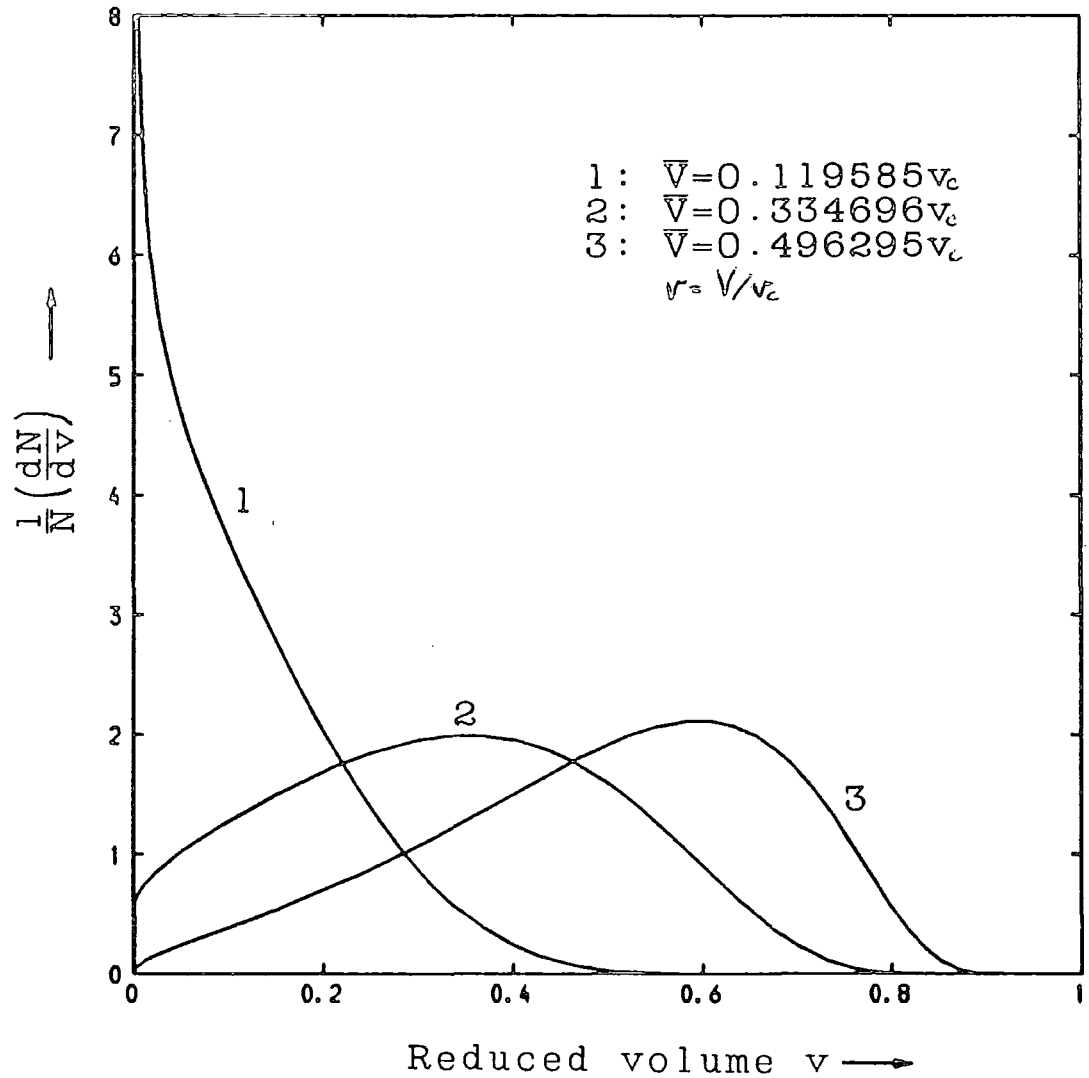

Fig 1. Particle volume distributions in the LSW region with growth rate limited by: 1-Surface reaction ('sticking'), 2-Bulk diffusion, 3-dislocation or grain boundary diffusion. The reduced volume v is related to the mean volume $\bar{V}$ as shown.

the growth is limited by: reaction rate at the precipitate boundary ($\bar{V} \propto t^{3/2}$); bulk diffusion ($\bar{V} \propto t$); and grain boundary or dislocation transport ($\bar{V} \propto t^{3/4}$). $\bar{V}$ is the average volume of the precipitate particles. If the volume fraction of the precipitate is greater than about 1% the distributions are broadened and particles grow faster (18 and see also 19).

5. Magnetic measurements and size distributions

The behaviour of microscopic particles of strongly magnetic material is usually size dependent (21). If a system of N particles is sufficiently disperse for particle-particle interactions to be negligible and an experiment measures its response G under conditions E then

$$G(E) = \int_0^\infty N g(E,V) f(V)\, dV \qquad (5)$$

where f(V) is the particle size distribution normalised so that

$$\int_0^\infty f(V)\, dV = 1 \qquad (6)$$

and g(E,V) is the expectation value of the response of a particle of volume V. The experiment conditions E would generally be a vector with components corresponding to the applied magnetic field, temperature, sample orientation and other relevant influences. The influence of f(V) on measurements of magnetisation torque and ferromagnetic resonance response will be discussed in chapter 4. Two problems are of practical importance (22):

(1) The distribution functions are known; calculate the magnetic properties of the sample.

(2) The magnetic properties have been measured; determine the distribution functions.

Kneller (22) gives references to several methods of solving these problems. It is not possible to determine particle volumes from magnetic measurements without relating a particle's volume to its magnetic properties by assumption. In some instances the assumptions can be investigated by microscopy (for example 23,24). Attempts have been made to determine the form of the particle size distribution from magnetisation measurements (25 and references therein); unfortunately the (magnetically) strong samples required to obtain good enough data to yield reasonable distributions experience interparticle interactions which invalidate, or render intractable, the analysis. If a distribution is unknown it is probably best characterised by its mean and standard deviation whch can be calculated very easily from a magnetisation curve using Cahn's method (26). The response functions g(E,V) for precipitates in iron doped MgO will be discussed in chapter 4 with particular attention to torque, ferrimagnetic resonance and magnetisation measurements.

6. The Fe/MgO system

Experimental measurements of the properties of MgO based systems are extremely sample dependent. Not only is it almost impossible to obtain reliable estimates of

impurity levels but the precise thermal history of a particular crystal can also seriously affect its properties (27). As mentioned in chapter 1 much of the extensive literature concerns the Fe/MgO system because of its importance in steel production chemistry. At the very low iron concentrations relevant to this work results are often difficult to interpret or conflicting but it is possible to draw some rather general conclusions.

The state and distribution of the iron in the Fe-Mg-O system depends on its environment. By choosing a reducing or oxidising atmosphere at high temperatures it can be treated as one of the pseudo-binary systems FeO-MgO or Fe_2O_3-MgO. The systems are pseudo-binary because each can contain different ratios of Fe^{2+} and Fe^{3+} ions (28,29).

6.1 The Fe/MgO system above ~1250K

In the Fe/MgO system above about 1250K the proportion of Fe^{3+} decreases with decreasing iron concentration (30,31) and decreasing oxygen partial pressure (for example 29,32). Woods and Fine (33) extrapolated from their magnetic measurements and estimated that the ratio Fe^{3+}/Fe^{2+} would be 10^{-3} at 1675K and 10^{-4}Pa oxygen partial pressure for 1% iron content. Groves and Fine (34) used Brynestad and Flood's (32) and Woods and White's (33) thermogravimetric data to estimate that at 1675K a 2% iron content sample in air at atmospheric pressure would contain 75% Fe^{3+} this proportion decreasing with increasing temperature. Wirtz and Fine (35)

suggested that polycrystalline MgO containing 1.2cation% iron sintered at 1850K in air contained 28% less Fe^{3+} than similar material sintered at 1715K; this result was inferred from magnetic measurements. White and collaborators (30,31) performed high temperature measurements but most other workers have used quenched samples. Recent work (36,37) has indicated that the cooling rates caused by quenching in air, water or liquid nitrogen are too slow to preserve the high temperature iron distribution.

Davidge (38) identified several forms of iron in samples heat treated in oxidising or reducing atmospheres: precipitates of metallic iron; substitutional Fe^{2+}; substitutional Fe^{3+}; and (at lower temperatures) precipitates of magnesioferrite $MgFe_2O_4$. He also discussed Fe^{3+}-vacancy association. Recently Kingery and co-workers (37,39,40) have calculated the energies of various defect aggregates found in iron doped MgO and used them to predict the equilibrium defect structures; the agreement between theory and experiment was good above 1575K and reasonable above 875K.

There have been several attempts to define the diffusion mechanisms and kinetics of iron in MgO (8-10,36,41-43). The results are not in agreement and it can only be concluded that if a vacancy mechanism is responsible then it will be extrinsic as a result of the impurities present in even the purest MgO (27,44) and it seems likely (8) that some other mechanism is active.

6.2 The Fe/MgO system below ~1250K

High temperature reactions between iron and MgO are often studied by rapidly quenching to normal temperatures. The quenched alloy is not at thermodynamic equilibrium and at room temperature is metastable. If the temperature is raised by a few hundred kelvin then diffusion can occur at a perceptible rate and the alloy can approach equilibrium.

Fine and co-workers (33-35,45,46) were interested in improving the physical properties of ceramics and examined the possibility of precipitation hardening in Fe/MgO. Their single crystal specimens were quenched in air from 1675K. Although electron microscopy and magnetisation measurements did not resolve any precipitate structure a powerful hardening was observed compared with when the experiment was conducted in non-oxidising conditions. It was concluded that the hardening indicated ordering of Fe^{3+} ions in the crystal. Using X-ray, magnetic, hardening and electron micrographic techniques they found that for Fe^{2+} diffusion limited oxidation led to surface and uneven intragranular precipitation. When Fe^{3+} was already present, dispersed in the lattice, the precipitation occurred entirely within, and evenly distributed throughout, the grains. Similar results were observed for polycrystalline samples. An explanation of the Fe^{2+} behaviour invokes two mechanisms (47-50). The oxygen in the lattice is arranged in a close packed array, the additional oxygen required for the $Fe^{2+} \rightarrow Fe^{3+}$ oxidation is at the surface so outward migration of Fe^{2+} is necessary.

The resultant change in Fe/O ratio within the grain allows some internal oxidation as well. The oxidation reaction was found to be diffusion limited for the range of oxygen partial pressures used ($2x10^4$ to 0.32Pa).

Evans and Cutler (10) suggested that spinodal decomposition might be responsible for nucleation and presented X-ray photographs in support. Using direct current conductivity measurements and optical spectroscopy they confirmed the work of Fine and his co-workers (up to 1175K, the latter's upper limit and discovered that above 1237K the precipitate ceased to be exclusively intragranular. McCollister and Van Vlack (51) found similar results in specimens of high iron content as did Davidge (38) using relatively low (5000ppm wt) iron concentrations

The precipitates of magnesioferrite which occur have been investigated with magnetic resonance at microwave frequencies by several workers (52-58). There is general agreement that the precipitates are regular octahedra and grow by a diffusion limited process (volume$\propto$time) with an activation energy for the growth rate equal to the value found by bulk diffusion experiments.

6.3 Magnesioferrite

The properties of material like magnesioferrite, the oxide spinels, have been reviewed by several authors (for example 59-62). They have the general formula $M'_{\delta}M_{1-\delta}[M'_{2-\delta}M_{\delta}]O_4$ where M and M' are di- and trivalent

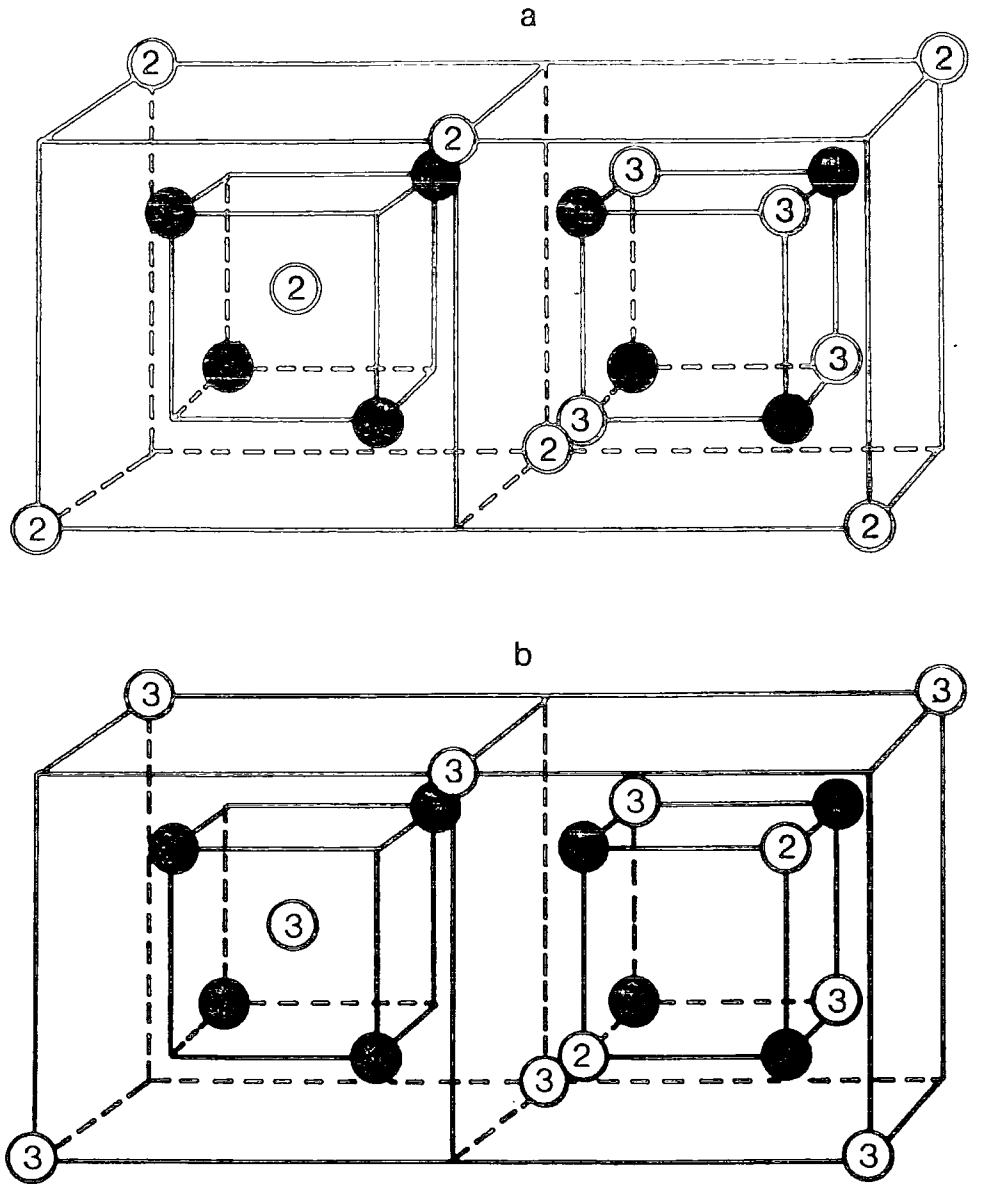

Fig 2. (a) Two octants of the regular spinel structure. Open circles represent di- and trivalent metal ions, solid circles are oxygen ions. (b) same for inverted structure. After (65).

Ion	4-fold	6-fold	Configuration
O^{2-}	0.138	0.140	$2p^6$
Mg^{2+}	0.057	0.072	$2p^6$
Fe^{2+}	0.063	0.078	$3d^6$
Fe^{3+}	0.049	0.062	$3d^5$

Table 1. Effective ionic radii (in nm) in 4-fold (tetrahedral site) and 6-fold (octahedral site) coordination (63).

cations respectively. $0 \leqslant \delta \leqslant 1$ is the degree of inversion, unbracketed cations occupying A (tetrahedral) sites and bracketed ions occupying B (octahedral) sites within the slightly distorted face-centred cubic oxygen lattice. The elementary cell of the structure contains 32 anions. Shannon's estimates (63) of the radii of ions comprising magnesioferrite are given in table 1. The magnetic behaviour of ferrites is usually described in terms of Néel's coupling scheme (64), the two magnetic sublattices comprising A sites and B sites respectively. There is a ferromagnetic ordering within each sublattice but a strong antiferromagnetic coupling between the two. If magnesioferrite had a completely inverted structure ($\delta=1$) it would have no spontaneous moment. In reality it is partially inverted ($\delta \sim 0.9$) and has a spontaneous moment of $\sim$1-2.4 Bohr magnetons per molecule (65) depending on preparation conditions. Magnesioferrite precipitated from a dilute Fe/MgO solution is expected to be saturated with MgO. Blackman (66) gives the solubility limit as 0.072 MgO per molecule of magnesioferrite independent of temperature below 1625K. Ignoring the influence of Fe^{2+} (which is present only in very small concentration) the spontaneous magnetisation of a precipitate particle will be

$$M_o = [5(x+1) - 10x\delta]\, 1{\cdot}25 \times 10^{5}\, J\, T^{-1} m^{-3} \qquad (7)$$

at 0K when there are x magnesium ions per molecule and a lattice constant of 0.84nm is assumed. The Curie

temperature of the precipitate is (35,66,67)

$$T_c = 200 + 490(1 - x + \delta x)\ K \qquad (8)$$

the temperature dependent spontaneous magnetisation M_s being (68)

$$M_s = M_o\left(1 - (T/T_c)^2\right) \qquad (9)$$

where T_c is the Curie temperature. The magnetocrystalline anisotropy of magnesioferrite is cubic and can be described by a single ion model (69-71) when the Fe^{2+} content is small. There have been several experimental studies of the effect of temperature, composition and cation distribution on the first order anisotropy constant K_1 (69,72-74). When $x \sim 1.0$-1.07 the results are summarised by

$$K_1 = -[(140 - 0.37T) \pm 5] \times 10^2\ Jm^{-3} \qquad (10)$$

Several workers have studied the effects of temperature on the degree of inversion in magnesioferrite (for example 67,68,75,76) which is given by (75)

$$\frac{(1-\delta)(2-x+(1-\delta)x)}{\delta(1-(1-\delta)x)} = \exp\left(-\frac{\theta_o + \theta_1\delta}{xT}\right) \qquad (11)$$

where $\theta_o = -2630K$ and $\theta_1 = 4480K$. Samples quenched from 1375K and annealed at 875K were found to come to equilibrium in about eight hours.

Yakovlev and co-workers (77) examined the ferrimagnetic resonance of single crystals of magnesioferrite and found that at 4.96GHz the line width was less than 0.6mT over the temperature range available (100-550K).

7. References

1. Behringer, R.E. Number of single, double and triple clusters in a system containing two types of atoms. J. Chem. Phys. (1958) 29, 537.

2. Crocker, A.G. Configurations of close-packed clusters of substitutional point defects in crystals. Phil. Mag. (1975) 32, 379.

3. Malik, A.Q., J.I. Akhtar, S.A. Ahmad and A.G. Crocker. The classification of mixed close-packed clusters of substitutional point defects in crystals. Phil. Mag. (1985) A51, 543.

4. Flynn, C.P. (1972) "Point defects and diffusion" Clarendon Press, Oxford.

5. Rice, S.A. Dynamical theory of diffusion in crystals. Phys. Rev. (1958) 112, 804.

6. Vineyard, G.H. Frequency factors and isotope effects in solid state rate processes. J. Phys. Chem. Solids (1957) 3, 121.

7. Sangster, M.J.L. and A.M. Stoneham. Calculations of off-centre displacements of divalent substitutional ions in CaO, SrO and BaO from model potentials. Phil. Mag. (1981) B43, 597.

8. Sangster, M.J.L. and A.M. Stoneham. Calculation of absolute diffusion rates in oxides. J. Phys. C. (1984) 17, 6093.

9. Blank, S.L. and J.A. Pask. Diffusion of iron and nickel in magnesium oxide single crystals. J. Amer. Ceram. Soc. (1969) 52, 669.

10. Evans, S.K. and. I.B. Cutler. Precipitation of magnesium ferrite from MgO-Fe_xO solid solutions. J. Mater. Sci. (1970) 5, 141.

11. Daniel, V. and H. Lipson. An X-ray study of the dissociation of an alloy of copper, iron and nickel. Proc. Roy. Soc. Lond. (1943) A181, 368.

12. Jain, S.C. and A.E. Hughes. Ostwald ripening and its application to precipitates and colloids in ionic crystals and glasses. J. Mater. Sci. (1978) 13, 1611.

13. Greenwood, G.W. Growth of dispersed precipitates in solutions. Acta Met. (1956) 4, 243.

14. Wagner, C. Theory of the ageing of precipitates by redissolution (Ostwald Maturing). Z. Elektrochem. (1961) 65, 581.

15. Lifshitz, I.M. and V.V. Slezov. Kinetics of diffusive decomposition of supersaturated solid solutions. Zh. Eksp. Teor. Fiz (1958) 35, 479.

16. Lifshitz, I.M. and V.V. Slezov. Theory of coalescence of solid solutions. Fiz. Tverd. Tela. (1960) 1, 1401.

17. Lifshitz, I.M. and V.V. Slezov. The kinetics of precipitation from supersaturated solid solutions. J. Phys. Chem. Solids (1961) 19, 35.

18. Marqusee, J.A. and J. Ross. Theory of Ostwald ripening: competitive growth and its dependence on volume fraction. J. Chem. Phys. (1984) 80, 536.

19. Marder, M. Correlations and droplet growth. Phys. Rev. Letts. (1985) 55, 2953.

20. Marqusee, J.A. and J. Ross. Kinetics of phase transitions: theory of Ostwald ripening. J. Chem. Phys. (1983) 79, 373.

21. This work, Chapter 4.

22. Kneller, E. (1969) Fine particle theory. pp.373-393 in A.E. Berkowitz and E. Kneller Eds. "Magnetism and Metallurgy" vol. 1, Academic Press, New York.

23. Kilner, M., S.R. Hoon, D.B. Lambrick, J. Potton and B.K. Tanner. Preparation and properties of metallic iron ferrofluids. IEEE Trans. Magn. (1984) MAG-20, 1735.

24. Hoon, S.R., D.B. Lambrick and D.M. Paige. An automated micrograph image size analyser. J. Phys. E. (1985) 18, 389.

25. Potton, J.A., G.J. Daniell and D. Melville. A new method for the determination of particle size distributions from superparamagnetic measurements. J. Phys. D. (1984) 17, 1567.

26. Cahn, J. Discussion in Trans. AIME J. Met. (1957) 209, 1309.

27. Quinn, N. Who will grow oxide crystals next? Brit. Assoc. Cryst. Growth Newsletter (1986) January, 10.

28. Phillips, B., S. Somiya and A. Muan. Melting relations of magnesium oxide-iron oxide mixtures in air. J. Amer. Ceram. Soc. (1961) 44, 167.

29. Phillips, B. and A. Muan. Phase equilibria in the system MgO-FeO-Fe_2O_3 in the temperature range 1400°C to 1800°C. J. Amer. Ceram. Soc. (1962) 45, 588.

30. Richards, R.G. and J. White. Phase relationships of iron oxide containing spinels Part II. Relationships in the systems Fe-Cr-O, Fe-Mg-O, Fe-Al-Cr-O and Fe-Al-Cr-Mg-O. Trans. Brit. Ceram. Soc. (1954) 53, 233.

31. Woodhouse, D. and J. White. Phase relationships of iron oxide containing spinels Part III. Further investigations on the systems Fe-Mg-O and Fe-Mg-Cr-O and general relationships in the system Fe-Mg-Cr-Al-O. Trans. Brit. Ceram. Soc. (1955) 54, 333.

32. Brynstad, J. and H. Flood. The redox reaction in wustite and solid solutions of wustite and MgO. Z. Electrochem. (1958) 62, 953.

33. Woods, K.N. and M.E Fine. MgO containing Fe^{2+}: Magnetic properties and clustering. J. Appl. Phys. (1969) 40, 3425.

34. Groves, G.W. and M.E. Fine. Solid solution and precipitation hardening in Mg-Fe-O alloys. J. Appl. Phys. (1964) 35, 3587.

35. Wirtz, G.P. and M.E. Fine. Superparamagnetic magnesioferrite precipitates from dilute solutions of iron in MgO. J. Appl. Phys. (1967) 38, 3729.

36. Weeks, R.A., J. Gastineau and E. Sonder. Distribution of Fe^{3+} in iron-doped MgO single crystals. Phys. Stat. Sol. (1980) A61, 265.

37. Yager, T.A. and W.D. Kingery. The equilibrium defect structure of iron-doped MgO in the range 600-1200°C. J. Mater. Sci. (1981) 16, 489.

38. Davidge, R.W. The distribution of iron impurity in single-crystal magnesium oxide and some effects on mechanical properties. J. Mater. Sci. (196) 2, 339.

39. Gourdin, W.H. and W.D. Kingery. The defect structure of MgO containing trivalent cation solutes: shell model calculations. J. Mater. Sci. (1979) 14, 2053.

40. Gourdin, W.H., W.D. Kingery and J. Driear. The defect structure of MgO containing trivalent cation solutes: the oxidation-reduction behaviour of iron. J. Mater. Sci. (1979) 14, 2074.

41. Carter, R.E. Mechanism of solid state reaction between MgO and Al_2O_3 and between MgO and Fe_2O_3. J. Amer. Ceram. Soc. (1961) 44, 116.

42. Wuensch, B.J. and T. Vasilos. Diffusion of transition metal ions in single crystal MgO. J. Chem. Phys. (1962) 37, 2917.

43. Rigby, E.B. and I.B. Cutler. Interdiffusion studies of the system Fe_x-MgO. J. Amer. Ceram. Soc. (1965) 48, 95.

44. Abraham, M.M., C.T. Butler and Y. Chen. Growth of high purity and doped alkaline earth oxides: I. MgO and CaO. J. Chem. Phys. (1971) 55, 3752.

45. Wirtz, G.P. and M.E. Fine. Precipitation and coarsening of magnesioferrite in dilute solutions of iron in MgO. J. Amer. Ceram. Soc. (1968) 51, 402.

46. Woods, K.N. and M.E. Fine. Nucleation and growth of magnesioferrite in MgO containing 0.9%Fe^{3+}. J. Amer. Ceram. Soc. (1969) 52, 186.

47. Schaeffer, W.L. and G.W. Brindley. Oxidation of magnesiowustite single crystals: I Optical and kinetic data. J. Phys. Chem. Solids (1963) 24, 919.

48. Ficalora, P.J. and G.W. Brindley. Oxidation of magnesiowustite single crystals: II Dependence on temperature, oxygen pressure and crystal composition. J. Amer. Ceram. Soc. (1967) 50, 662.

49. Brindley, G.W. and W.L. Schaeffer. Volume changes of magnesiowustite crystals in oxidation-reduction cycles. Trans. Brit. Ceram. Soc. (1964) 63, 31.

50. Sonder, E., T.G. Stratton and R.A. Weeks. Kinetics of Fe^{2+} oxidation and Fe^{3+} reduction in MgO single crystals. J. Chem. Phys. (1979) 70, 4603.

51. McCollister, H. and L.H. Van Vlack. MgO-$MgFe_2O_3$ microstructures. Bull. Amer. Ceram. Soc. (1965) 44, 915.

52. de Biasi, R.S. and T.C. Devezas. Crystal anisotropy of superparamagnetic particles as measured by resonance. Phys. Letts. (1974) 50A, 137.

53. de Biasi, R.S. and T.C. Devezas. Ferrimagnetic resonance study of the growth rate of superparamagnetic precipitates of magnesioferrite in MgO. J. Amer. Ceram. Soc. (1976) 59, 55.

54. de Biasi, R.S. and T.C. Devezas. Anisotropy field of small magnetic particles as measured by resonance. J. Appl. Phys. (1978) 49, 2466.

55. Dubowik, J. and J. Baszyński. Superparamagnetic properties of thin films and small particles of magnesium ferrite. IEEE Trans. Magn. (1980) MAG-16, 649.

56. Inglis, A.D., G.J. Russell and J.S. Thorp. Magnesioferrite formation in low-concentration Fe/MgO single crystals. J. Mater. Sci. (1982) 17, 2939.

57. de Biasi, R.S. and T.C. Devezas. Shape anisotropy of ultrafine magnesium ferrite precipitates. J. Magn. Magn. Mater. (1983) 35, 121.

58. Dubowik J. and J. Baszyński. FMR study of coherent fine magnesioferrite particles in MgO - Line shape behaviour. J. Magn. Magn. Mater. (1986) 59, 161.

59. Smit, J. and H.P. Wijn (1959) "Ferrites" John Wiley, New York.

60. Craik, D.J. Ed. (1975) "Magnetic oxides" John Wiley, New York.

61. Krupička, S. and P. Novak (1982) Oxide spinels. In E.P. Wohlfarth, Ed. "Ferromagnetic materials" vol. 3, North-Holland, Amsterdam.

62. Pollert, E. Crystal chemistry of magnetic oxides part 1: general problems - spinels. Prog. Cryst. Growth Charact. (1984) 9, 263.

63. Shannon, R.D. Revised effective ionic radii and systematic studies of interatomic distances in halides and chalcogenides. Acta Cryst. (1976) A32, 751.

64. Néel, L. Magnetic properties of ferrites: ferromagnetism and antiferromagnetism. Ann. Phys. (1948) 3, 137.

65. Corliss, L.M., J.M. Hastings and F.G. Brockman. A neutron diffraction study of magnesium ferrite. Phys. Rev. (1953) 90, 1013.

66. Blackman, L.C.F. On the solubility of MgO in magnesium ferrite. Trans. Faraday Soc. (1959) 55, 391.

67. Epstein, D.J. and B. Frackiewicz. Some properties of quenched ferrites. J. Appl. Phys. (1958) 29, 376.

68. Kriessman, C.J. and S.E. Harrison. Cation distributions in ferrospinels. Magnesium-manganese ferrites. Phys. Rev. (1956) 103, 857.

69. Folen, V.J. and G.T. Rado. Magnetocrystalline anisotropy of Mg-Fe ferrites: temperature dependence, ionic distribution effects, and the crystalline field model. J. Appl. Phys. (1958) 29, 438.

70. Yosida, K. and M. Tachiki. On the origin of the magnetic anisotropy energy of ferrites. Prog. Theor. Phys. (1957) 17, 331.

71. Slonczewski, J.C. Anisotropy and magnetostriction in magnetic oxides. J. Appl. Phys. Suppl. (1961) 32, 253S.

72. Belson, H.S. and C.J. Kriessman. Ionic distribution and ferrimagnetic resonance in magnesium ferrite. J. Appl. Phys. Suppl. (1959) 30, 170S.

73. Arai, K.I. and N. Tsuya. Measurement of magnetostriction and anisotropy of Mg-ferrite. J. Phys. Chem. Solids (1973) 34, 431.

74. Brabers, V.A.M., T. Merceron, M. Porte and R. Krishnan. Magnetic anisotropy of magnesium ferrous ferrites. J. Magn. Magn. Mater (1980) 15-18, 546.

75. Mozzi, R.L. and A.E. Paladino. Cation distributions in nonstoichiometric magnesium ferrite. J. Chem. Phys. (1963) 39, 435.

76. Knoch, H. and H. Dannheim. Temperature dependence of the cation distribution in magnesium ferrite. Phys. Stat. Sol. (1976) A37, K135.

77. Yakovlev Yu. M., É.V. Rubal'skaya, L.G. Godes, B.L. Lapovok and T.N. Bushueva. Single crystals of ferrospinels giving a narrow FMR line. Fiz. Tverd. Tela (1971) 13, 1151.

CHAPTER 4

Fine particle magnetism

1. Introduction

The magnetic behaviour of microscopic particles of strongly magnetic material such as the magnesioferrite precipitates discussed in this work, differs from that of macroscopic samples in two respects: the formation of any domain structure is energetically very unfavourable and, under typical experimental conditions, thermal fluctuations are comparable with the particles' energy of interaction with the applied magnetic field. The term superparamagnetic (SPM) refers to single domain particles whose magnetisation behaves anhysterisially under the applied field's influence. The formation of a dispersed precipitate of magnesioferrite in MgO has been described (1); the particles are regular octahedra, dominated by cubic crystalline anisotropy and particle-particle interactions are negligible for the concentration of iron used in this study (2). Fine particle magnetism and superparamagnetism have been reviewed by several authors (3-7).

2. The fine particle approximation

The magnetic domain structure of strongly magnetic material (8) results from a trade-off between two terms in

the Hamiltonian: the dipole-dipole interaction (9) is minimised by a large number of small domains, the exchange energy (10) is maximised under such conditions. Frenkel and Dorfman (11) proposed that below a critical size a particle would be entirely uniformly magnetised; real materials exhibit a variation of coercivity with particle size consistent with this idea (12). Some authors attempted to solve the problem by comparing the energy of a uniformly magnetised particle with various non-uniform configurations (for example 11,13-17). This model of the behaviour predicts the disappearance of hysterisis at the critical size (18) and experiments (12) do not agree with this conclusion. To obtain reasonable agreement with experiment it is necessary to consider the mechanism of access to the uniformly magnetised state (18,19), rigorous solutions exist for ellipsoids with predominant shape anisotropy. Quantitative solutions have not been found yet for the case of dominant crystalline anisotropy even for ellipsoids (5) and the critical dimension for a magnesioferrite particle must be estimated by assuming that it is no smaller than the domain wall thickness in large crystals (20). For stoicheiometric magnesioferrite the wall thickness is about 100nm.

3. Size dependence of magnetic properties

The properties of crystals are usually interpreted in terms of an ideal lattice possessing translational and

rotational symmetries. A real crystal has its translational symmetry broken by its surfaces and some size dependence of its bulk properties must be expected. For instance, the definition of a (non-zero) Curie temperature for a strong-weak magnetic phase transition is problematic for a finite sample (3,21). The rotational symmetry of the crystal affects its magnetocrystalline anisotropy and Néel suggested (22) that the large proportion of atoms on the surface of a fine particle would cause its anisotropy to differ significantly from large sample behaviour. These effects have been reviewed by Jacobs and Bean (4), theoretical and experimental evidence indicate that they are unimportant for particles larger than 2nm diameter in a reasonably matched host lattice.

The interface between two phases in coexistence is not perfectly sharp; in going from one phase to another the concentration changes gradually over several atomic distances (23). Kneller and others (24,25) assumed a trapezoidal concentration profile and were able to derive a temperature-dependent effective volume which was in agreement with experimental results. They found that for spherical particles in 74-2-24% Cu-Fe-Ni alloy the correction was significant for particles smaller than about 8nm radius.

4. Thermal Effects

A fine particle's temperature affects its behaviour in

a way that can be conveniently separated into two parts. Its material properties (spontaneous magnetisation M_s, crystalline anisotropy K etc.) depend on temperature; as explained earlier it is usual to assume that they have the values found for bulk samples of the material. The second part of the effect arises because the work needed to cause an appreciable divergence of the magnetisation within the particle is relatively large compared with the enthalpy associated with different orientations of the magnetisation with respect to the crystal axes. The magnetic enthalpy of a particle is proportional to its volume V and has contributions due to the magnetocrystalline anisotropy ($\sim KV$), the demagnetising fields ($<\mu_o VM_s^2/2$) and the external field B ($\sim BM_s V$). The last two magnetostatic contributions are discussed in detail in chapter 5. For most materials when the particle volume is small enough for single domain behaviour these terms can be comparable with the energies of room temperature thermal fluctuations. The theory of the thermal fluctuations of fine particles is mainly the work of Néel (26-28) and Brown (29,30 and references therein). Brown adapted the theory of Brownian motion to the fluctuations of a fine particle's magnetisation and found values for f_o in the approximate expression for the transition rate

$$W_{ij} = f_o \exp\left(-[E_m - E_i]/kT\right) \qquad (1)$$

from a state i (energy E_i) to a state j separated by an

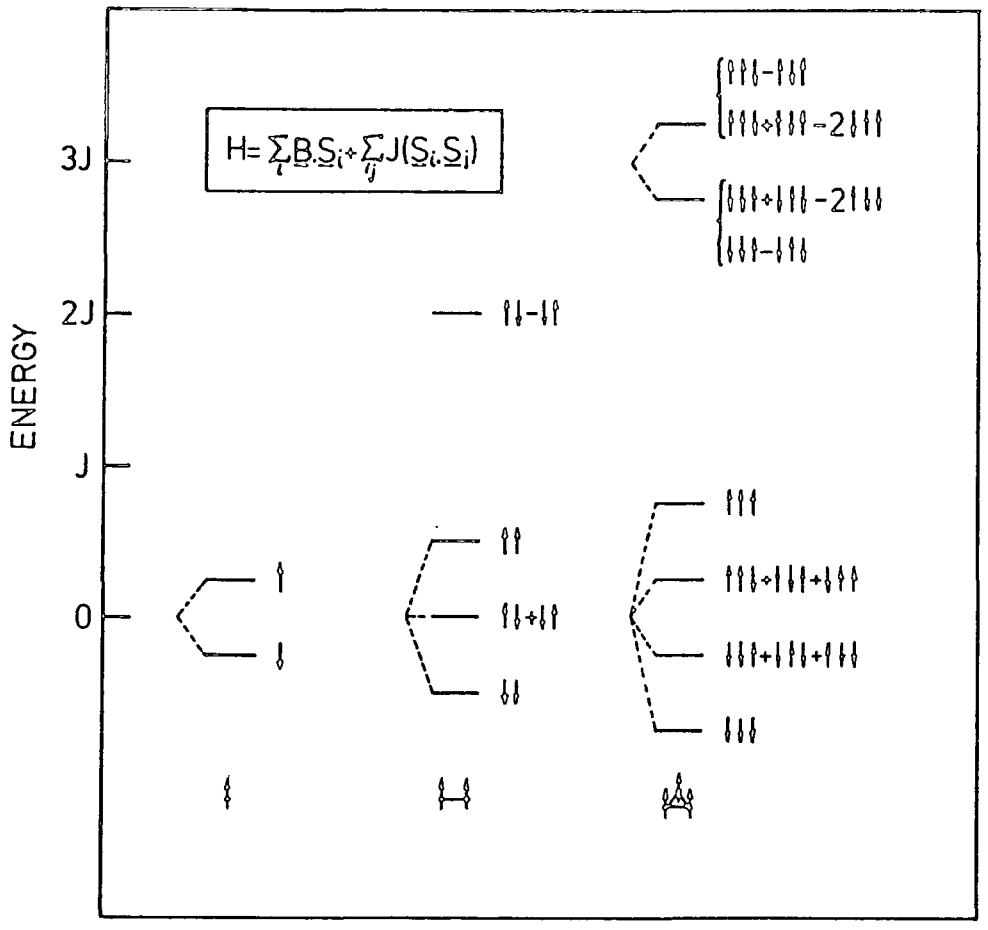

Fig 1. Illustration of the energy levels of clusters of spins in a small magnetic field interacting via isotropic exchange. The eigenfunctions are unnormalised and use a 'free spin product' basis.

energy barrier E_m. The rapid variation of the exponential factor means that $f_o \sim 10^{10} s^{-1}$ is an adequate approximation in most cases.

5. Quantum mechanics and fine particles

The link between the classical and quantum descriptions of fine particle magnetism can be simply illustrated by considering a system of a few atoms described by a Heisenberg spin Hamiltonian (10,31)

$$H = \left(\frac{qe}{2m}\right) \sum_i \underset{\sim}{B} . \underset{\sim}{S}_i - \sum_{ij} J_{ij} \left(\underset{\sim}{S}_i . \underset{\sim}{S}_j\right) \qquad (2)$$

where J_{ij} are the exchange integrals and $\underline{S}_i$ is the spin operator for the ith atom. The effects of anisotropic exchange and dipolar interactions between the N atoms will be mentioned later. The energy levels and eigenfunctions of equation 2 are illustrated in figure 1 for clusters of one, two and three atoms. The classical treatments of the preceding sections qualitatively describe the behaviour of a cluster of only three atoms. A ferromagnetic material has positive exchange integrals and the lowest energy states have a uniform magnetisation, that is all atoms have the same spin projection m_s. A cluster at low temperatures ($kT \ll J$) responds to a magnetic field like a single $S=N/2$ particle. Higher temperatures will populate the $S<(N/2)-1$ 'spinwave' states. Individual spinwave eigenstates do not in general, have a uniform magnetisation. The averaged magnetisation of degenerate spinwaves is uniform however, so

when the temperature is increased the spontaneous magnetisation reduces but remains uniform (provided the magnetic splitting is much less than kT and the magnetisation is averaged for longer than the thermal correlation time $h/kT \sim 10^{-13}$s at 300K (32)).

The Heisenberg model was first discussed by Heisenberg (33) and Frenkel (34) and it has been shown that equation 2 is a first approximation to the exact Hamiltonian (35). Magnetocrystalline anisotropy can be incorporated by adding an anisotropic exchange term (10). The demagnetisation fields (9,36-38) can be represented by a dipole-dipole interaction between atoms. A magnetic quadrupole interaction between atoms has also been investigated as a possible source of anisotropy (39,49 for example). Models based on equation 2 can describe the behaviour of many strongly magnetic materials if the exchange integrals are inferred from experiments (41). Calculations of the exchange integrals (42) directly from the electrostatic interactions they represent (43) suggest that indirect exchange interactions are the microscopic mechanism responsible for strong magnetism in most materials (44-46). This is not a great disadvantage, the response of a system of strongly interacting particles to low energy excitations is often not very sensitive to the exact nature of the microscopic interactions (47).

6. Magnetic response of fine particles

A fine particle will reach internal equilibrium for a particular orientation of its magnetisation in a time of about h/kT. At room temperature T~300K this relaxation time is about 10^{-13}s, several orders of magnitude shorter than the time it takes the magnetisation to come to equilibrium with the particle's surroundings (29). Even the smallest particles of interest contain thousands of atoms, enough to be able to specify accurately the magnetisation by classical coordinates and define a magnetic subsystem energy $F(\theta,\phi)$. This comprises all contributions to the total system's free energy which depend on its magnetisation (30). The expectation value of an observable $A(\theta,\phi)$ is then

$$\langle A \rangle = \frac{\sum_i A(\theta_i,\phi_i)\exp\left(-F(\theta_i,\phi_i)/kT\right)}{\sum_i \exp\left(-F(\theta_i,\phi_i)/kT\right)} \qquad (3)$$

where the sums extend over all possible states i of the magnetisation. If the separation of energy levels is small compared with kT the summations of equation 3 can be approximated by integrals. At a particular temperature using a spherical polar coordinate system (48) to describe the direction of magnetisation $\underline{M}$ with respect to the crystal axes

$$F(\theta,\phi) = -\underline{\underline{B}}.\underline{M}V + \frac{\mu_0}{2}\underline{M}\left(\tilde{N} - \tilde{\gamma}_3\right)\underline{M}V + K(\theta,\phi)V \qquad (4)$$

where $\tilde{N}$ is the particle's demagnetisation tensor. The

second term in equation 4 is discussed later (9), it depends on the shape of the particle and the orientation of the magnetisation $\underline{M}$ with respect to its axes. This shape anisotropy can be described by adding a uniaxial term to $K(\theta,\phi)$. For regular octahedra there is no shape anisotropy. $K(\theta,\phi)$ can be expressed as a sum of spherical harmonics (49) or other functions chosen to reflect the crystal symmetry (59). Magnesioferrite exhibits cubic magnetocrystalline anisotropy (51,52) so, neglecting high order terms and applying the magnetic field at angle (ψ,ω) to the crystal axes (53)

$$F(\theta,\phi;M_s,V,K_1,B,\gamma,\omega) = -BM_sV(\cos\theta\cos\gamma+\sin\theta\sin\gamma\cos(\phi-\omega)) + \frac{K_1V}{4}(\sin^4\theta\sin^2 2\phi+\sin^2 2\theta) \quad (5)$$

Magnetostrictive effects are incorporated into the definition of K_1 (54). The rest of this chapter discusses evaluation of equation 5 with particular reference to magnetisation, torque and FMR measurements.

6.1 Magnetisation

A conventional magnetometer measures a sample's magnetic dipole moment projection in the direction of the applied field so the operator A is $(V\underline{M}.\hat{\underline{B}})$ for a single fine particle of volume V and

$$\langle MV\rangle = M_sV\langle\cos\theta\cos\gamma+\sin\theta\sin\gamma\cos(\omega-\phi)\rangle \quad (6)$$

If the particle is isotropic this is exactly the expression

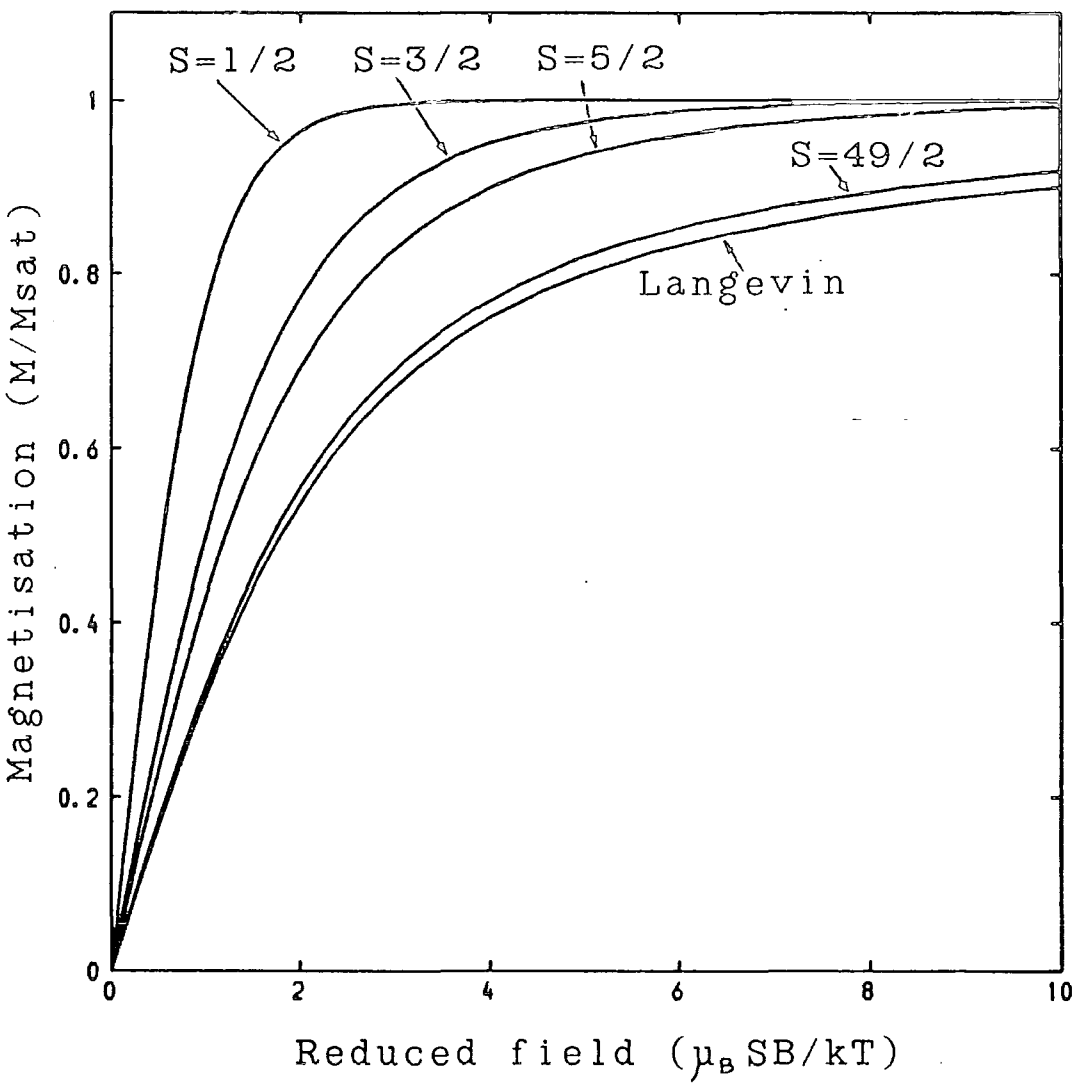

Fig 2. Reduced magnetisation of a weakly interacting (paramagnetic) system compared with (S=∞) Langevin behaviour.

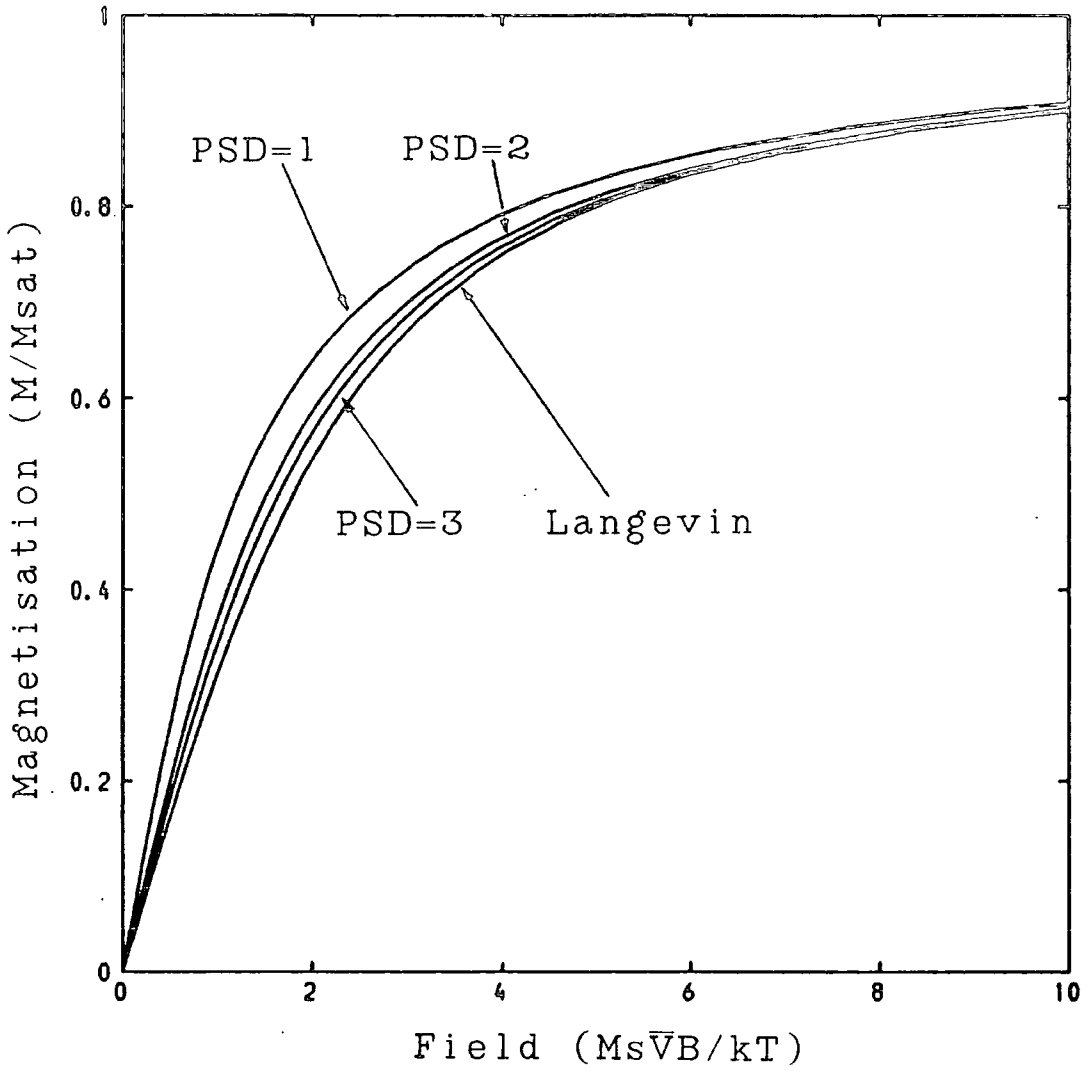

Fig 3. Reduced magnetisation of a system of isotropic fine particles, average volume $\bar{V}$, for each of the LSW particle size distributions (chapter 3, fig 1).

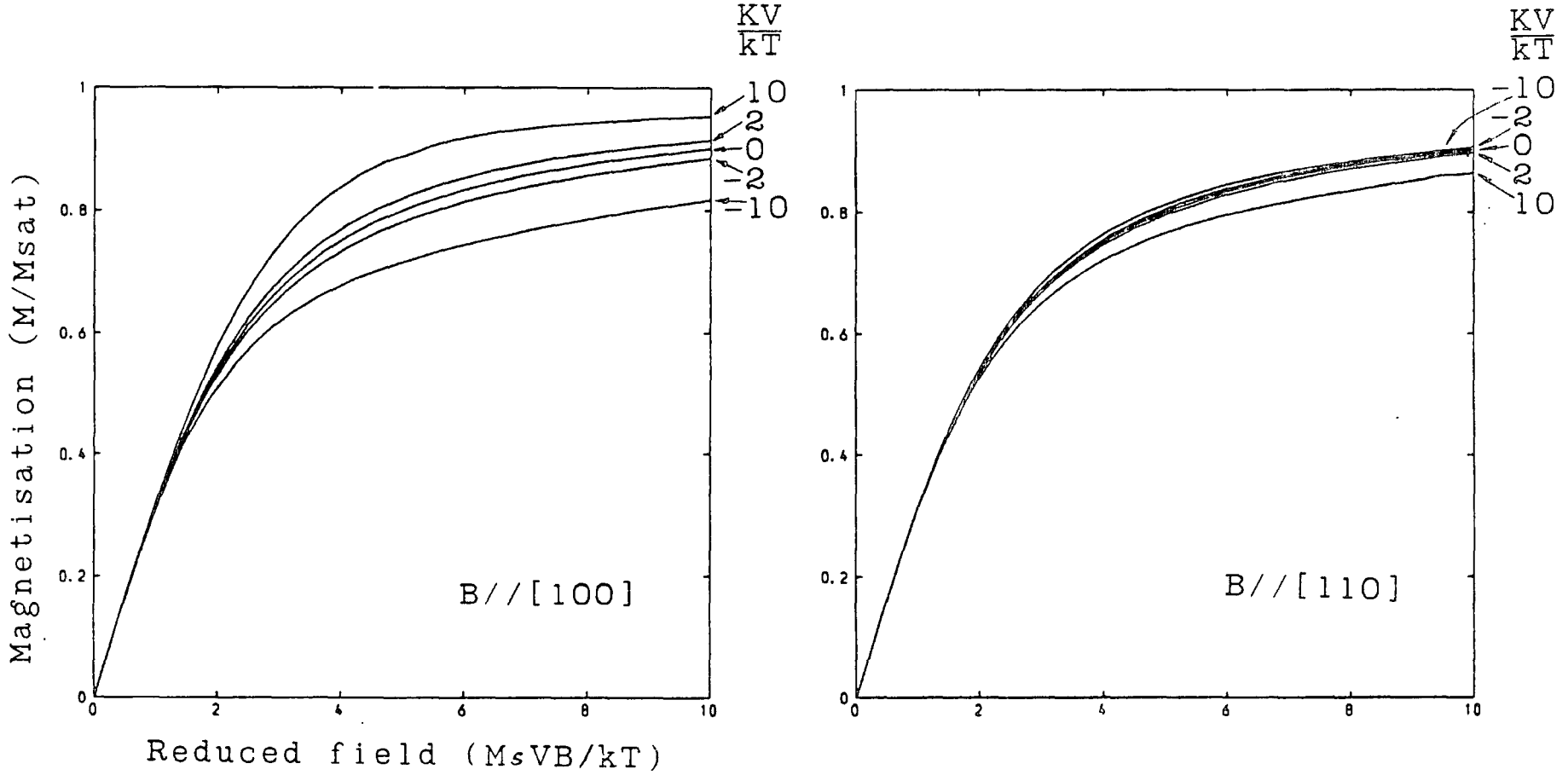

(Fig 4. Continued on next page.)

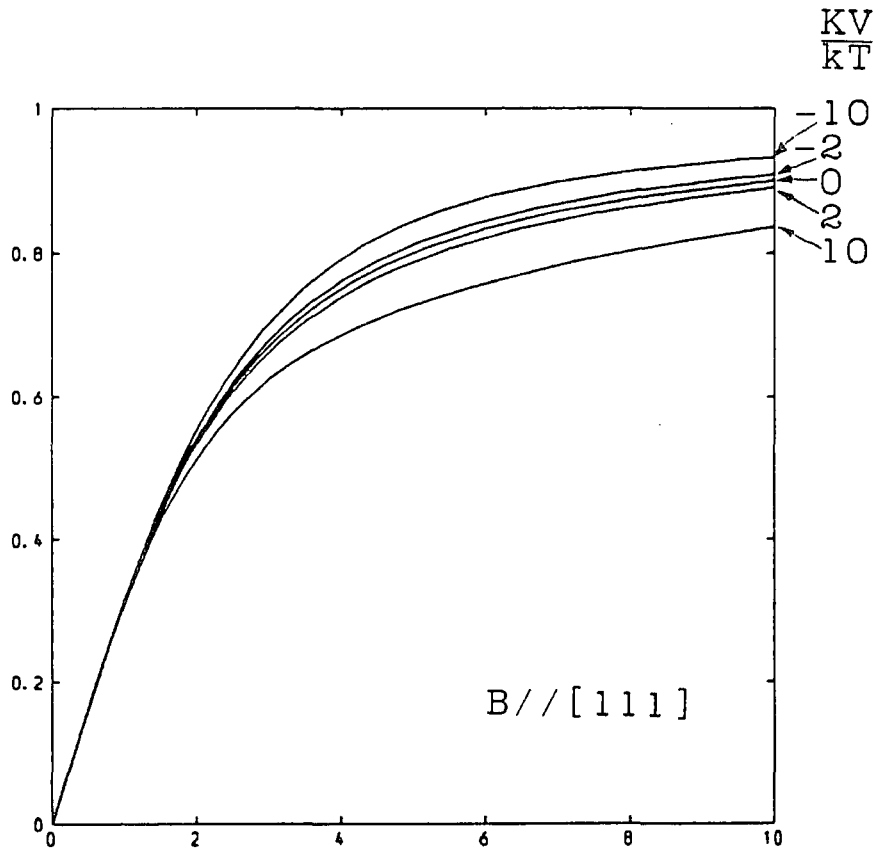

Fig 4 (cont.). Magnetisation of assembly of orientated fine particles with first order cubic anisotropy for field B applied in three directions.

for the behaviour of a particle of spin $S=M_s V/g\hbar\mu_B$ (55) where g is the particle's gyromagnetic ratio. Figure 2 compares the magnetisation curves of particles with the classical limit ($S=\infty$, Langevin behaviour) and shows that fine particles with as few as fifty magnetic atoms are reasonably described classically. This means that for the particles of several thousand atoms studied in this work the summations in equation 3 can be replaced by integrals. The effects of the particle size distributions discussed in chapter 3 on a system of isotropic, weakly interacting fine particles have been calculated numerically and the results are shown in figure 3. It is a consequence of the triangle inequality that the initial susceptibility of any such system is a minimum (for a given saturation magnetisation and mean volume) when all the particles have equal volumes. Asimow (53) calculated the effects of cubic anisotropy on the magnetisation of an assembly of randomly orientated SPM particles. Lin (56) and West (57) gave analytic results for orientated particles with uniaxial anisotropy. There have been several calculations of the coercivity and remanence of particles with cubic and other anisotropies (5) but apparently no publications have given explicit results for orientated particles with cubic anisotropy at equilibrium. The effects of first order cubic anisotropy on magnetisation curves taken along {100}, {110} and {111} directions have therefore been calculated numerically and are shown in figure 4, the result that the initial susceptibility of a

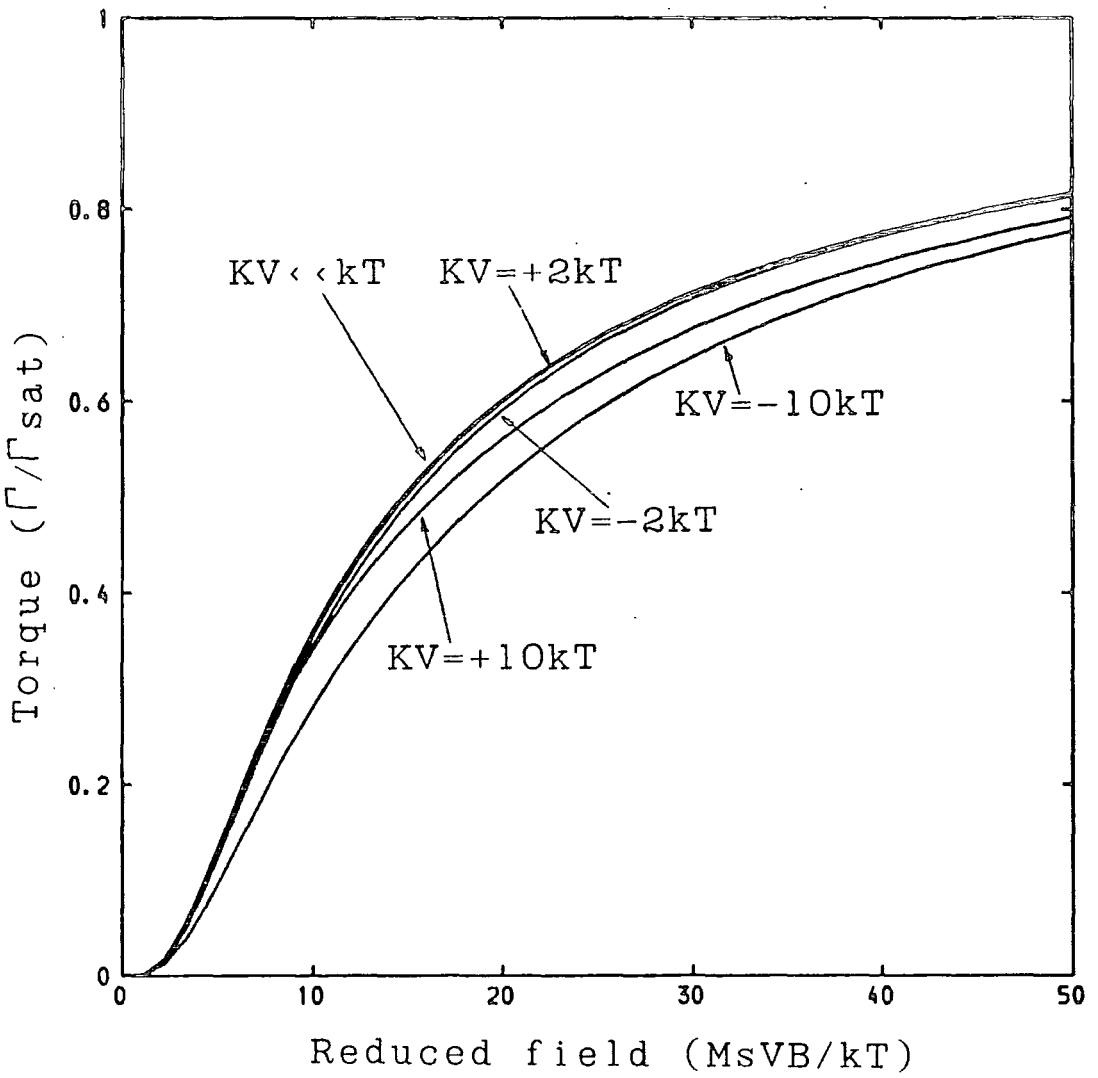

Fig 5. Reduced torque amplitude of a system of orientated fine particles with first order cubic anisotropy and volume V for various values of the anisotropy constant K.

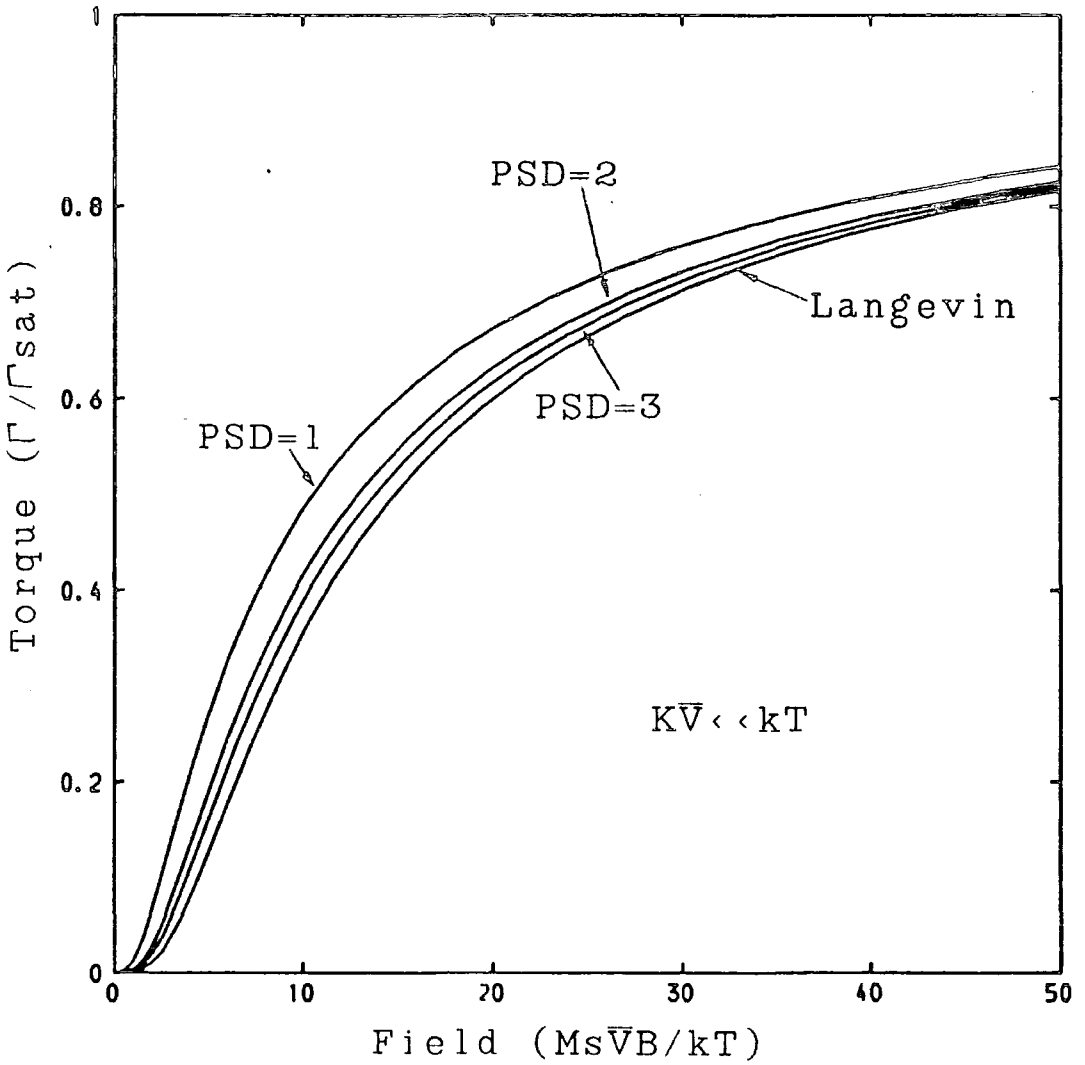

Fig 6. Reduced torque amplitude of a system of orientated fine particles with cubic anisotropy and average volume $\bar{V}$, for each of the LSW particle size distributions (chapter 3, fig 1).

particle is unaffected by cubic anisotropy complements Bean's predictions (58).

6.2 Torque

The experiments described in the next chapter measured the torque about the [001] axis of the sample due to the magnetic field $\underline{B}$ applied in the (001) plane at an angle ω to the [100] axis. The operator A is $(V\underline{M}_{\wedge}\underline{B})_z$ and the torque on a single particle is given by

$$\langle \Gamma \rangle = M_s V \langle \sin\theta \sin(\phi-\omega) \rangle \qquad (7)$$

Analytic approximations exist for cases when $|K_1V| \ll kT$ and $|K_1V| \gg kT$ (59). The torque curves have the symmetry expected for a saturated sample but reduced in amplitude, in the cubic $|K_1V| \ll kT$ case, by a fraction

$$\frac{\langle \Gamma \rangle}{\Gamma_{sat}} = 1 - \frac{10\coth X}{X} + \frac{45}{X^2} - \frac{105\coth X}{X^3} + \frac{105}{X^4} \qquad (8)$$

$$X = \frac{M_s V B}{kT} \qquad (9)$$

When $|K_1V|$ is not small compared with kT the results must be calculated numerically (figure 5). The influence of the particle size distributions described in the previous chapter on the torque amplitude when $|K_1V| \ll kT$ is shown in figure 6.

6.3 Ferromagnetic Resonance

Ferromagnetic resonance (FMR) was first observed by

Griffiths (60) and Zavoiskii (61). Luttinger and Kittel (62) and Richardson (63) obtained expressions for the eigenstates of a specimen undergoing FMR by adding demagnetisation factors to a Heisenberg Hamiltonian. Polder (64) gave a general proof of the equivalence of the classical and quantum mechanical interpretations. Van Vleck (65) and Oguchi (66) have given general quantum mechanical treatments of the problem and there have been many classical solutions (for example 67,68). Wangsness (69,70) investigated ferrimagnetic resonance and concluded that the equations describing ferromagnetic resonance can be applied to ferrimagnets if the value of g', the spectroscopic splitting factor, is suitably chosen.

Since its discovery there have been over a thousand publications concerning FMR so the following discussion has been restricted to material relevant to fine particles and references to experimental results are illustrative rather than exhaustive. Some of the earliest FMR investigations were of fine particle systems (71-76). Metal colloids were used to eliminate problems caused by the small ($\sim\mu$m) skin depth of metals at microwave frequencies. The observed resonances were many times broader than those of macroscopic crystals of the same materials. Although it was not realised until later those broad "lines" and the broad absorption envelopes of polycrystalline ferrites (77,78 and references therein) have the same basic cause: the resonance field B_{res} of a single domain crystal depends on the

orientations of the magnetisation and external field with respect to its axes (66). Reasonable approximations to the experimental line shapes of polycrystalline materials have been obtained (77-79). Rather few papers treat the theoretical problem of the FMR response of SPM particles (59,80-85). Livingstone and Bean (59) outlined a qualitative calculation and said that the apparent anisotropy measured using resonance would be larger than that found with a torque experiment. Dorfman (80) estimated that the width of the FMR line of an assembly of randomly orientated SPM particles would be ~10-100mT. Theories which ignore thermal fluctuations (for instance those originally developed for polycrystalline ferrites) have been applied to SPM systems (86,87)! Gekht and co-workers (81,84) used a statistical description of the dynamics of the magnetisation and obtained approximate results for an <u>isotropic</u> SPM particle. They suggested that their theory could explain the results of Bagguley (73) but did not mention a more likely possibility - that the colloid's particles were not perfectly spherical and were thus not isotropic (9). Griscom made an approximate calculation of the temperature and size dependence of the FMR absorption intensity but the agreement with experiment was problematic (85). De Biasi and Devezas (82,83) calculated the average value of the anisotropy field B_A defined by

$$\frac{h\nu}{g\mu_B} = B_0 + B_A = B_0 + \alpha \frac{K}{M} \qquad (10)$$

(where α is a numerical constant) as $\langle B_A \rangle = \langle K \rangle / \langle M \rangle$. They did not mention the fact that $K = K' P_n(\cos\theta)$ and $M = M_s \cos\theta$ (their definitions) are correlated so $\langle K/M \rangle \neq \langle K \rangle / \langle M \rangle$. Similar remarks apply to their treatment of the shape anisotropy. The only comparison with experimental results made for this theory used unpublished data (88) which had a ratio of 0.59 between the anisotropy field of SPM cobalt particles measured by torque and resonance, the value expected by de Biasi and Devezas being 0.49. In spite of these criticisms, which do not seem to have been made previously, the theory has the merit of simplicity and has been used by several authors (85,89-92). In summary, although the literature contains various methods of parameterising the FMR spectra of SPM samples, there has been nothing published suitable for direct application in this work.

The spin Hamiltonian describing the magnetic moment of a fine particle can be constructed from the classical magnetic enthalpy (equation 4) defining a spin operator $\underline{S}$ by $\hbar \underline{M} V = g\mu_B \underline{S}$. The demagnetisation term vanishes if the particle is a regular octahedron, and when there is first order cubic magnetocrystalline anisotropy

$$H_S = \left(\frac{ge}{2m}\right)\left(B_x S_x + B_y S_y + B_z S_z\right) + \frac{K_1 V}{(\hbar s)^4}\left(S_x^2 S_y^2 + S_y^2 S_z^2 + S_x^2 S_z^2\right) \qquad (11)$$

where the spin quantum number s is large and m is the electron mass. If the microwave radiation, frequency ν, is of low intensity P_o and thermal fluctuations are small the resonance condition

$$gB(\cos\theta\cos\gamma + \sin\theta\sin\gamma\cos(\phi-\omega)) =$$

$$\frac{K_1}{2M_s}\left(5\sin^2\theta\left[4\cos^2\theta+\sin^2\theta\sin^2 2\phi\right]-4\right)$$

$$\pm\left(\left[\frac{h\nu}{\gamma_B}\right]^2+\left[\frac{3K_1\sin^2\theta}{2M_s}\right]^2\left[\left(4\cos^2\theta-(1+\cos^2\theta)\sin^2 2\phi\right)^2+\cos^2\theta\sin^2 4\phi\right]\right)^{1/2} \quad (12)$$

can be otained by assuming a linear response (38,67). Under high power or high temperature (large thermal fluctuations) conditions the nonlinearity caused by the anisotropy and large deviations from equilibrium would invalidate such treatments (93).

When $\underline{B}$ is applied in a {100} direction equation 11 becomes

$$H_S = \left(\frac{ge}{2m}\right)B_z S_z + \frac{K_1 V}{(\hbar s)^4}\left(S_x^2 S_y^2 + S_z^2(S^2-S_z^2)\right) \quad (13)$$

assuming the deviation from the field direction is small the term $S_x^2 S_y^2$ can be neglected. S^2 and S_z commute so the energy levels of (13) are

$$E_m = g\mu_B B m_s + K_1 V\frac{m_s^2}{s^2}\left(1-\frac{m_s^2}{s^2}\right) \quad (14)$$

If the microwave radiation is polarised with its magnetic vector $\underline{b}\exp(-i2\pi\nu t)$ normal to $\underline{B}$ allowed transitions have $|\Delta m_s|=1,2,3,4$. Since $|m_s|$ is extremely large only the $|\Delta m_s|=1$ transitions have a significant intensity, approximately proportional to $(s^2-m_s^2)b^2$ and absorption can occur when

$$h\nu = g\mu_B B + \frac{K_1 V(2m_s+1)}{s^2}\left(1-\frac{(2m_s+1)}{s^2}\right) \quad (15)$$

The average power absorbed by the fine particle with $\underline{B}$ applied in a {100} direction is

$$P \propto P_o \left(\frac{M_s V}{\mu_B}\right)^2 \langle \sin^2\theta \, L(B-B_{res}) \rangle \qquad (16)$$

where L, the intrinsic line shape of a magnetic dipole transition for the particle, is normalised and $P_o \propto b^2$. Neglecting terms of higher order than θ^2 equation 16 becomes

$$B_{res} = \left(\frac{h\nu}{g\mu_B}\right) - \frac{2K_1}{M_s}\left(1 - \theta^2/2\right) \qquad (17)$$

The theory will be valid when the wavelength of the microwave field is long enough for the particle to experience a uniform field, and $M_s VB >> kT$ and $M_s VB >> -K_1 V + kT$. Under these conditions the magnetic subsystem energy is

$$F \simeq -BM_s V\left(1 - \delta\psi^2/2 - \sin^2\psi\,\delta\omega^2/2\right)$$
$$+ \left(K_\theta \delta\psi + K_\phi \delta\omega + K_{\theta\phi}\delta\psi\delta\omega + K_{\theta\theta}\delta\psi^2/2 + K_{\phi\phi}\delta\omega^2/2\right)V \qquad (18)$$

where $\theta = \psi + \delta\psi$, $\phi = \omega + \delta\omega$ and the partial derivatives of the anisotropy energy are evaluated at (ψ, ω). When $K_{\theta\phi} = 0$ the approximate partition function for the magnetic subsystem can be written as the product of two single dimensional integrals. If the SPM particle has first order cubic anisotropy this separation of variables occurs when $\underset{\sim}{B}$ is parallel to a {100} or {111} direction. In the {100} case $\psi = 0$ so

$$F \simeq -BM_s V\left(1 - \delta\psi^2/2\right) + K_1 V \delta\psi^2 \qquad (19)$$

and, to a good approximation, the distribution of magnetisation orientations about the direction of $\underline{B}$ is a Gaussian. Setting the constant of proportion to unity

because absolute measurements of absorption are unusual and excluding the case $K_1=0$ the average absorption will be

$$P(B) = \frac{\int_0^{2\pi} d\phi \int_0^{\pi} d\theta\, L(B-B_{res})\,(M_s V)^2 P_0 \sin^3\theta \exp(-F/kT)}{\mu_B^2 \int_0^{2\pi} d\phi \int_0^{\pi} d\theta \exp(-F/kT)\sin\theta} \tag{20}$$

If terms of order θ^4 are discarded and the line shape L is narrow enough to be approximated by a delta function then

$$P(B) \simeq \frac{P_0 V}{kT}(BM_s+2K_1)\left(\frac{M_s V}{\mu_B}\right)^2 \theta_{res}^3 \exp\left(-\theta_{res}^2 (BM_s+2K_1)V/2kT\right) \tag{21a}$$

$$\theta_{res}^2 = \frac{M_s}{K_1}\left(B - \frac{h\nu}{g\mu_B} + \frac{2K_1}{M_s}\right) \tag{21b}$$

$P(B)=0$ if $\theta^2_{res}<0$ and in the special case $K_1=0$

$$P(B) \simeq P_0 \left(\frac{M_s V}{\mu_B}\right)^2 \frac{2kT}{BM_s V} L\left(B - \frac{h\nu}{g\mu_B}\right) \tag{22}$$

Spectrometers usually record the derivative power absorption.

7. References

1. This work, chapter 3.

2. This work, chapters 6,7.

3. Bean, C.P. and J.D. Livingstone. Superparamagnetism. J. Appl. Phys. Suppl. (1959) 30, 120S.

4. Jacobs, I.S. and C.P. Bean. (1963) Fine particles, thin films and exchange anisotropy. In G.T. Rado and H. Suhl, Eds. "Magnetism" Vol. 3, Academic Press, New York.

5. Kneller, E. (1969) Fine particle theory. In A.E. Berkowitz and E. Kneller, Eds. "Magnetism and metallurgy" Vol. 1, Academic Press, New York.

6. Richardson, J.T. Magnetism and catalysis. J. Appl. Phys. (1978) 49, 1781.

7. Dormann, J.L. Le phénomène de superparamagnétisme. Revue Phys. Appl. (1981) 16, 275.

8. Tebble, R.S. (1969) "Magnetic domains" Halsted, New York.

9. This work, chapter 5.

10. Tyablikov, S.V. (1967) "Methods in the quantum theory of magnetism" Plenum Press, New York.

11. Frenkel, J. and J. Dorfman. Spontaneous and induced magnetisation in ferromagnetic bodies. Nature (1930) 126, 274.

12. Luborsky, F.E. Development of elongated particle magnets. J. Appl. Phys. Suppl. (1961) 32, 171S.

13. Néel, L. Propriétés d'un ferromagnétique cubique en grains fins. Compt. Rend. (1947) 224, 1488.

14. Stoner, E.C. and E.P. Wohlfarth. A mechanism of magnetic hysterisis in heterogeneous alloys. Phil. Trans. Roy. Soc. (1948) A240, 599.

15. Kittel, C. Physical theory of ferromagnetic domains Rev. Mod. Phys. (1949) 21, 541.

16. Amar, H. Magnetization mechanism and domain structure of multidomain particles Phys. Rev. (1958) 111, 149.

17. Amar, H. Size dependence of the wall characteristics in a two-domain iron particle. J. Appl. Phys. (1958) 29, 542.

18. Frei, E.H., S. Shtrikman and D. Treves. Critical size and nucleation field of ideal ferromagnetic particles. Phys. Rev. (1957) 106, 446.

19. Brown Jr., W.F. Criterion for uniform micromagnetisation. Phys. Rev. (1957) 105, 1479.

20. Wohlfarth, E.P. (1963) Permanent magnet materials. In G.T. Rado and H. Suhl. Eds. "Magnetism" Vol. 3, Academic Press, New York.

21. Thomas, H. Paramagnetisches Verhalten dünner ferromagnetischer Schichten oberhalb des Curie-Punktes. Z. Angew. Phys. (1963) 15, 201.

22. Néel, L. Anisotropie magnétique superficielle et surstructures d'orientation. J. Phys. Radium (1954) 15, 225.

23. Cahn, J.W. and J.E. Hilliard. Free energy of a nonuniform system. I. Interfacial free energy. J. Chem. Phys. (1958) 28, 258.

24. Kneller, E. and M. Wolff. Anomalous superparamagnetism and interface effect. J. Appl. Phys. (1966) 37, 1350.

25. Kneller, E., M. Wolff and E. Egger. Temperature variation of the magnetisation curve of superparamagnetic alloys. J. Appl. Phys. (1966) 37, 1838.

26. Néel, L. Influence des fluctuations thermiques sur l'aimantation de grains ferromagnétiques très fins. Compt. Rend. (1949) 228, 664.

27. Néel, L. Théorie du trainage magnétique des ferromagnétiques en grains fins avec applications aux terres cuites. Ann. Geophys. (1949) 5, 99.

28. Néel, 1. Thermoremanent magnetization of fine powders. Rev. Mod. Phys. (1953) 25, 293.

29. Brown Jr., W.F. Thermal fluctuations of a single-domain particle. Phys. Rev. (1963) 130, 1677.

30. Brown Jr., W.F. Thermal fluctuations of fine ferromagnetic particles. IEEE Trans. Magn. (1979) MAG-15, 1196.

31. This work, chapter 2 section 4.5.

32. Callen, H.B. and T.A. Welton. Irreversibility and generalized noise. Phys. Rev. (1951) 83, 34.

33. Heisenberg, W. Theory of ferromagnetism. Z. Phys. (1928) 49, 619.

34. Frenkel, J. Elementary theory of the magnetic and electric properties of metals at the absolute zero of temperature. Z. Phys. (1928) 49, 31.

35. Arai, T. Exchange interaction and Heisenberg's spin Hamiltonian. Phys. Rev. (1962) 126, 471.

36. Holstein, T. and H. Primakoff. Field dependence of the intrinsic domain magnetisation of a ferromagnet. Phys. Rev. (1940) 58, 1098.

37. Van Vleck, J.H. Concerning the theory of ferromagnetic resonance absorption. Phys. Rev. (1950) 78, 266.

38. Oguchi, T. Note on the ferromagnetic resonance absorption. Prog. Theor. Phys. (1957) 17, 659.

39. Van Vleck, J.H. On the anisotropy of cubic ferromagnetic crystals. Phys. Rev. (1937) 52, 1178.

40. Potapkov, N.A. The Hamiltonian of a uniaxial ferromagnet. Dokl. Akad. Nauk. SSSR (1962) 144, 297.

41. Vonsovskiĭ, S.V. (1974) "Magnetism" Vol. 2, Halsted Press, New York.

42. Freeman, A.J., R.K. Nesbet and R.E. Watson. Two-electron Heisenberg exchange interaction between neighbouring atoms. Phys. Rev. (1962) 125, 1978.

43. Dirac, P.A.M. Quantum mechanics of many-electron systems. Proc. Roy. Soc. Lond. (1929) A123, 714.

44. Anderson, P.W. (1963) Exchange in insulators: superexchange, direct exchange and double exchange. In G.T. Rado and H. Suhl, Eds. "Magnetism" Vol. 1, Academic Press, New York.

45. Herring, C. (1966) Exchange interactions in metals. In G.T. Rado and H. Suhl, Eds. "Magnetism" Vol. 2, Academic Press, New York..

46. Kittel, C. Indirect exchange in metals Sol. Stat. Phys. (1968) 22, 1.

47. Domb, C. Critical phenomena: a brief historical survey. contemp. Phys. (1985) 26, 49.

48. Spiegel, M.R. (1968) "Mathematical handbook" McGraw-Hill, New York.

49. Paige, D.M. (1983) Ph.D. thesis, University of Durham, U.K.

50. Doring, W. The direction dependence of crystal energy. Annln. Phys. (1958) Ser 7, 1, 102.

51. Slonczewski, J.C. Anisotropy and magnetostriction in magnetic oxides. J. Appl. Phys. Suppl. (1961) 32, 253S.

52. Brabers, V.A.M., T. Merceron, M. Porte and R. krishnan. Magnetic anisotropy of magnesium ferrous ferrites. J. Magn. Magn. Mater. (1980) 15-18, 545.

53. Asimow, R.M. The measurement of superparamagnetic particle shapes and size distribution. Trans. Met. Soc. AIME (1965) 233, 401.

54. Brown, Jr., W.F. (1963) "Micromagnetics" Wiley (Interscience), New York.

55. Crangle, J. (1977) "The magnetic properties of solids" Edward Arnold, London.

56. Lin, C.J. Behavior of ferro- or ferrimagnetic very fine particles. J. Appl. Phys. Suppl. (1961) 32, 233S.

57. West, F.G. General superparamagnetic behaviour of an aligned assembly of uniaxially anisotropic particles. J. Appl. Phys. Suppl. (1961) 32, 249S.

58. Bean, C.P. Hysterisis loops of mixtures of ferromagnetic micropowders. J. Appl. Phys. (1955) 26, 1381.

59. Livingstone, J.D. and C.P. Bean. Anisotropy of superparamagnetic particles as measured by torque and resonance. J. Appl. Phys. Suppl. (1959) 30, 318S.

60. Griffiths, J.H.E. Anomalous high-frequency resistance of ferromagnetic metals. Nature (1946) 158, 670.

61. Zavoiskii, E.K. Russian Title. Zh. Teor. Eksp. Fiz. (1946) 17, 883.

62. Luttinger, J.M. and C. Kittel. Eine Bemerkung zu Quantentheorie der ferromagnetischen Resonanz. Helv. Phys. Acta (1948) 21, 480.

63. Richardson, J.M. Quantum theory of ferromagnetic resonance. Phys. Rev. (1949) 75, 1630.

64. Polder, D. On the theory of ferromagnetic resonance. Phil. Mag. (1949) 40, 99.

65. Van Vleck, J.H. Ferromagnetic resonance. Physica (1951) 17, 234.

66. Oguchi, T. Note on the ferromagnetic resonance absorption. Prog. Theor. Phys. (1957) 17, 659.

67. Bloembergen, N. Magnetic resonance in ferrites. Proc. Inst. Radio Engrs. (1956) 44, 1259.

68. Artman, J.O. Microwave resonance relations in anisotropic single crystal ferrites. Phys. Rev. (1957) 105, 62.

69. Wangsness, R.K. Sublattice effects in magnetic resonance. Phys. Rev. (1953) 91, 1085.

70. Wangsness, R.K. Magnetic resonance in ferrimagnetics. Phys. Rev. (1954) 93, 68.

71. Bagguley, D.M.S. Ferromagnetic resonance in colloidal suspensions. Proc. Phys. Soc. Lond. (1953) A66, 765.

72. Bagguley, D.M.S. and N.J. Harrick. The temperature dependence of ferromagnetic resonance in colloidal nickel. Proc. Phys. Soc. Lond. (1954) A67, 46.

73. Bagguley, D.M.S. Ferromagnetic resonance absorption in colloidal suspensions. Proc. Roy. Soc. (1955) A228, 549.

74. Anderson, J.C. and B. Donovan. Internal ferromagnetic resonance in nickel. Proc. Phys. Soc. Lond. (1959) 73, 593.

75. Anderson, J.C. Internal ferromagnetic resonance in small cobalt particles. Proc. Phys. Soc. Lond. (1960), 75, 33.

76. Anderson, J.C. and B. Donovan. Internal ferromagnetic resonance in magnetite. Proc. Phys. Soc. Lond. (1960) 75, 149.

77. Schlömann, E. Inhomogeneous broadening of ferromagnetic resonance lines. Phys. Rev. (1969) 182, 632.

78. Gurevich, A.G. (1963) "Ferrites at microwave frequencies" Consultants Bureau, New York.

79. Griscom, D.L. Ferromagnetic resonance condition and powder pattern analysis for dilute, spherical, single-domain particles of cubic crystal structure J. Magn. Reson. (1981) 45, 81.

80. Dorfman, Ya. G. On the theory of the influence of ferromagnetic particles on EPR Spectra of dielectrics. Zh. Eksp. Teor. Fiz. (1965) 48, 715.

81. Gekht, R.S., V.A. Ignatchenko, Yu. L. Raikher and M.I. Schliomis. Magnetic resonance of an isotropic superparamagnet. Zh. Eksp. Teor. Fiz. (1976) 70, 1300.

82. de Biasi, R.S. and T.C. Devezas. Crystal anisotropy of superparamagnetic particles as measured by resonance. Phys. Letts. (1974), 50A, 137.

83. de Biasi, R.S. and T.C. Devezas. Anisotropy field of small magnetic particles as measured by resonance. J. Appl. Phys. (1978) 49, 2466.

84. Gekht, R.S. and V.A. Ignatchenko. Magnetodipole broadening of a resonance line in a superparamagnet. Zh. Eksp. Teor. Fiz. (1979) 76, 164.

85. Griscom, D.L. Particle size effects in the FMR spectra of fine-grained precipitates in glass. IEEE Trans. Magn. (1981) MAG-17, 2718.

86. Gopel, W. and B. Weichmann. Magnetic anisotropies of single domain particles as determined by ferromagnetic resonance (FMR). J. Vac. Sci. Technol. (1982) 20, 219.

87. Griscom, D.L., E.J. Friebele and D.B. Shin. Ferromagnetic resonance of spherical of α-iron precipitated in fused silica. J. Appl. Phys. (1979) 50, 2402.

88. Reference 6 of (82).

89. Sharma, V.K. and A. Baiker. Superparamagnetic effects in the ferromagnetic resonance of silica supported nickel particles. J. Chem. Phys. (1981) 75, 5596.

90. Inglis, A.D., G.J. Russell and J.S. Thorp. Magnesioferrite formation in low-concentration Fe/MgO single crystals. J. Mater. Sci. (1982) 17, 2939.

91. Malhotra, V.M. and W.R.M. Graham. Detection of magnetite particles in coal by ferromagnetic resonance. J. Appl. Phys. (1985) 57, 1270.

92. Dubwik, J. and J. Baszynski. FMR study of coherent magnesioferrite particles in MgO-line shape behaviour. J. Magn. Magn. Mater. (1986) 59, 161.

93. Fairbairn, W. organised chaos a signature of nonlinearity. Phys. Bull. (1986) 37, 300.

CHAPTER 5

Demagnetisation tensors of fine particles

1. Introduction

The demagnetisation field of a fine particle (or other sample) can have a large, shape dependent effect on its magnetic behaviour. The demagnetisation energy is due to the dipolar interaction of the sample's microscopic moments. This energy is usually calculated by integration and assuming that the magnetised medium is continuous. The precipitation of microscopic octahedra of strongly magnetic magnesioferrite particles from a dilute solution of Fe_2O_3 in MgO was described in chapter 3. Published literature contains no discussion of either the demagnetisation energy of octahedra or the applicability of macroscopic calculations to microscopic samples containing only a few hundreds of atoms. This chapter addresses these problems.

2. Definitions and properties of demagnetisation tensors

The magnetic flux density $\underline{B}$ due to a region V of magnetisation $\underline{M}$ is

$$\underline{B}(\underline{r}_0) = \frac{\mu_0}{4\pi}\int_V \frac{3(\underline{M}\cdot\underline{r})\underline{r} - \underline{M}r^2}{r^5}\, d^3r' \qquad (1a)$$

$$\underline{r} = \underline{r}' - \underline{r}_0 \qquad (1b)$$

Obtaining the magnetisation configuration $\underline{M}(\underline{r})$ can be

difficult because it depends on the local magnetic field; after effects such as magnetostriction, anisotropy and thermal fluctuations have been included in the formulation, there are no general solutions (1). If a sample is either very small and ferromagnetic (2) or is in a large external field ($B_{ext} >> \mu_o M$) then its magnetisation can deviate only slightly from being uniform. Under these circumstances it is usual to assume a uniform magnetisation ($\underline{\nabla} . \underline{M} = 0$) and define a "demagnetisation" tensor $\tilde{N}_p(\underline{r}_o)$ by

$$\underset{\sim}{B}(\underline{r}_o) = -\mu_o \tilde{N}_p(\underline{r}_o) . \underline{M} \qquad (2)$$

$\tilde{N}_p(\underline{r}_o)$ is called the point demagnetisation tensor, it is second-rank, symmetric and has trace (3,4)

$$Tr\left(\tilde{N}_p(\underline{r}_o)\right) \begin{cases} = 1 \; ; \; \underline{r}_o \text{ inside surface} \\ = 0 \; ; \; \underline{r}_o \text{ outside surface} \end{cases} \qquad (3)$$

Ballistic demagnetisation factors $\tilde{N}_b$ are elements of $\tilde{N}_p$ averaged over the sample's central cross-section transverse to the magnetisation. $\tilde{N}_b$ is not a tensor but its elements are useful for interpreting ballistic magnetometer measurements (5,6). The volume average of $\tilde{N}_p$ over the sample forms the magnetometric demagnetisation tensor $\tilde{N}_m$, also of unit trace. $\tilde{N}_m$ is symmetric, has non-negative diagonal elements and can be diagonalised by an orthogonal transform $\tilde{U}$ (4)

$$\tilde{N}_m' = \tilde{U}^T \tilde{N}_m \tilde{U} \qquad (4)$$

The principal values of $\tilde{N}_m'$ are the demagnetisation factors

of the Brown-Morrish equivalent ellipsoid (7)*. The Stoner-Wohlfarth model (8) for the behaviour of a uniformly magnetised ellipsoid predicts at most two stable antiparallel equilibrium magnetisation states the absence of magnetocrystalline anisotropy. An interesting consequence of the Brown-Morrish theorem is that the Stoner-Wohlfarth predictions apply to a uniformly magnetised particle of any geometry. This is surprising because one might intuitively expect an octahedron, for example, to have six equilibrium states.

A microscopic picture of solid state magnetism associates magnetic moments $\underline{m}_i$ with discrete sites at $\underline{r}_i$ on a lattice and the resultant dipolar field varies rapidly over distances comparable with the lattice structure. However, if the macroscopic magnetisation $\underline{M}$ diverges no faster than linearly with position then Lorentz's argument relating the microscopic and macroscopic fields by considering the influence of the nearby lattice (9,10) is applicable and the field acting on a site can be found. Inside and away from the surface of an object comprising a cubic lattice of identically orientated and similar dipoles the local field at a site $\underline{r}_i$ due to all other sites $\underline{r}_j \neq \underline{r}_i$ is

$$B(\underline{r}_i) = B_{ext} - \mu_0 \left(\tilde{N}_p(\underline{r}_i) - \tilde{1/3} \right) . \underset{\sim}{M} \qquad (5)$$

---

*The Brown-Morrish theorem is that any uniformly magnetised object behaves, in a uniform external field, identically to a suitably chosen "equivalent" ellipsoid.

Sample geometry	Types	Ref.	Remarks
Ellipsoid of revolution	B=M=P	12	Analytic result in terms of elementary functions
	B=M=P	13	Tables for wide range of ellipticity
	M	*	M calculated by evaluation of lattice sums
General ellipsoid	B=M=P	14	Various analytic approximations, exact expressions in terms of elliptic integrals with tables and graphs
Circular cylinder	M	11	Tables of inductance [15a] used to tabulate M
	P	16	P in terms of elliptic integrals (see also [17])
	B,M	18	Analytic results in terms of elliptic integrals, tabulated for a range of aspect ratios
	M	*	M calculated by evaluation of lattice sums
	B	19	Experimental deterimination using an electrolytic tank and resistance networks
Hollow cylinder	M	20	Results in terms of elliptic integrals and tables
	B	19	Experimental method as [19] above
Elliptic cylinder	M,P	21	M given in terms of elliptic integrals, P numerically obtained for extreme positions
Rectangular prism	M	22	Analytic results in terms of elementary functions
	B,M	5	Tables for infinitely long, transversely magnetised bar
	B,M,P	23	Results in terms of analytic functions, graph of B
	M	24,*	Numerical calculations for a prism of square section and various degrees of elongation
Polygonal prisms	M	4,25	Refer to text
Octahedron	M	*	M calculated by evaluation of lattice sums

Table 1. Calculations of demagnetising factors (B=Ballistic, M=Magnetometric, P=Point) for uniformly magnetised samples. *=Reference to this work.

For such an object of volume V the magnetic potential energy E is related to its magnetometric demagnetisation factor by (11)

$$E/V = -\underset{\sim}{B}_{ext}.\underset{\sim}{M} + \frac{\mu_0}{2}|\underset{\sim}{M}|^2 + \frac{\mu_0}{2}\underset{\sim}{M}.(\tilde{N}_m - \tilde{V}_3)\underset{\sim}{M} \qquad (6)$$

3. Previous calculations of the demagnetising field

Maxwell presented the first accessible treatment of the field within a uniformly magnetised body and, following a method ascribed to Poisson, calculated its internal field and demonstrated that inside ellipsoids, and only ellipsoids, the demagnetising field is invariant with position; in the case of ellipsoids of revolution it is expressible in terms of elementary functions (12). Subsequent authors have generalised demagnetising tensors and applied them not only to uniformly magnetised samples as described earlier and summarised in table 1, but also to composites comprising two or more regions of differing (but still uniform magnetisation (26,27) and even to rings of cylindrically symmetric magnetisation (28,29).

Brown's 'Inductive Analogy' (11), relating the self-inductance of a finite solenoid to the magnetometric demagnetisation tensor of a similarly shaped sample, resulted in the publication of demagnetisation factors for polygonal prisms (4,25) based on tables of inductance (15). These results appear to be in disagreement with other work (5,22,23,24 and this work) in the case of rectangular

prisms. Other cases have not been checked but the disagreement is caused by the approximate method used to calculate the inductance tables and is likely to affect all of the shapes.

Attempts to predict the behaviour of domains resulted in numerous related calculations, based on the minimisation of the magnetic energy associated with particular patterns of domains (for example 5,22,30,31). A few calculations have let the magnetisation vary continuously (16,32,33). Recent work by Brug and Wolf and others (34 and references 14 and 15 therein) have investigated samples with both non-linear susceptibility and non-uniform magnetisation. The results are of limited general applicability and probably most useful for designing experiments to minimise the effects of sample shape.

Except for casual remarks (35,36) that regular octahedra would be expected to have a small positive shape anisotropy, there has been no previous discussion of demagnetisation tensors for octahedra: in fact regular octahedra are isotropic. Magnetometric demagnetisation tensors have been widely used to discuss the shape anisotropy of fine particles (volumes $\lesssim 10^{-24} m^3$) but there has apparently been no discussion of effects caused by such particles being too small for Lorentz's argument to be applied.

4. Magnetometric demagnetisation tensors in small samples

To examine the effects of shape and size on the magnetic behaviour of a sample consisting of N dipoles, each of moment $\underline{m}$ it is useful to define a quantity $\tilde{S}_N$ by analogy with equation 6 as

$$\frac{N}{2}\mu_0 \underline{m}.(\tilde{S}_N - \tilde{1}/3).\underline{m} = \frac{-\mu_0}{8\pi}\sum_{\substack{j \\ j\neq i}}^{N} \frac{3(\underline{m}.\underline{r}_{ij})^2 - |\underline{m}|^2|\underline{r}_{ij}|^2}{|\underline{r}_{ij}|^5} \qquad (7)$$

This definition is equivalent to an average over the entire assembly of the quantum mechanical point demagnetisation factor defined by Van Vleck (37,38). $\tilde{S}_N$ is related to the magnetometric demagnetisation tensor $\tilde{N}_m$ defined earlier by

$$\tilde{N}_m = \lim_{N\to\infty} \tilde{S}_N \qquad (8)$$

By defintion $\underline{r}_{ij}=-\underline{r}_{ji}$ and the nine elements of $\tilde{S}_N$ are given by

$$S_N^{kl} = \frac{\delta_{kl}}{3} - \frac{1}{2\pi N}\sum_{i>j}^{N}\sum_{j=1}^{N} \frac{3(\hat{\underline{e}}_k.\underline{r}_{ij})(\underline{r}_{ij}.\hat{\underline{e}}_l) - \delta_{kl}|\underline{r}_{ij}|^2}{|r_{ij}|^5} \qquad (9)$$

where $\{\hat{\underline{e}}_k\}$ are the basis of the cartesian coordinate system being used and $(\hat{\underline{e}}_k.\hat{\underline{e}}_l)=\delta_{kl}$. These elements are real and, since $\tilde{S}_N$ is symmetric, it can be diagonalised by an appropriate orthogonal transformation $\tilde{U}$. The Brown-Morrish theorem (7) can now be generalised to cover small assemblies of dipoles: the assembly of N dipoles described behaves, in a uniform field, like an ellipsoid of uniform magnetisation and moment $N\underline{m}$ with principle axes $\{\tilde{U}.\hat{\underline{e}}_k\}$ and demagnetisation tensor $\tilde{U}^T\tilde{S}_N\tilde{U}$.

5. Calculation of $\tilde{S}_N$

A typical fine particle might have a diameter of 5nm and contain about 10^4 dipoles; a direct calculation of $\tilde{S}_N$ from equation 9 would involve summing almost 10^8 terms and yield a result with four significant figures lost to round-off errors (39). A computer programme to perform this direct calculation would have taken over 24 CPU-hours to run for the maximum particle size of interest (65000 dipoles) on the Amdahl 470/V8 available. This execution time is O(2) in the number of dipoles N*. A systematic study of the size and shape dependences of $\tilde{S}_N$ using this method would have been beyond the available computing resources so a rather faster strategy was developed and used in the form of a computer programme called DIPOLE.

DIPOLE represents a particle by a list of integers, each the coordinate of a dipole J on the assembly's cubic lattice structure, with

```
LIST[J]:=(K*X)+(L*Y)+Z                    (10)
```

where K and L are constants selected with reference to the assembly's dimensions and X,Y,Z are the coordinates. The relative position of two dipoles I and J is then

```
R:=LIST[J]-LIST[I]                        (11)
```

---

*A process is O(m) in N if the execution time is proportional to N^m.

A second array DIFFERENCE has elements addressed by R. Starting with all elements of DIFFERENCE zero the code

```
for I:=1 to N-1 do
  for J:=I+1 to N do begin
    R:=LIST[J]-LIST[I];
    DIFFERENCE[R]:=DIFFERENCE[R]+1;
  end{for};
```

compiles a table of the number of occurrences of all possible values of $\underline{r}_{ij}$ in DIFFERENCE. This process is referred to as enumeration. Evaluation of $\tilde{S}_N$ from this table is O(1) in N and, compared with direct evaluation of equation 9, the number of significant figures lost to round-off is halved. The execution of the loops is extremely rapid and the total calculation is 25 times faster than the direct evaluation.

A method which will be called threading was developed to further increase execution speed. Threading is equivalent to a discrete form of Gauss's theorem. There are rows of adjacent dipoles within the assembly which can be entirely described by the coordinates of their start and finish. The threader identifies these coordinates by searching LIST for sequences of J where LIST[J+1]=LIST[J]+1 holds. For a sufficiently large assembly DIFFERENCE can be calculated from a list of threads by an O(5/3) in N procedure, in practice the performance is closer to O(3/2) due to the loops' overheads. Compared with the enumeration method threading produces identical results

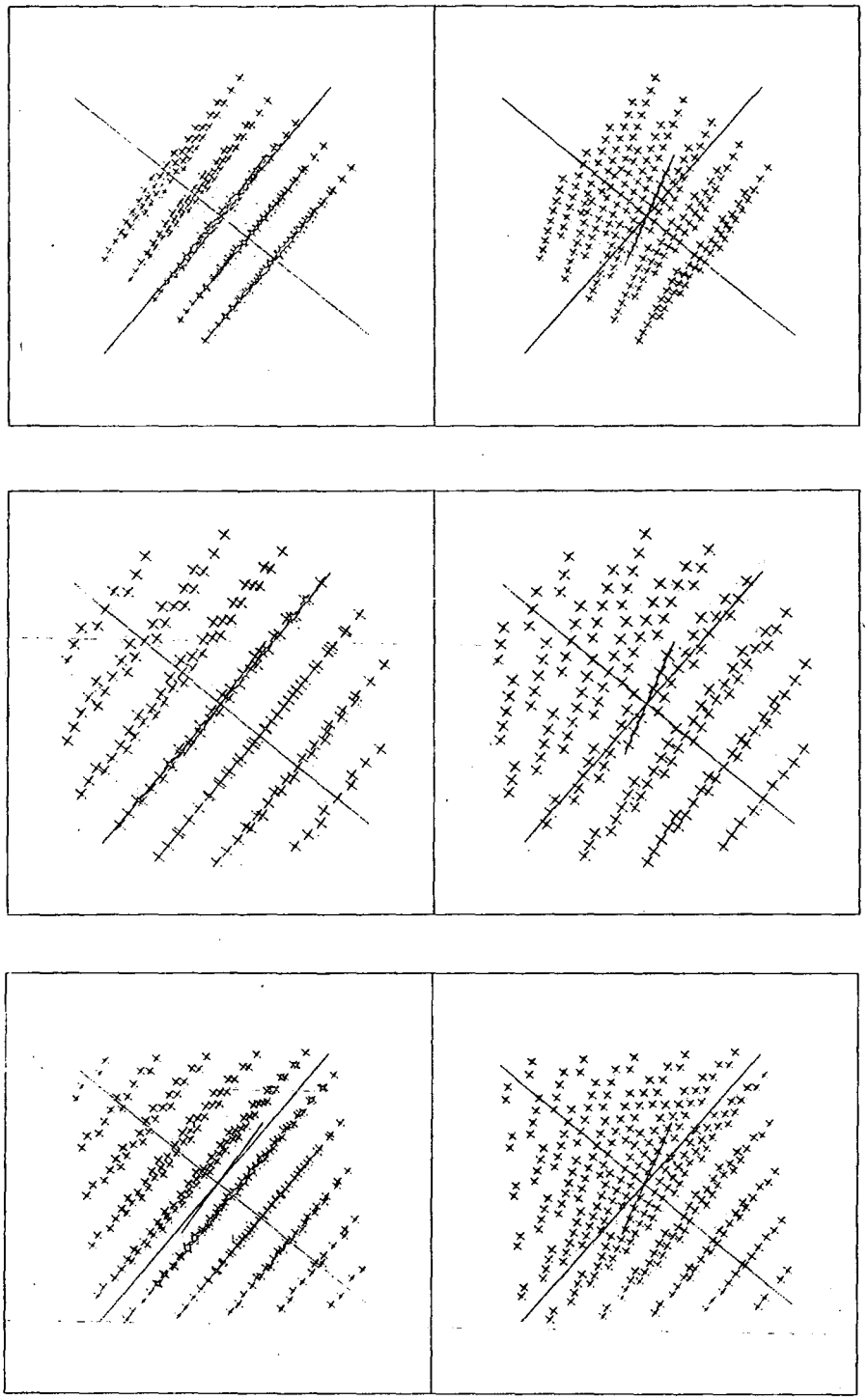

Fig 1. Examples of the stereogram output from DIPOLE used to check the coordinate list generation. (Suitable viewers are available from Philip Harris Biological Ltd.)

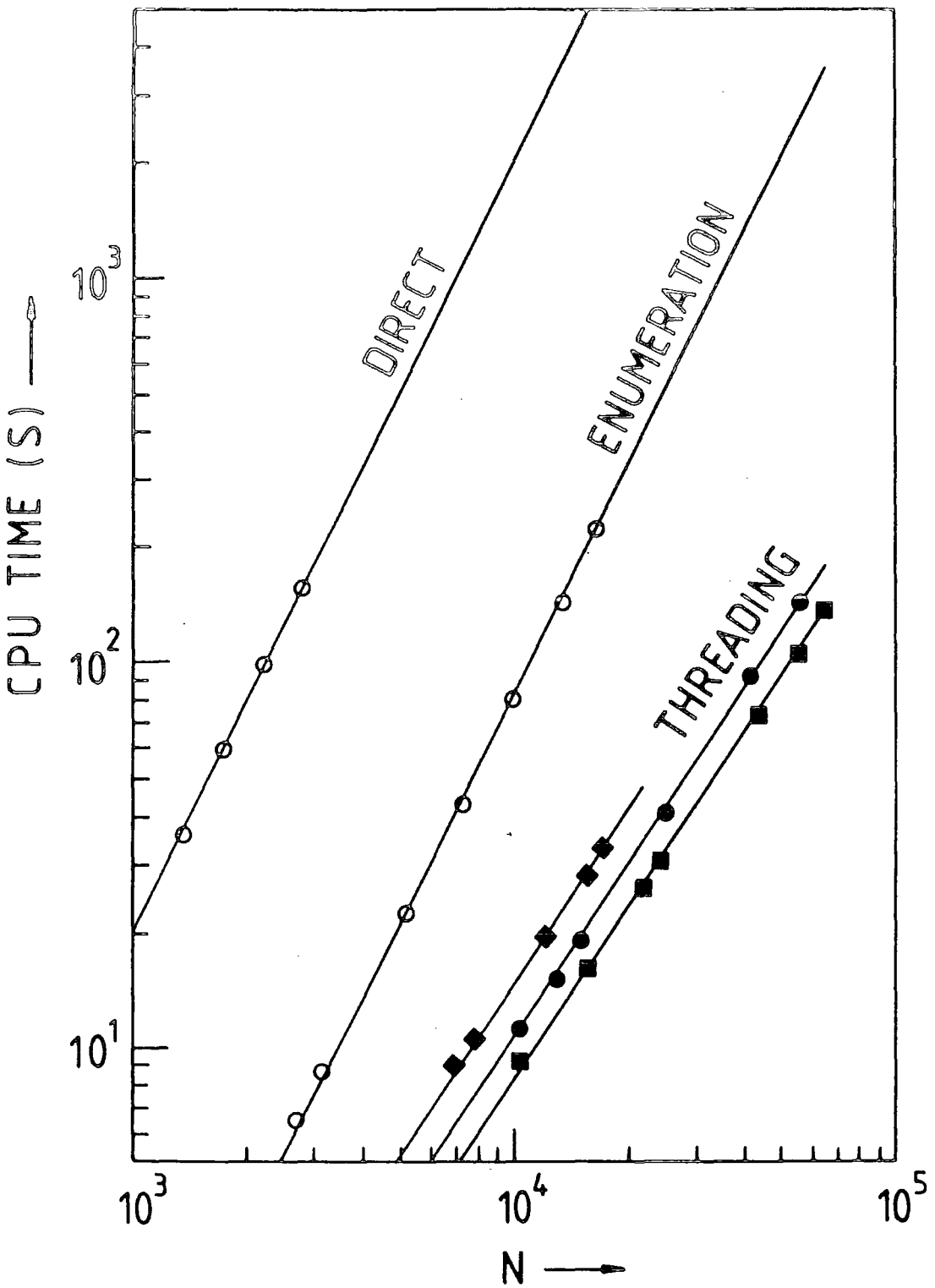

Fig 2. C.P.U. time needed to calculate S_N by various methods. o all shapes, ● spheres, ■ cubes, ◆ regular octahedra.

up to 23 times faster for N$\sim$65000.

DIPOLE is written in the computer programming language Pascal (40). Execution flow and error handling are controlled by set structures. Stereoscopic graphical output can be used to check visually the coordinate lists (figure 1 is some examples). DIPOLE recognises fault conditions and issues warnings or modifies execution flow as necessary; some errors likely to arise from careless modifications to the source code are also trapped. The extent of this checking renders the debug and check code generated by the compiler unnecessary and it can be suppressed with a consequent increase in execution speed. An IBM Pascal compiler (41) generated optimised object code for the Amdahl 470/V8 computer running under the Michigan Terminal System (42) operating system at Durham. Figure 2 displays the CPU time required to calculate $\tilde{S}_N$ for various shapes and methods. Results were accumulated in a log file which was subsequently used as direct input to an analysis programme.

The analysis consisted of sorting the results into shapes with the same aspect ratios and performing regression analysis; particular care was taken to avoid the problems of significance loss (39) which affect many regression techniques when they are applied to almost constant data. The exact results quoted in tables 2 and 3 were evaluated from analytic expressions in the literature (table 1) with a Hewlett-Packard Company HP15c programmable calculator (43), significance loss was monitored by separately accumulating

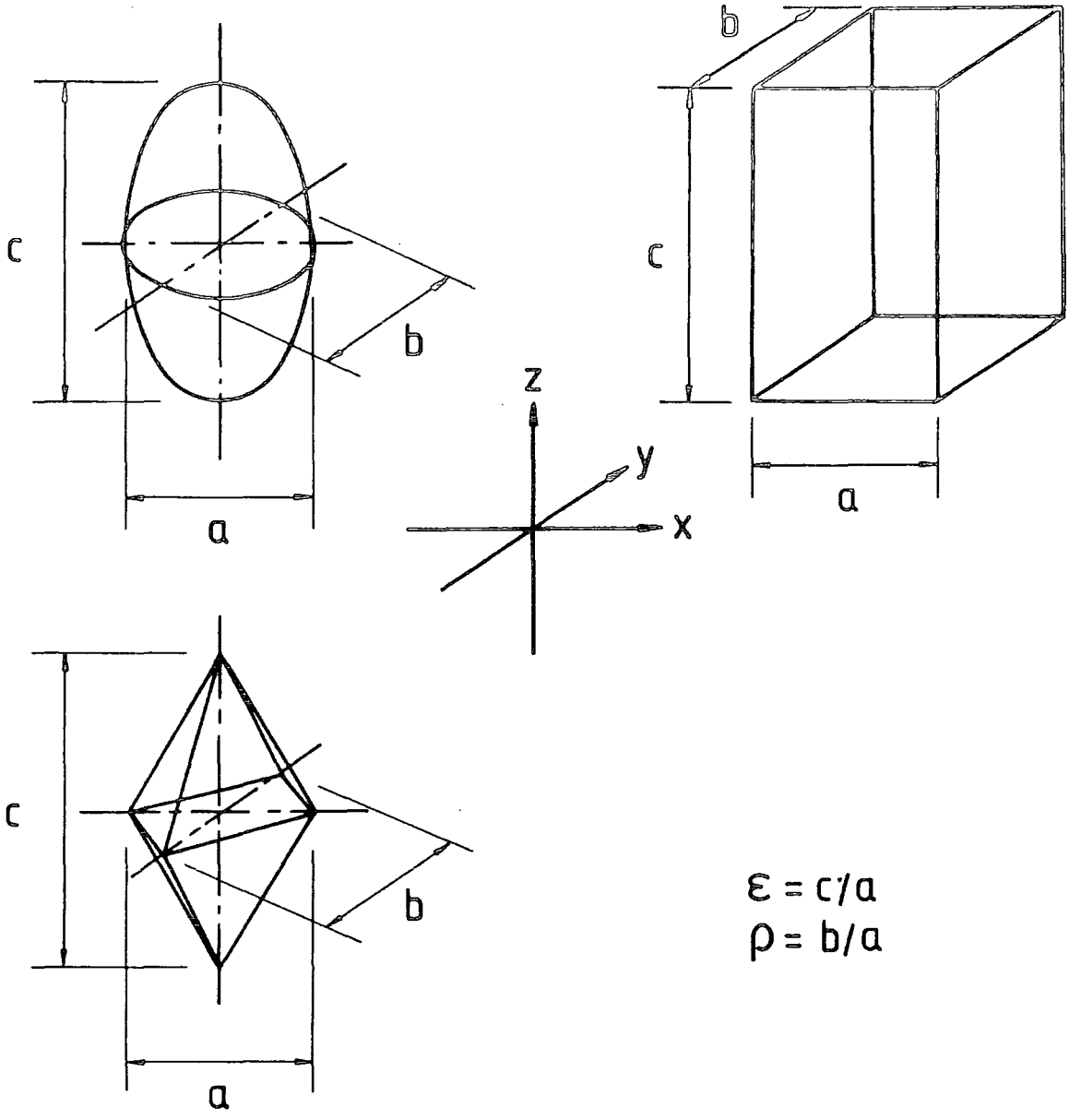

Fig 3. Definition of elongation and broadening for cuboids, ellipsoids and octahedra. Their principal axes coincide with the x,y and z directions.

positive and negative contributions to sums. The elliptic integrals were evaluated using Gauss's formula for the arithmogeometrical mean (44).

6. Results and discussion

If a uniformly magnetised sample is small enough for $\tilde{S}_N$ to differ noticeably from $\tilde{N}_m$ then the contribution to the total magnetic energy $\frac{V}{2}\mu_o(\underline{M}.\tilde{N}_m.\underline{M})$ must be replaced by $\frac{N}{2}\mu_o(\underline{N}.\tilde{S}_N.\underline{M})$. It is reasonable to believe that $\tilde{S}_N$ is approximately equal to $\tilde{N}_m$ with corrections for the missing interactions because of the surfaces, edges and corners of the assembly:

$$N\tilde{S}_N = N\tilde{N}_m + N_{surface}\tilde{\Delta} + N_{edges}\tilde{\Delta}' + N_{corners}\tilde{\Delta}'' \qquad (12)$$

$N_{surface}$, N_{edges}, $N_{corners}$ are the numbers of dipoles in the surfaces, edges and corners and the $\tilde{\Delta}$s are constants for given sample shape. Dividing equation 12 by N, noting that $\tilde{S}_\infty = \tilde{N}_m$, and renormalising the $\tilde{\Delta}$s gives

$$\tilde{S}_N = \tilde{S}_\infty + \tilde{\Delta}N^{-1/3} + \tilde{\Delta}'N^{-2/3} + \tilde{\Delta}''N^{-1} + \ldots \qquad (13)$$

For the three geometries illustrated in figure 3 (cuboidal, ellipsoidal and octahedral) $\tilde{S}_N$ was calculated using DIPOLE: keeping the x and y dimensions equal (ρ=1) with about forty elongations (ε=0.15 to 8) $\tilde{S}_N$ was evaluated for a wide range of N. The coordinate axes of figure 3 coincided with the

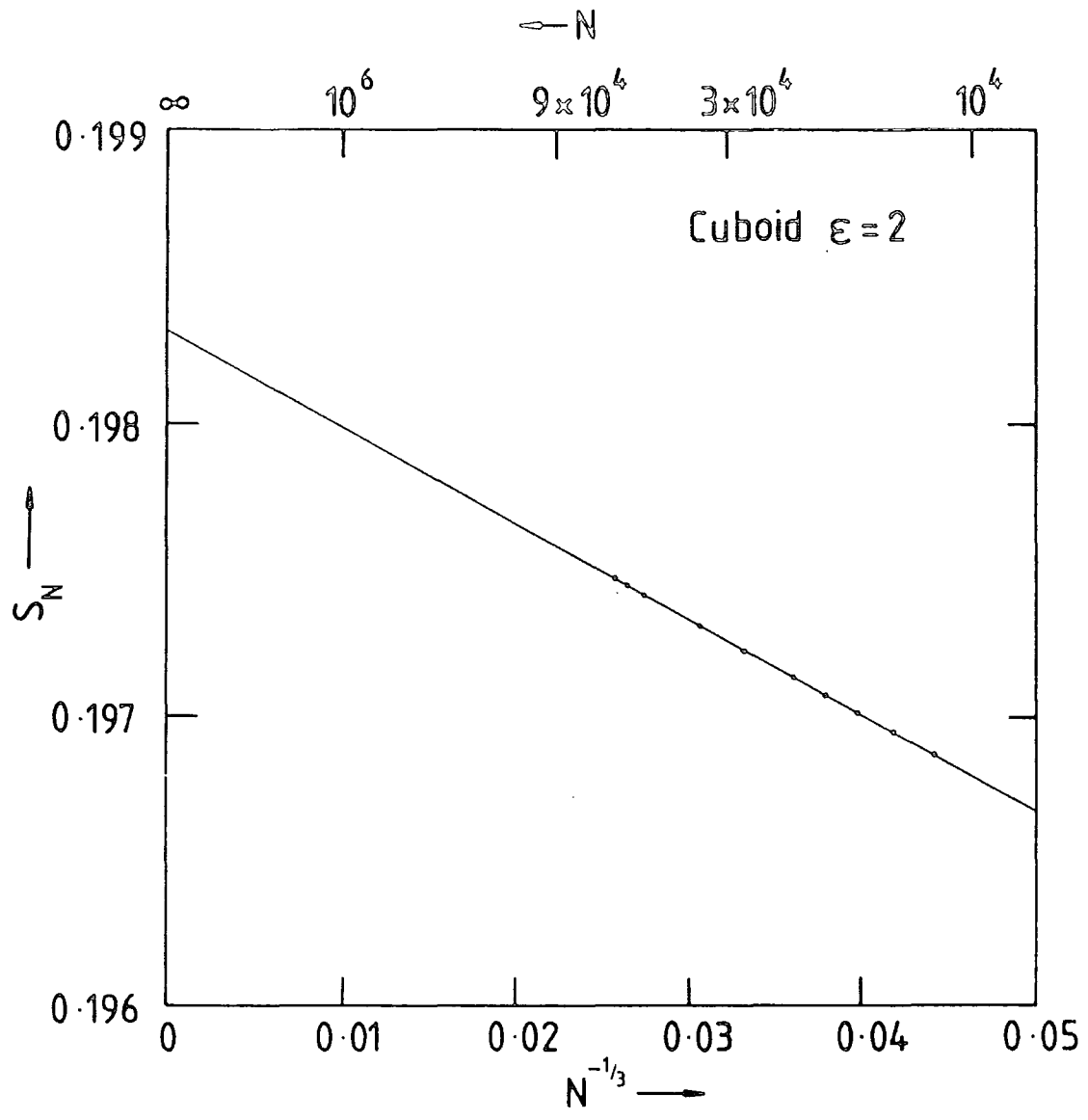

Fig 4. S_N as a function of $N^{-1/3}$ for cuboids of elongation $\varepsilon=2.5$ and $\rho=1$.

ε	Sharma [24]	Exact result (See text)	This work, O(1) method
0.1	0.816	0.8050776	0.805085
0.2	0.701	0.6941941	0.694199
0.5	0.499	0.4959220	0.495924
0.8	0.387	0.3842979	0.384299
1.0	0.334	0.3333333	0.333333
2.0	0.199	0.1983162	0.198313
5.0	0.0886	0.0883157	0.088308
8.0	0.05686	0.0566698	0.056658
10.0	0.04589	0.0457312	0.045716

Table 2. Comparison of the first order method of extrapolation used in this work with a previous worker's numerical calculation of the Z-component of a prism's magnetometric demagnetisation factor for various lengths and a square cross-section.

ε	Ellipsoids of revolution		Octahedra
	Analytic	Large N extrapolation of S_N	
0.15	0.80259	0.80338(48)	0.81770(320)
0.20	0.75048	0.75075(42)	0.77440(280)
0.25	0.70364	0.70358(28)	0.72949(240)
0.30	0.66135	0.66155(32)	0.68458(300)
0.35	0.62302	0.62328(32)	0.64632(200)
0.40	0.58815	0.58844(24)	0.60570(182)
0.45	0.55633	0.55625(26)	0.57153(220)
0.50	0.52720	0.52728(24)	0.54234(144)
0.55	0.50045	0.50005(24)	0.51778(200)
0.60	0.47583	0.47580(20)	0.48824(186)
0.65	0.45310	0.45321(22)	0.46278(260)
0.70	0.43207	0.43233(26)	0.43828(158)
0.75	0.41256	0.41242(26)	0.41541(144)
0.80	0.39444	0.39429(24)	0.40052(130)
0.85	0.37757	0.37786(20)	0.38164(186)
0.90	0.36182	0.36211(20)	0.36819(240)
0.95	0.34711	0.34710(22)	0.34592(192)
1.00	0.33333	0.33334(.5)	0.33346(4)
1.50	0.23298	0.23286(15)	0.22704(69)
2.00	0.17356	0.17323(13)	0.16743(37)
2.50	0.13515	0.13499(11)	0.12884(63)
3.00	0.10871	0.10875(11)	0.10415(25)
3.50	0.08965	0.08959(13)	0.08506(45)
4.00	0.07541	0.07560(9)	0.07167(29)
4.50	0.06445	0.06426(13)	0.06094(58)
5.00	0.05582	0.05563(10)	0.05341(30)
5.50	0.04889	0.04883(8)	0.04669(34)
6.00	0.04323	0.04302(8)	0.04174(25)
6.50	0.03854	0.03846(7)	0.03756(35)
7.00	0.03461	0.03450(8)	0.03289(29)
7.50	0.03127	0.03101(10)	0.03040(37)
8.00	0.02842	0.02841(7)	0.02707(30)

Table 3. Z component of magnetometric demagnetisation factor for ellipsoids of revolution and octahedra of square cross-section for various degrees of elongation in the Z direction. The definition of S_N and the extrapolation procedure are described in the text.

[100], [010], [001] directions of the cubic lattice used by DIPOLE. In these circumstances $\tilde{S}_N$ is diagonal and completely defined by S_N^{ZZ} since $S_N^{YY}=S_N^{XX}$. To simplify notation the zz superscript will be dropped henceforth.

6.1 Cuboids

The cuboids were orientated with each face parallel to one of the {100}, planes of the cubic lattice. Making each dimension an exact multiple of the lattice constant results in a cuboid with well defined, smooth faces and edges. Figure 4 shows the variation of S_N with $N^{-1/3}$ for such cuboids with elongation $\varepsilon=2$. An estimate of S_∞ is given by the intercept and it is clear from the excellent fit to the straight line

$$S_N = S_\infty + \Delta N^{-1/3} \qquad (14)$$

that the higher-order terms in equation 13 have a rather small effect under these conditions. Table 2 lists, for various elongations: first-order estimates of S_∞ from fitting equation 14 to values of S_N for N in the range 10^4 to 6×10^4; exact values of N_m; and results of an attempt by Sharma (24) to calculate N_m numerically. The S_∞ estimates are typically in error by a single count in the fifth decimal place. If a second-order extrapolation is used with the same values for S_N the estimates of S_∞ agree with exact values for N_m to better than eight decimal places.

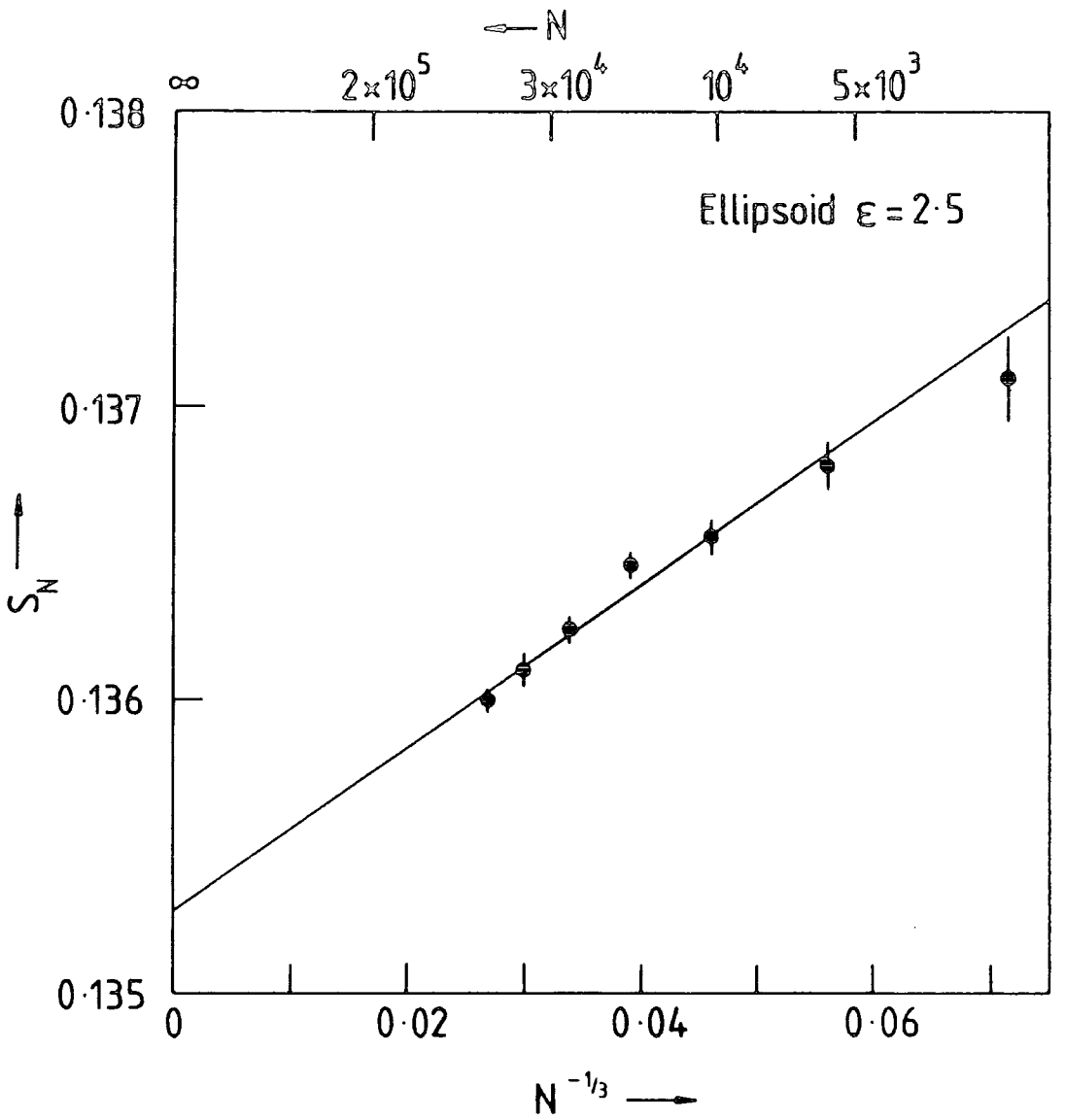

Fig 5. Estimated value of S_N as a function of $N^{-1/3}$ for ellipsoids of elongation $\varepsilon=2.5$ and $\rho=1$.

6.2 Ellipsoids

Several assemblies of points on a cubic lattice can be constructed to represent any particular ellipsoid. These possibilities differ relatively slightly in volume (the number of points used) but the exact arrangement of the surface may vary considerably depending on where the ellipsoid's centre is positioned within a unit cell. A second, and similar, effect occurs because an ellipsoid's dimensions can vary continuously but the configuration of lattice points representing it cannot: a lattice point either is or is not included. Consequentially, although the expected value of $\tilde{S}_N$ is the smooth function of N described by equation 13, calculated values of $\tilde{S}_N$ fluctuate about the expected value. By randomly selecting the ellipsoids' volumes from the range of interest the fluctuations were made to behave in an apparently random manner; the calculated values $\tilde{S}'_N$ could then be treated as if

$$\tilde{S}'_N = \tilde{S}_N + \tilde{\phi}(N) \qquad (15)$$

where $\tilde{S}_N$ is the expected value and $\tilde{\phi}(N)$ is drawn at random from a distribution of zero mean and a variance that is a smooth function of N. Figure 5 shows some typical results for an ellipsoid of elongation $\varepsilon=2.5$, the estimates of S_N and the associated standard errors* were obtained by binning values of similar N.

*The standard error estimates are based on the estimated variance of $\phi(N)$ which has a distribution rather closer to rectangular than Gaussian.

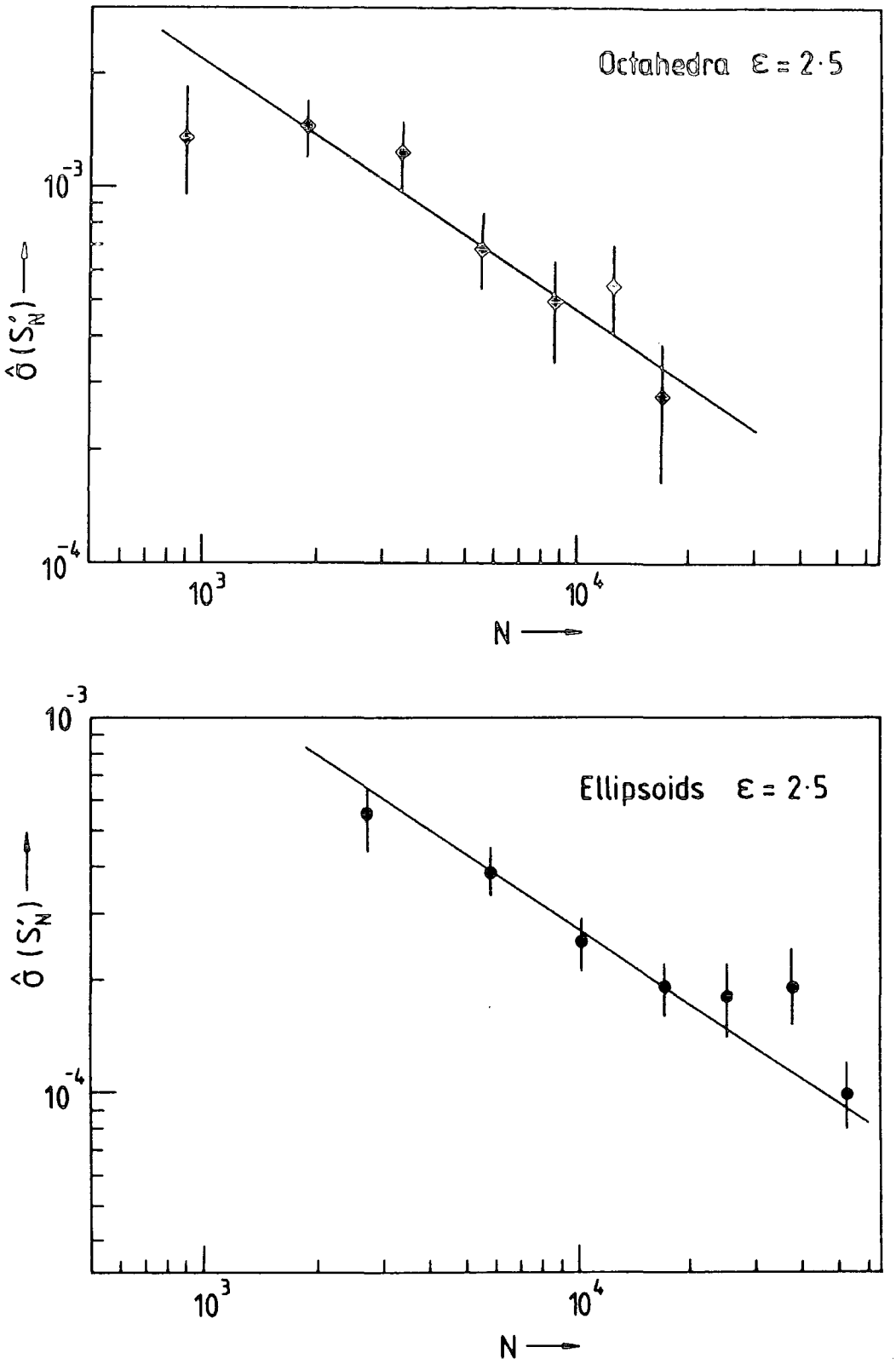

Fig 6. Estimated standard deviation of S'_N compared with the predicted $N^{-2/3}$ behaviour.

If it is assumed that the variance of $N_{surface}$ is proportional to the surface area of the ellipsoid and that the effects of correlation between N and $N_{surface}$ are negligible then the variance associated with NS'_N is approximately given by

$$Var(NS'_N) \propto N^{2/3} \qquad (16)$$

so

$$var(S'_N) \propto N^{-4/3} \qquad (17)$$

Figure 6a compares $\hat{\sigma}(S'_N)$ the standard deviation estimate of S'_N with the predicted $N^{-2/3}$ dependence for an ellipsoid (ε=2.5, ρ=1). Similar checks were made for octahedra (figure 6b) and oblate (ε=0.4) geometries. No significant deviation from the expected behaviour was found.

Since the variance of S'_N changes considerably over the range of N fitting equation 14 with equally weighted values of S'_N would yield poor estimates of S_∞ and Δ, and their associated errors (45). The problem is overcome by giving each S'_N a weight proportional to $N^{-2/3}$. The estimates of S_∞ and their standard errors s_e have been calculated, using values of N from 6000 to 65000, by this method for ellipsoids of revolution (table 3)*. A useful check on the reliability of the method is the behaviour of the quantity

$$\lambda = (N_m - \hat{S}_\infty)/\hat{s}_e \qquad (18)$$

which is expected to be a random variable drawn from a

*The figures in parentheses in table 3 refer to the standard error of the associated estimate. For example 0.80338(48) could be written 0.80338±0.00048 in a less compact notation.

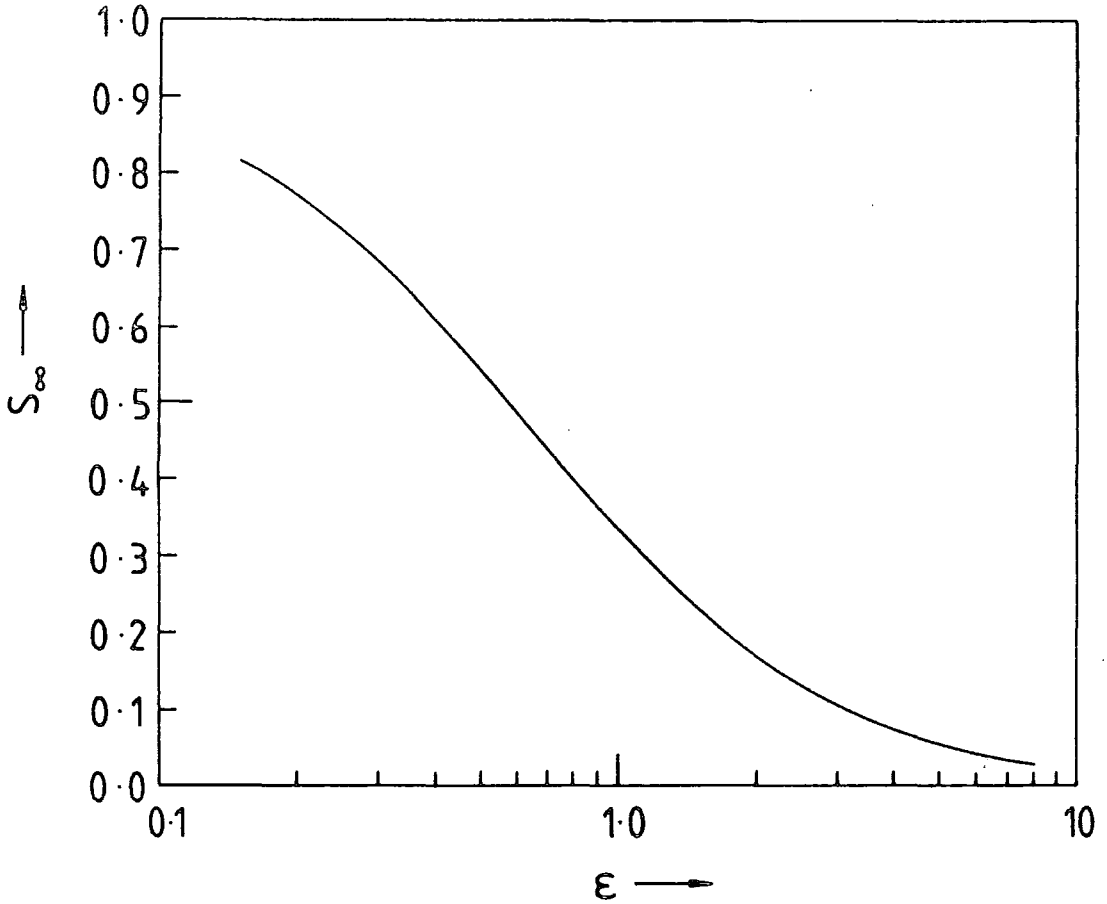

Fig 7. Magnetometric demagnetisation factors for macroscopic octahedra with $\rho=1$.

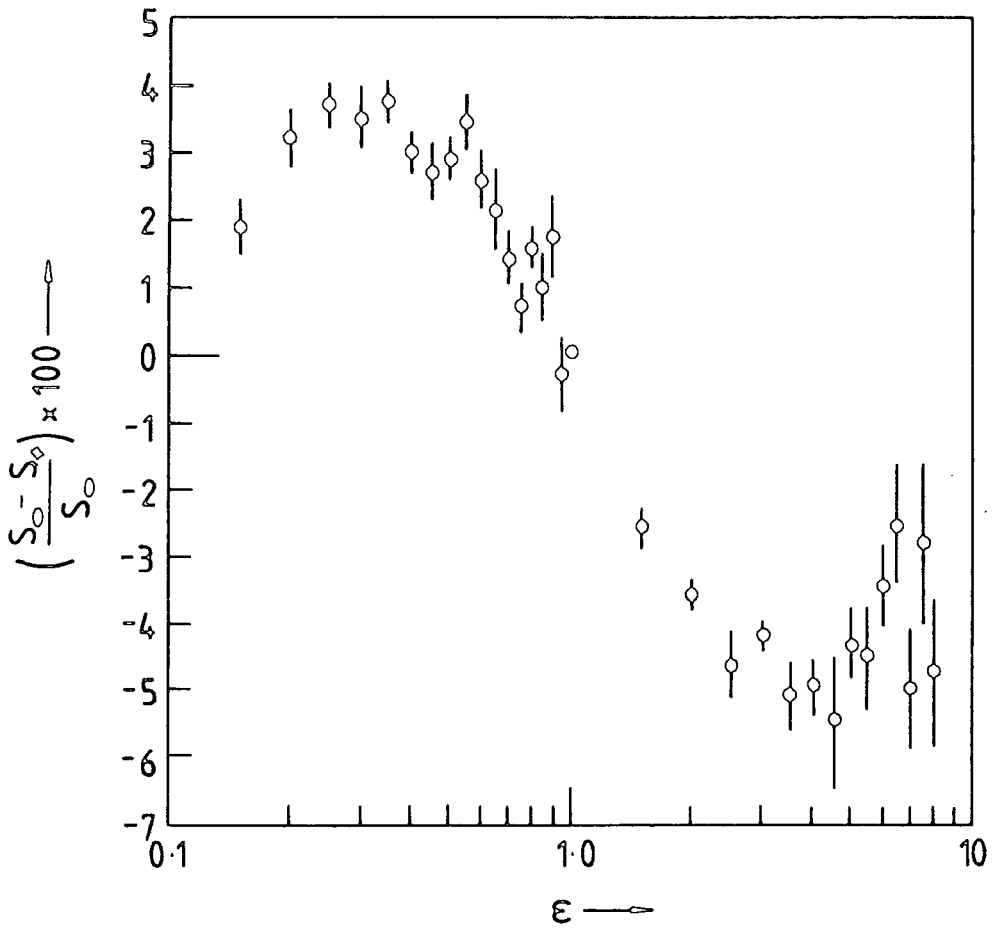

Fig 8. Difference between the magnetometric demagnetisation factors of an ellipsoid and an octahedron ($\rho = 1.$)

nearly Gaussian distribution of zero mean and unit standard deviation. When calculated from the values of table 3 the estimates of the λ population mean and standard deviation are $\bar{\lambda}=0.24\pm0.23$, $\hat{\sigma}(\lambda)=1.31\pm0.32$: over the range $\varepsilon=0.15$ to 8 there is therefore no significant evidence that the estimates of S_∞ are unreliable.

6.3 Octahedra

To calculate S_∞ and Δ for the octahedra the definition of the surface shape was changed from

$$\left(\frac{x}{a}\right)^2+\left(\frac{y}{b}\right)^2+\left(\frac{z}{c}\right)^2=\frac{1}{4} \qquad (19)$$

to

$$\left|\frac{x}{a}\right|+\left|\frac{y}{b}\right|+\left|\frac{z}{c}\right|=\frac{1}{2} \qquad (20)$$

and the procedure used for ellipsoids repeated. The estimates of S_∞ for the octahedra (table 3, figures 7 and 8) have rather larger error estimates than the ellipsoids' because the present version of the MTS operating system cannot support a single array larger than 1MBytes: this limits the maximum octahedron volume to about 20000 dipoles in an arrangement with a relatively large surface to volume ratio.

6.4 Size effects

The effect of size on the magnetometric demagnetisation factor for a sample is characterised nicely by

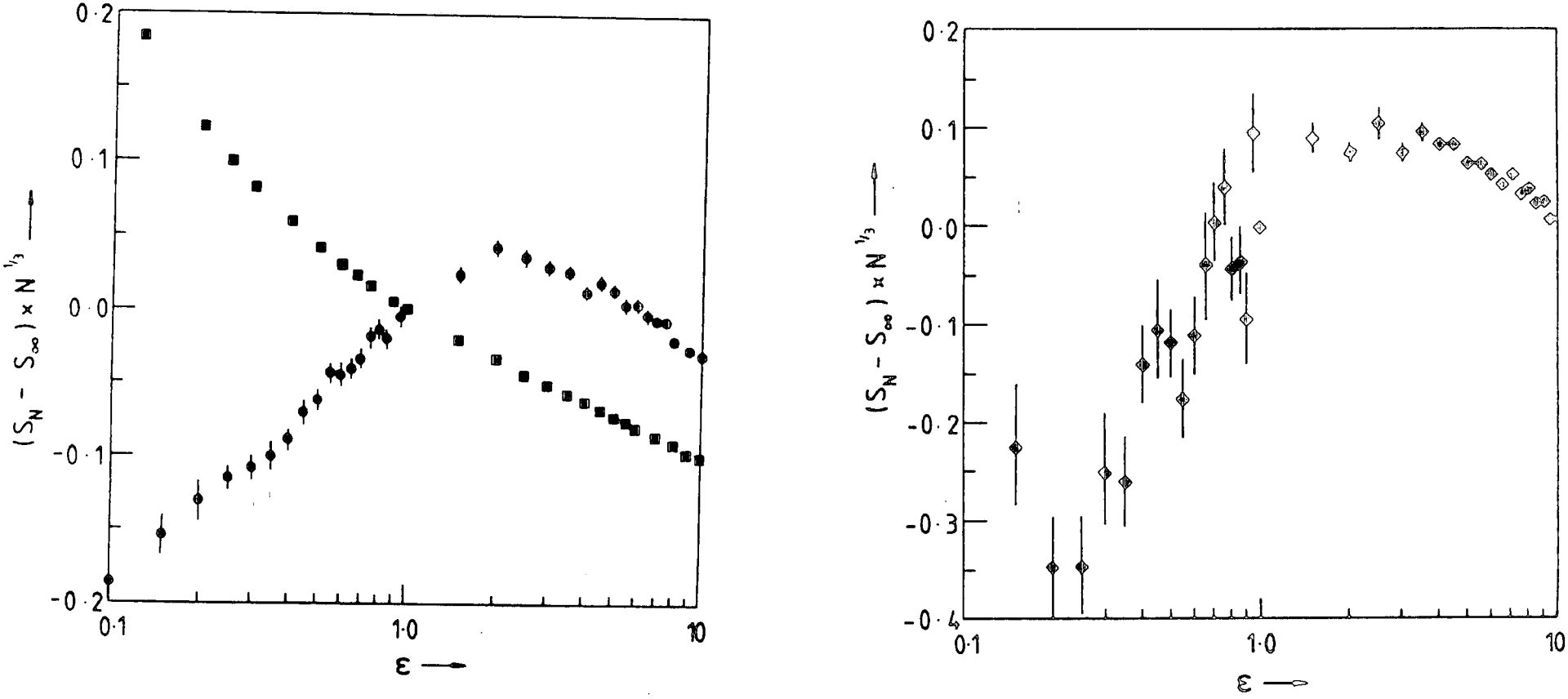

Fig 9. Size dependence of magnetometric demagnetisation factors for various elongations (ρ=1) for ■ cuboids, ● ellipsoids and ◆ octahedra.

$$(S_N - S_\infty) N^{1/3} = \Delta \qquad (21)$$

Estimates of Δ were obtained at the same time as those for S_∞ and values for cuboids, ellipsoids and octahedra are plotted for various elongations as figure 9. For these shapes with elongations ε lying between 0.5 and 10 (ρ=1) the size of particles comprising as few as 1000 dipoles affects their magnetometric demagnetisation factor by no more than one or two counts in the second decimal place.

7. Conclusions

An analogue $\tilde{S}_N$ of the magnetometric demagnetisation tensor has been defined for an assembly of N, similarly orientated, identical dipoles. $\tilde{S}_N$ has been used to extend the Brown-Morrish theorem's applicability to any arrangement of such dipoles. If the dipoles are on a lattice it is possible to evaluate $\tilde{S}_N$ rapidly and DIPOLE, a computer programme that performs the calculation, has been described. An analytic expansion in terms of $N^{-1/3}$ was used to investigate the variation of $\tilde{S}_N$ with size: for cuboids, ellipsoids and octahedra with elongations in the range 0.5 to 10 and N greater than 1000 S_N differed from S_∞ by less than 0.02. These are the first reported calculations of the magnetometric demagnetisation tensors of octahedra and it has been shown that, for the range of elongations studied (ε=0.15 to 8) the magnetometric demagnetisation tensor differed by less than six percent from its value for ellipsoids of the same elongation.

8. References

1. Brown Jr., W.F. (1963) "Micromagnetics" Wiley (Interscience), New York.

2. Kneller, E. (1969) Fine particle theory. pp.373-393 in A.E. Berkowitz and E. Kneller, eds. "Magnetism and metallurgy" Vol. 1, Academic Press, New York.

3. Schlömann, E. A sum rule concerning the inhomogeneous demagnetizing field in non-ellipsoidal samples. J. Appl. Phys. (1962) 33, 2825.

4. Moskowitz, R. and E. Della Torre. Theoretical aspects of demagnetization tensors. IEEE Trans. Magn. (1966) MAG-2, 739.

5. Brown Jr., W.F. (1962) "Magnetostatic principles in ferromagnetism" North-Holland Publ., Amsterdam.

6. Bates, L.F. (1963) "Modern magnetism" Cambridge Univ. Press, Cambridge.

7. Brown Jr., W.F. and A.H. Morrish. Effect of a cavity on a single-domain magnetic particle. Phys. Rev. (1957) 105, 1198.

8. Stoner, E.C. and E.P. Wohlfarth. A mechanism of magnetic hysterisis in heterogeneous alloys. Phil. Trans. Roy. Soc. (1948) A240, 599.

9. Lorentz, H.A. (1909) "The theory of electrons" pp. 137-9 and notes 54-5. B.G. Teubner, Leipzig.

10. Jeans, J. (1925) "The mathematical theory of electricity and magnetism" 5th edn. Arts 426-51, Cambridge Univ. Press, Cambridge.

11. Brown Jr., W.F. Single domain particles: New uses of old theorems. Amer. J. Phys. (1960) 28, 542.

12. Maxwell, J.C. (1881) "A treatise on electricity and magnetism" Vol. 2, 2nd edn., Clarendon Press, Oxford.

13. Stoner, E.C. The demagnetizing factors for ellipsoids. Phil. Mag. (1945) 36, 803.

14. Osborn, J.A. Demagnetizing factors of the general ellipsoid. Phys. Rev. (1945) 67, 351.

15. Grover, F.W. (1962) "Inductance calculations" 2nd edn. Dover Publications, New York.

16. Joseph, R.I. and E. Schlömann, Demagnetizing field in nonellipsoidal bodies. J. Appl. Phys. (1965) 36, 1579.

17. Kraus, L. The demagnetization tensor of a cylinder. Czech. J. Phys. (1973) B23, 512.

18. Joseph, R.I. Ballistic demagnetizing factor in uniformly magnetized cylinders. J. Appl. Phys. (1966) 37, 4639.

19. Okoshi, T. Demagnetizing factors of rods and tubes computed from analog measurements. J. Appl. Phys. (1965) 36, 2382.

20. Kaczér, J. and Z. Klem. The magnetostatic energy of coaxial cylinders and coils. Phys. Stat. Sol. (1976) A35, 235.

21. Wanas, M.A. and N.H. Hegazi. The demagnetizing field of elliptical cylindrical domains. J. Phys. D. (1976) 9, 1461.

22. Rhodes, P. and G. Rowlands. Demagnetizing energies of uniformly magnetised rectangular blocks. Proc. Leeds Phil. Lit. Soc. Sci. Sec. (1954) 6, 191.

23. Joseph, R.I. Ballistic demagnetizing factor in uniformly magnetised rectangular prisms. J. Appl. Phys. (1967) 38, 2405.

24. Sharma, P.V. Demagnetization effect of a rectangular prism. Geophysics (1968) 33, 132.

25. Moskowitz, R., E. Della Torre and F.M.M. Chen. Tabulation of magnetometric demagnetization factors for regular polygonal cylinders. Proc. Inst. Elect. Electronics Engrs. (1966) 54, 1211.

26. Iwata, T. A diagonal sum rule concerning demagnetisation tensors in composite bodies. J. Appl. Phys. (1968) 39, 3094.

27. Kaczér, J. and L. Murtinová. On the demagnetizing energy of periodic magnetic distributions. Phys. Stat. Sol. (1974) A23, 79.

28. Hegedus, C.J., G. Kadar and E. Della Torre. Demagnetisation matrices for cylindrical bodies. J. Inst. Maths. Applics. (1979) 24, 279.

29. Kadar, G., C.J. Hegedus and E. Della Torre. Cylindrical demagnetisation matrix. IEEE Trans. Magn. (1978) MAG-24, 276.

30. Williams, H.J., R.M. Bozorth and W. Schockley. Magnetic domain patterns on single crystals of silicon iron. Phys. Rev. (1949) 75, 155.

31. Tebble, R.S. (1969) "Magnetic domains" Halsted, New York.

32. Bozorth, R.M. and D.M. Chapin. Demagnetising factors of rods. J. Appl. Phys. (1942) 13, 320.

33. Ruehli, A.E. and D.M. Ellis. Numerical calculation of magnetic fields in the vicinity of a magnetic body. IBM J. Res. Develop. (1971) 14, 478.

34. Brug, J.A. and W.P. Wolf. Demagnetizing fields in magnetic measurements. 1. Thin discs. J. Appl. Phys. (1985) 57, 4685.

35. Wirtz, G.P. and M.E. Fine. Superparamagnetic magnesioferrite precipitates from dilute solutions of iron in MgO. J. Appl. Phys. (1967) 38, 3729.

36. de Biasi, R.S. and T.C. Devezsas. Shape anisotropy of ultra fine magnesium ferrite precpitates. J. Magn.Magn. Mater. (1983) 35, 121.

37. Van Vleck, J.H. The influence of dipole-dipole coupling on the specific heat and susceptibility of a paramagnetic salt. J. Chem. Phys. (1937) 5, 320.

38. Van Vleck, J.H. Concerning the theory of ferromagnetic resonance absorption. Phys. Rev. (1950) 78, 266.

39. Atkinson, K.E. (1978) "An introduction to numerical analysis" Wiley, New York.

40. British Standards Institution, BS6192:1982 "Specification for computer programming language Pascal" London.

41. IBM Corporation (1985) "Pascal/VS Reference Manual" Publication SH20-6168-2, New York.

42. Salisbury, R.A. ed. (1984) "The Michigan Terminal System" The University of Michigan computer Center, Ann Arbor, Michigan.

43. Hewlett-Packard Company (1982) "HP-15C owner's handbook" Publication 00015-90001, Corvallis, Oregon.

44. Abramowitz, M. and I. Stegun eds. (1972) "Handbook of Mathematical Functions" 17.3, 17.6., National Bureau of Standards, Washington D.C.

45. Hamilton, W.C. (1964) "Statistics in physical science" Chapter 5, Ronald Press, New York.

CHAPTER 6

Materials and experimental details

1. Introduction

This chapter describes the experiments and the methods used to perform them. Representative results are presented but the bulk of the data, in reduced form, are contained in the next chapter. The computer programme used to perform the reduction is mentioned and some physical data for MgO and magnesioferrite are given. The experiments were designed to provide reliable values for the magnetisation, torque and FMR spectra of the SPM precipitates of magnesioferrite. This is the first report of such a set of measurements being applied to pieces of the same Fe/MgO sample which have been subjected to identical heat treatments.

2. MgO samples

At atmospheric pressure MgO has a face-centred cubic (NaCl) structure (1). Each magnesium atom occupies a site with six nearest neighbours of oxygen at the vertices of a regular octahedron. The lattice parameter at 294K is 0.42112nm (1) corresponding to a defect free sample density of $3.585 \times 10^{3} kgm^{-3}$. Shannon (2) gives the effective radii of Mg^{2+} and O^{2-} in octahedral configuration as 0.072nm and 0.140nm respectively. Pure MgO melts at 3075K under atmospheric pressure (3). There have been several quite

successful attempts to calculate its electronic structure (4 and references therein). The reactions of iron oxides with MgO have been discussed earlier (5). In December 1985 the INSPEC database held more than 3600 references to publications concerning MgO.

The samples used for this work were cleaved from material supplied by W. & C. Spicer Ltd. of Cheltenham. They were grown using an electrical fusion method (6,7) from 4N (99.99%) purity MgO powder doped with iron oxide. The iron content of the batch (reference 76) was found to be 8500ppm iron by weight using X-ray fluorescence spectroscopy. The analysis was performed by Johnson Matthey Chemicals, Herts. and although it seems likely that there is some variation within the batch Spicer's have "not encountered evidence of any great divergence from the stated figure" (8). The 4N grading refers to cation impurities; infrared, EPR and nuclear studies (9,10) indicate that hydrogen is associated with some defect sites and carbon can be present in significant amounts ($\sim$3000ppm wt). Non-transition metal ions tend to precipitate at grain boundaries during the cooling phase of crystal growth (11-14). These precipitates make the grain structure visible; grains are typically 0.5-2mm diameter misorientated by $\sim 10^{-5}$ radians. Table 1 describes the samples used in the experiments.

Sample ref.	Mass (mg)	Dimensions (mm)	Purpose
19850206/1a	132.10(2)	8.1x7.4x0.64	VSM/Torque
19850206/1b	24.65(2)	1.7x7.4x0.56	ESR/FMR
19850606/1c	16.12(2)	---	Control

Table 1. Samples used. Cleaved along {100} planes from Spicer's (ref. 76) Fe/Mgo single crystal material. The dimensions are approximate.

Treatment number	Treatment time at 973K		Total effective time at 973K
	Actual	Effective	
1	15	17.3(1)	17.3(1)
2	15	17.3(1)	34.6(2)
3	45	50.4(2)	85.0(3)
4	110	117.0(2)	202.0(3)

Table 2. Heat treatment schedule, all times in minutes. Treatments were in oxygen at atmospheric pressure.

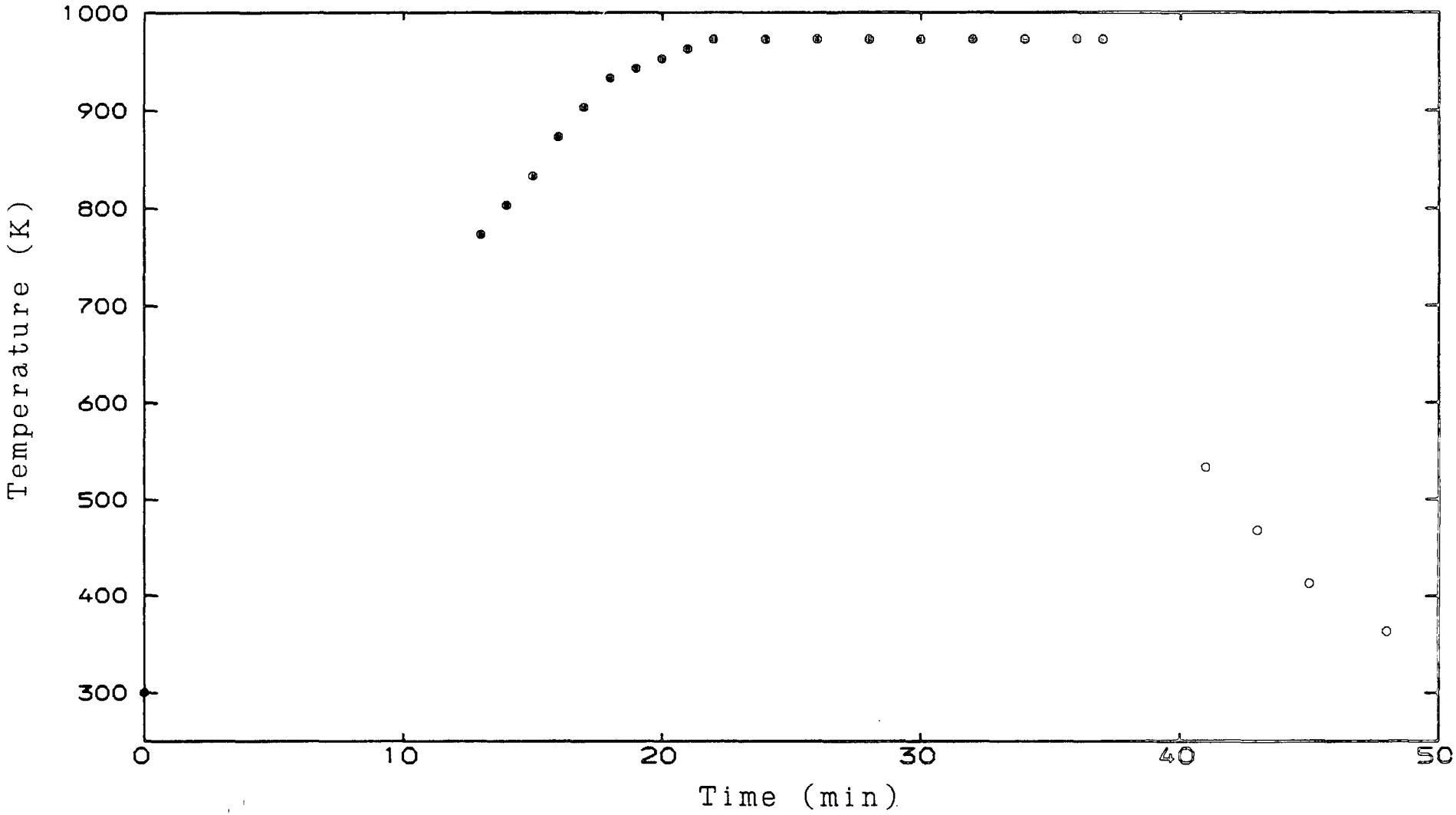

Fig 1. Furnace temperature during treatment 1. The controller was switched on at Time=0.

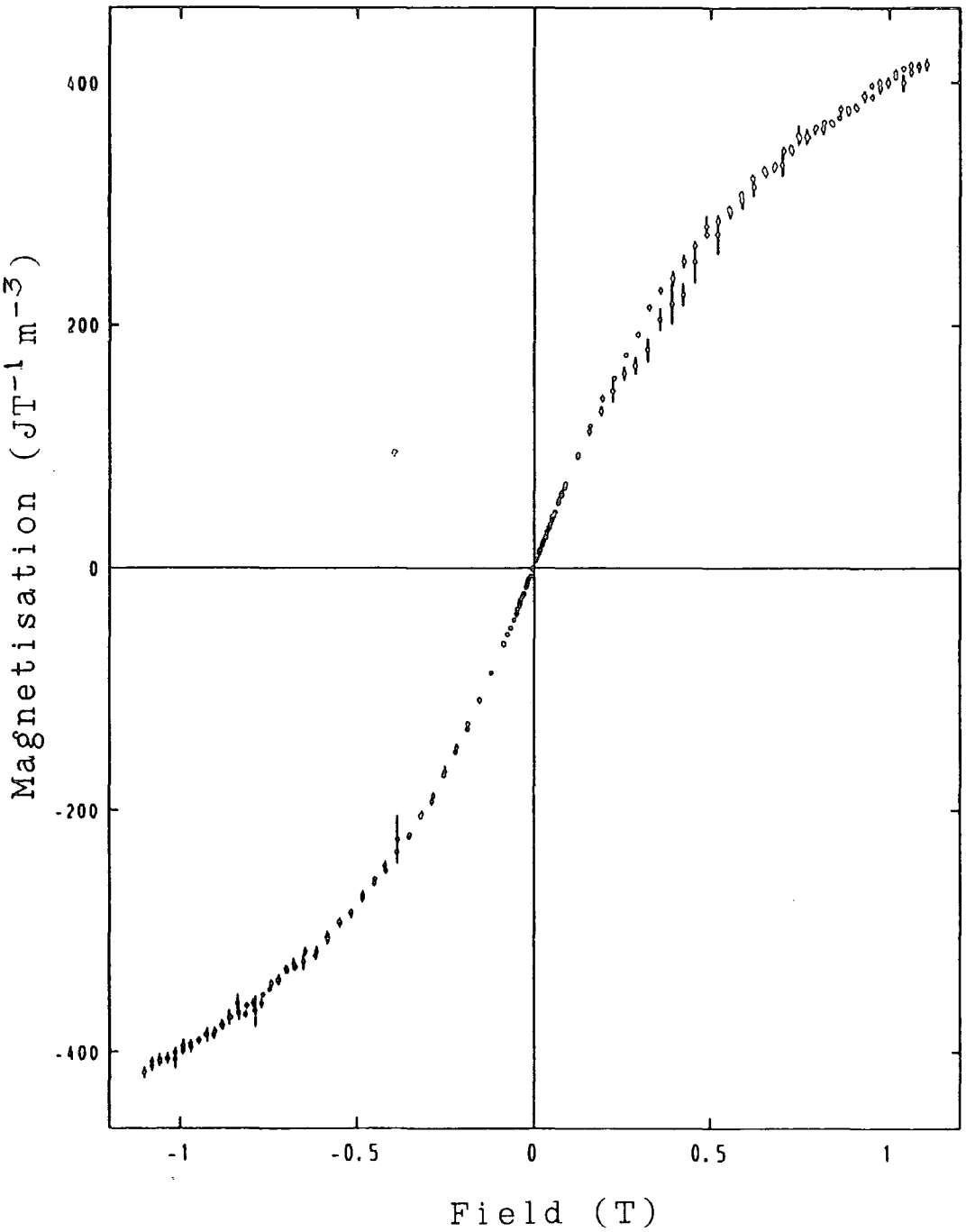

Fig 2. Example of magnetisation curve. Sample 19850206/1a B//[100] T=297K after second heat treatment (34.6min@973K).

3. Heat treatment

Measurements were made on the samples as received and after each of four periods of heat treatment. This was performed in a furnace attached to a Eurotherm controller, a slow flow of oxygen (about $2Lh^{-1}$) provided the oxidising atmosphere. Before each treatment the samples and the alumina boat which held them were carefully cleaned. The temperature was monitored with a thermocouple positioned just above the samples. Figure 1 is the measured temperature schedule of the first treatment. The heating and cooling times are significant compared with the total time spent at the nominal 973K ageing temperature. The rate of growth of the precipitates is expected to be governed by an activation energy of about $(5.1\pm0.2)\times10^{-19}$J(15). On this basis an effective ageing time for each treatment has been calculated; this is how long an ideal furnace, heating and cooling instantaneously, would keep the samples at 973K to achieve the same growth as the practical arrangement. Timings for the four heat treatments are in table 2. The solenoid winding of the furnace subjects its contents to a longitudinal magnetic field amplitude of $\sim$5mT which could cause preferential growth of the precipitate along the field axis.

4. Magnetisation measurements

The magnetisation in fields up to 1.2T of the 19850206/1a sample was measured using a vibrating sample

magnetometer (VSM) (16,17). The VSM was operated by D.B. Lambrick. The magnetising field was measured with a Bell 640 incremental gaussmeter which had been calibrated against a proton magnetometer. Measurements were made with the magnetising field applied along the MgO [100] and [110] directions. A 4N purity nickel single crystal (18,19) was used to calibrate the system before and after each magnetising cycle. Drift in the sensitivity reflecting the change in instrument temperature during the course of a cycle is the main source of error in the results. Stability was ameliorated by allowing a reasonable warm-up time. After the last heat treatment measurements were made at a range of temperatures between 15 and 300K. An Oxford Instruments KF1200 gas flow cryostat and DTC-2 controller provided the variable temperature environment. The AuFe-chromel thermocouple used for measurement and control was calibrated in situ with a secondary standard RhFe resistance thermometer (20). Figure 2 is a typical set of magnetisation measurements, each point is the mean of several readings which are also used to estimate its standard error.

5. Torque measurements

The torque, in fields up to 0.7T, acting on the 19850206/1a sample was measured at room temperature using a torque magnetometer (21). The magnetising field was applied in the (001) plane (normal to the sample's short dimension).

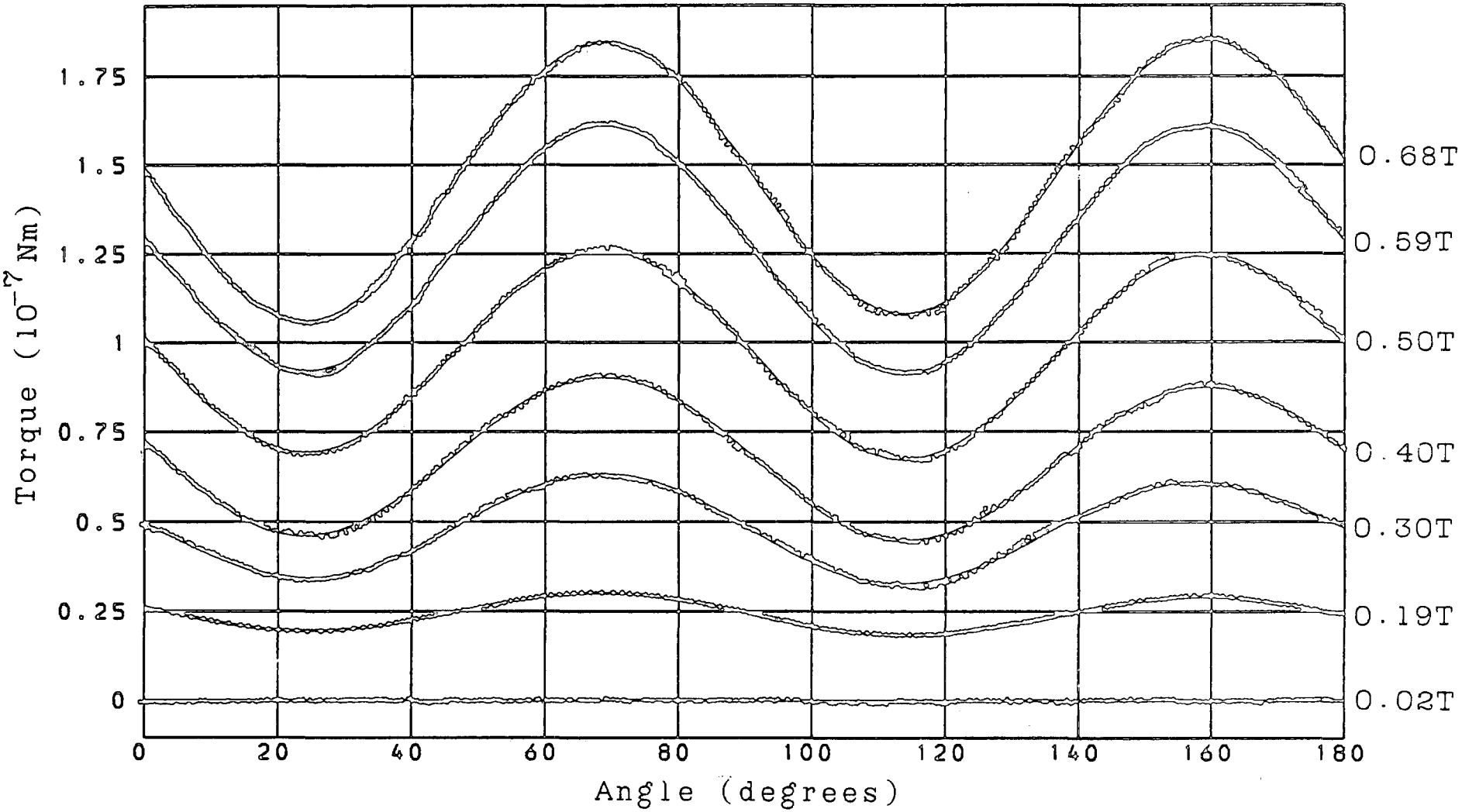

Fig 3. Torque curves after treatment for 202mins at 973K using a range of measuring fields between 0 and 0.68T (sample 19850206/1a).

Figure 3 shows a typical set of curves. In view of the extremely small torques being measured the usual mechanical calibration (2) was considered unsatisfactory. A small coil was used to replace the sample and its equivalent area was determined from measurements of the field and rotation rate of the magnet. A small constant current was then passed through the coil and the torque acting on it measured. Potential sources of error (ferromagnetic impurities in the copper coil, induced potential differences across the connecting wires and stiffness of the connecting wires) were either eliminated or corrected for. A small, linear field dependence of the sensitivity was identified. The standard error of the final calibration constant was estimated as 1.2%. The torque curves obtained were digitised ready for analysis.

6. Magnetic resonance measurements

ESR and FMR spectra were obtained using a Varian Associates V4502 spectrometer. The magnetic field was generated by a Varian 12" electromagnet and a VFR5203 power supply. The operating frequency was about 9.25GHz. Calibration involved a standard sample (DPPH dissolved in benzene) and a proton magnetometer. The usual precautions were taken to ensure that spectra were free from instrumental distortion (23). Sample 19850206/1b was mounted on a quartz glass rod with a very small quantity of Apiezon M vacuum grease. A Goniometer held the support rod

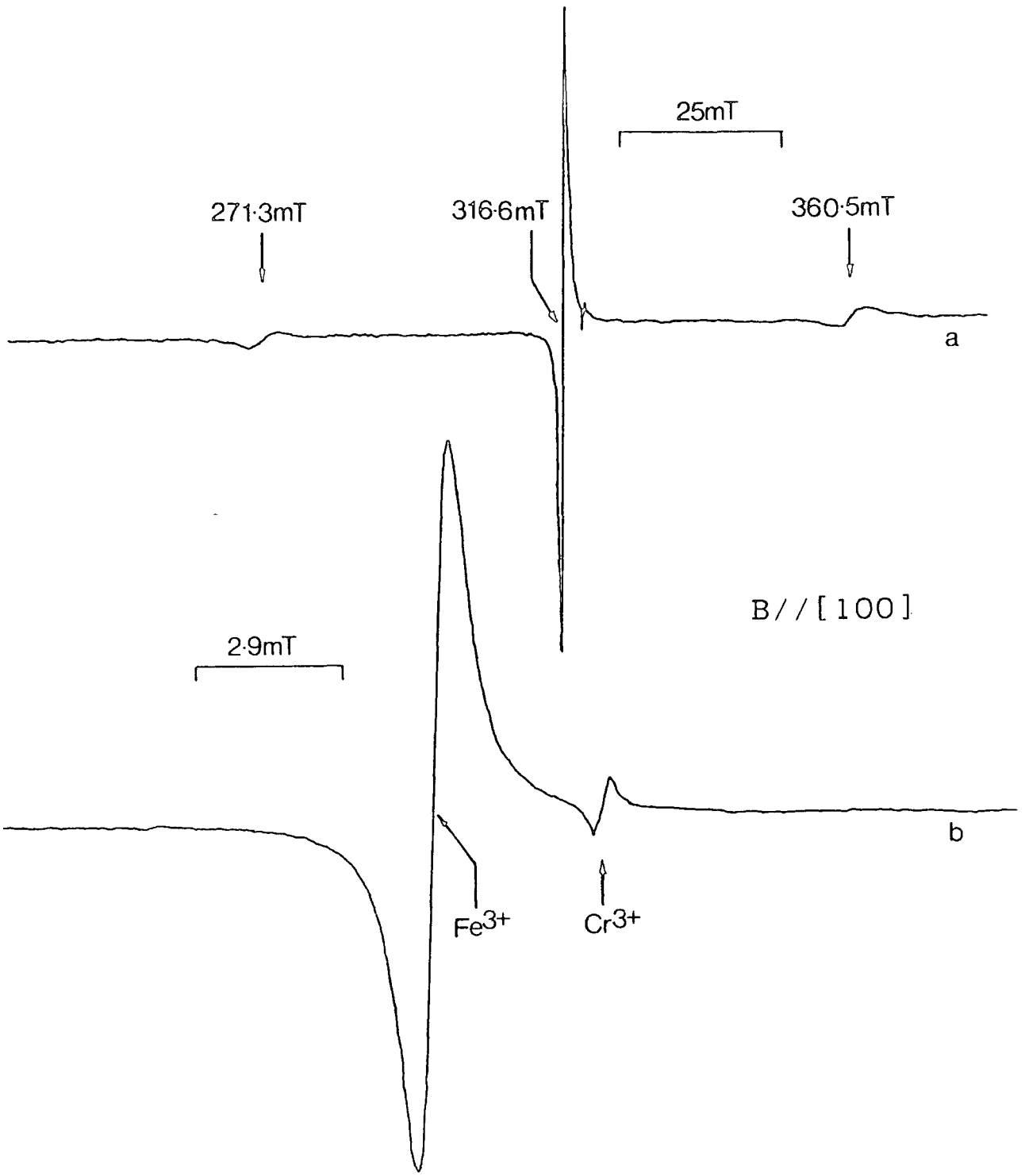

Fig 4. (a) Typical 9.256GHz ESR spectrum of as received sample (19850206/1b) at 293K. (b) Same expanded to show detail.

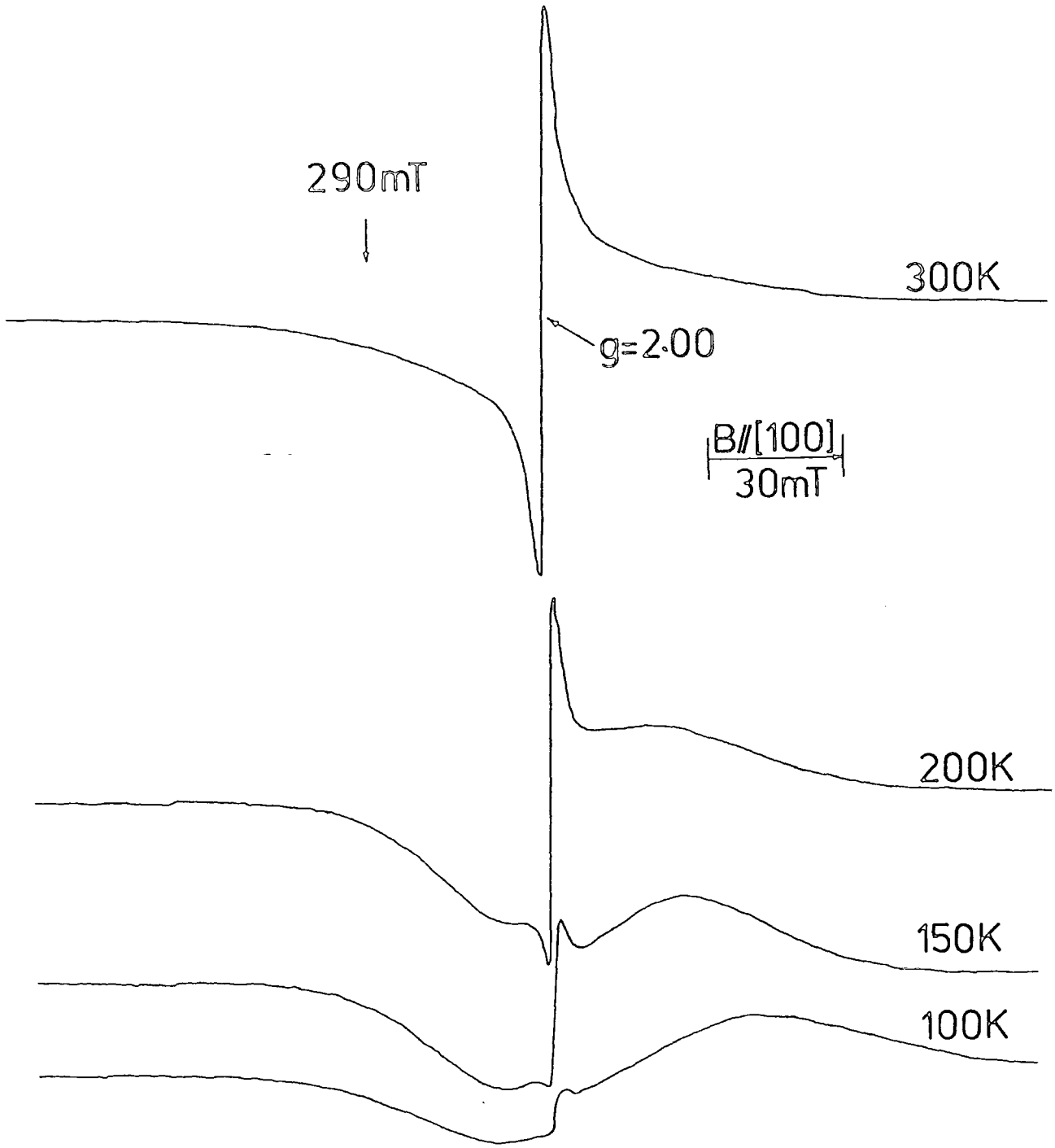

Fig 5a. 9.256GHz FMR (derivative absorption) of sample 19850206/1b after 202 minutes heat treatment. B//[100].

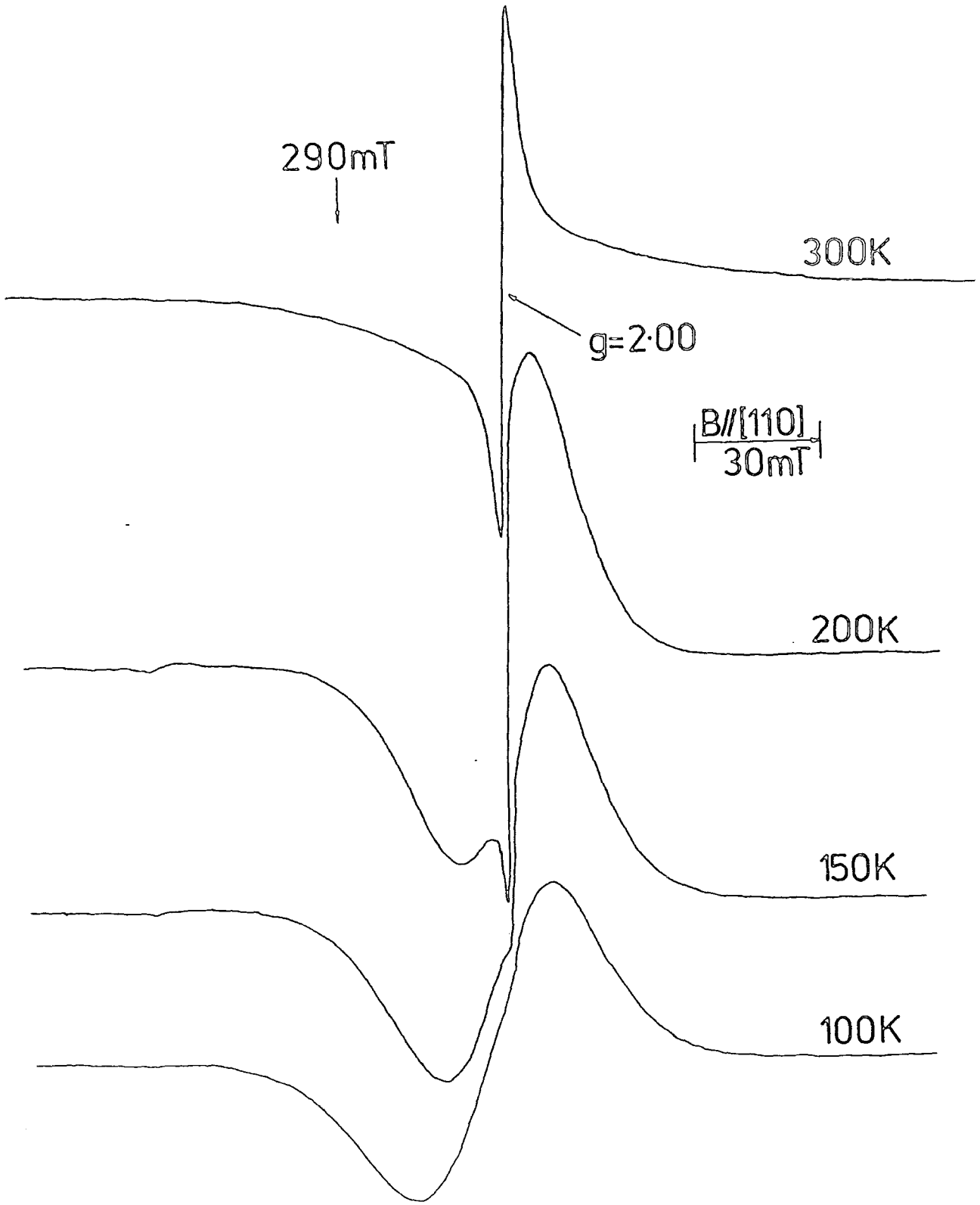

Fig 5b. As 5a but B//[110].

and allowed 2π rotation about an axis perpendicular to the static magnetic field. The sample was mounted with a [100] direction parallel to the rotation axis. A variable temperature environment was provided by an Oxford Instruments ESR9 gas flow cryostat (24). Figures 4 and 5 are examples of the spectra obtained.

7. Data analysis

A general purpose computer programme called FIT was written to perform the data analysis and plotting involved in this work. Most of the graphs in this thesis were drawn by it. Experimental data and processing instructions are stored in files, FIT uses these as input for a non-linear, weighted least-squares analysis (25). Estimates of parameters, their standard errors and the moments of the residual distribution are calculated. Statistics for non-parametric assessment of fit quality (26 for example) based on residuals' signs are also provided.

8. References

1. Wycoff, R.W.G. (1965) "Crystal structures" Vol. 1, Wiley (Interscience), New York.

2. Shannon, R.D. Revised effective ionic radii and systematic studies of interatomic distances in halides and chalcogenides. Acta Cryst. (1976) A32, 751.

3. Phillips, B., S. Somiya and A. Muan. Melting relations of magnesium oxide-iron oxide mixtures in air. J. Amer. Ceram. Soc. (1961) 44, 167.

4. Taurian, O.E., M. Springborg and N.E. Christensen. Self-consistent electronic structures of MgO and SrO. Sol. Stat. Commun. (1985) 55, 351.

5. This work, chapter 3 section 6.

6. Abraham, M.M., C.T. Butler and Y. Chen. Growth of high purity and doped alkaline earth oxides I: MgO and CaO. J. Chem. Phys. (1971) 55, 3752.

7. Quinn, N. Who will grow oxide crystals next? Brit. Assoc. Cryst. Growth Newsletter (1986) January, 10.

8. Quinn, N. Priv. Commun. (1986).

9. Henderson, B. and J.E. Wertz (1977) "Defects in the alkaline earth oxides" Taylor and Francis, London.

10. Freund, F., G. Debras and G. Demortier. Carbon content of magnesium oxide single crystals grown by the arc fusion method. J. Cryst. Growth (1977) 38, 277.

11. Bowen, D.H. Observation of impurity precipitates in magnesium oxide. Trans. Brit. Ceram. Soc. (1963) 62, 771.

12. Bowen, D.H. and F.J.P. Clarke. Impurity precipitates in magnesium oxide. Phil. Mag. (1963) 8, 1257.

13. Bowen, D.H. and F.J.P. Clarke. The growth of neutron irradiated magnesium oxide. Phil. Mag. (1964) 9, 413.

14. Venables, J.D. Identification of precipitates on grown-in dislocations in MgO. J. Appl. Phys. (1963) 34, 293.

15. Sonder, E., T.G. Stratton and R.A. Weeks. Kinetics of Fe^{2+} oxidation and Fe^{3+} reduction in MgO single crystals. J. Chem. Phys. (1979) 70, 4603. (Estimate derived from data in table 1).

16. Willcock, S.N.M. Ph.D. Thesis (1986), University of Durham, U.K.

17. Hoon, S.R. and S.N.M. Willcock. Vibrating sample magnetometry: The design and operation of an automated double crank VSM. Internal report, Dept. of Physics, University of Durham, U.K. (1986). Submitted to J. Phys. E.

18. Pauthenet, R. Spin-waves in nickel, iron, and yttrium-iron garnet. J. Appl. Phys, (1982) 53, 2029.

19. Pauthenet, R. Experimental verification of spin-wave theory in high fields. J. Appl. Phys. (1982) 53, 8187.

20. Lambrick, D.B. Priv. Commun. (1986).

21. Paige, D.M. The use of torque magnetometry in determining particle anisotropy and orientation distributions in magnetic tape materials. Internal report, Dept. of Physics, University of Durham, U.K. (1986).

22. Paige, D.M. Ph.D. Thesis (1983), University of Durham, U.K.

23. This work, chapter 2, section 4.1.

24. Campbell, S.J., I.R. Herbert, C.B. Warwick and J.M. Woodgate. A continuous flow cooling unit for ESR experiments over the temperature range 3.7-300K. J. Phys. E. (1976) 9, 443.

25. Adby, P.R. and M.A.H. Dempster (1974) "Introduction to optimization methods" Chapman and Hall, London.

26. Kreyzig, E. (1979) "Advanced engineering mathematics" John Wiley, New York.

CHAPTER 7

Results and conclusions

1. Introduction

The results of the experiments described in the previous chapter, some 200 resonance spectra and more than 1Mbyte of torque and magnetisation data, are compared with a theoretical model of the precipitate's magnetic behaviour in this chapter. The magnetisation and torque measurements are used to characterise the growth of the magnesioferrite fine particle system. The conclusions drawn from the static measurements are used to confront several theoretical interpretations of magnetic resonance spectra with the experimental results. References between solidi are to earlier parts of this thesis. The final section is a summary of the work and its main conclusions.

2. As received samples

The material as received (sample 19850206/1a) had a susceptibility of $(1.01\pm0.06)\times10^{-4}$ at 292K. The magnetisation was proportional to the applied field with no observable hysteresis (some data are shown in figure 4). The diamagnetic susceptibility of the MgO host ($\sim10^{-6}$) and demagnetisation correction are negligible so the magnetic behaviour indicates that the upper limit of the average

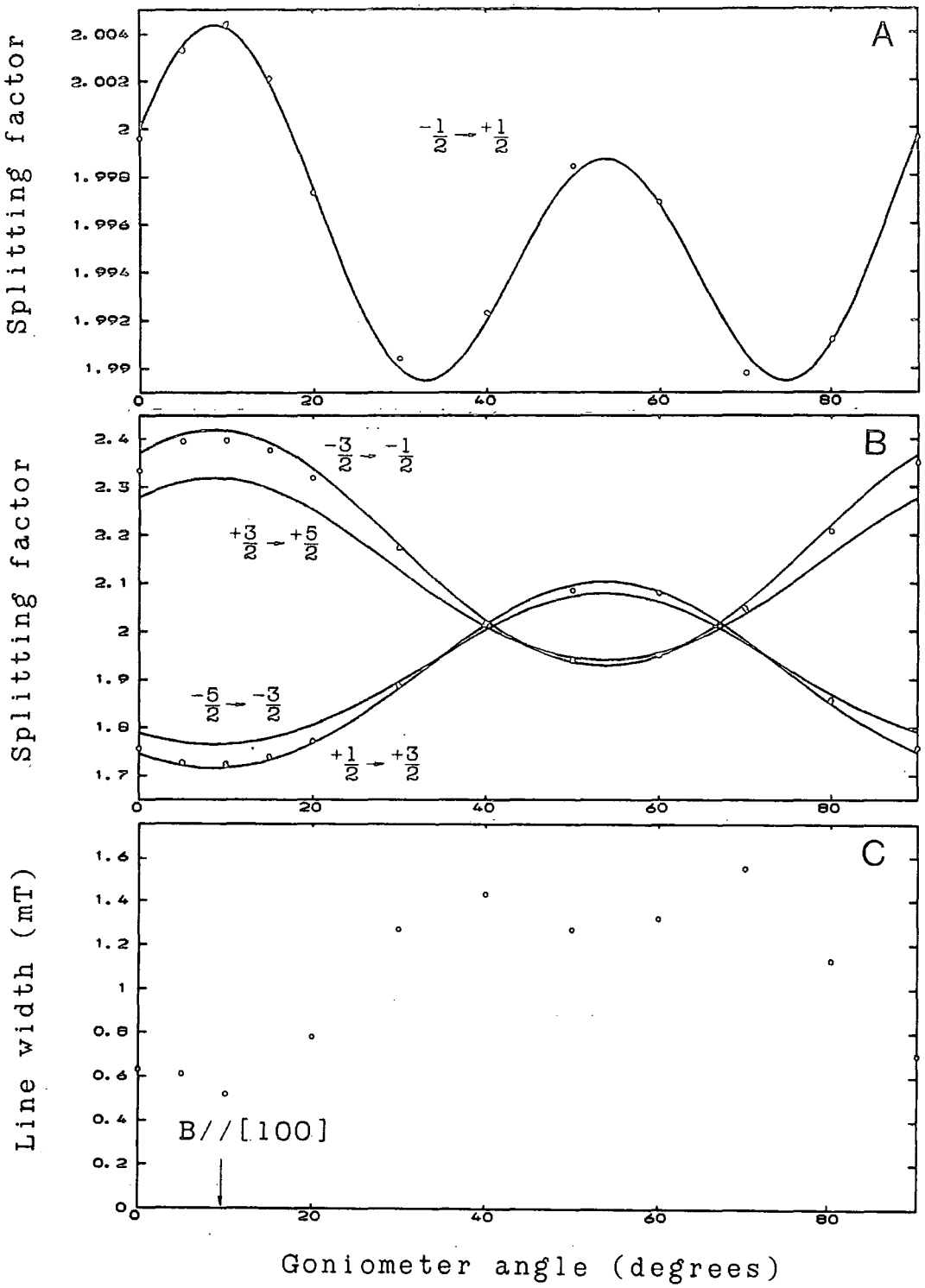

Fig 1. Angular dependence of 9.256GHz ESR spectra of unheated sample (19850206/1b). Curves indicate the fit to a cubic spin Hamiltonian (see text).

moment of the microscopic dipoles responsible is $\sim 500\mu_B$ /ch4,fig2/. If the 8500ppm wt. iron was entirely present as Fe^{3+} (S=5/2) in isolated octahedral sites (g=2.00) the expected susceptibility at 292K would be 1.03×10^{-4} /ch2,sec 3/. Any torque exerted by a 0.7T field was undetectable ($\lesssim 10^{-9}$Nm) using the available instrument.

The ESR spectra of sample 19850206/1b are dominated by the signal from Fe^{3+} in octahedral sites /ch6,fig4/. The spin Hamiltonian parameters /ch2,sec3/ $g=2.0044 \pm 0.0002$, $a=(2.10 \pm 0.03) \times 10^{-2} cm^{-1}$ obtained by fitting the $-\frac{1}{2} \rightarrow +\frac{1}{2}$ transition data (figure 1a) also fit the anisotropic fine structure lines (figure 1b) although these are too broad ($\Delta B_{pp} \sim 3mT$) to be fully resolved. These estimates for g and a are in agreement with the values found by other workers (1-4). The isotropic line at $g=1.9800 \pm 0.0002$ /ch6,fig4/ is due to Cr^{3+} in cubic sites (2,4). Other lines were detected, but were very weak; these are caused by Mn^{2+}, $\Delta m_s > 2$ transitions of Fe^{3+} (3,5) and possibly iron in non-cubic sites and pairs (4). Fe^{2+} present in cubic sites would have an isotropic g=3.4277 line at low temperatures (4,6). The spectra taken at 25K had no such feature more intense than 10% of the Fe^{3+} $-\frac{1}{2} \rightarrow +\frac{1}{2}$ transition.

Room temperature line width data for the Fe^{3+} $-\frac{1}{2} \rightarrow +\frac{1}{2}$ transition is also given in figure 1. Several groups have investigated the line widths and intensities and various theoretical descriptions of their results have been proposed (2,6-16). Figure 1c resembles other published results which

are rather sample dependent. The line widths found are far too narrow (16) to be explained by assuming that most of the Fe^{3+} participates in a Kittel-Abrahams mechanism /ch2,sec4.6/ and several other possibilities have been suggested: long-range (indirect) 'exchange narrowing' (13,14), dipolar interactions with Fe^{2+} (9), and clustering of the iron ions (12). The first two suggestions can probably be discounted (15,16) whilst hardness measurements (17) and the rapid nucleation of magnesioferrite precipitates support the clustering description. It is not possible however, to draw any conclusions about the microscopic nature of the cluster distribution from line width data - however by including 'clustering parameters' /ch2,sec4.6/ in the Kittel-Abrahams model a reasonable phenomenology of the observed line widths is possible (12,16). The line widths of figure 1c are almost independent of temperature being $\sim$0.2mT narrower than their room temperature values below 100K. Greater broadening of the anisotropic fine structure lines was also observed, this is to be expected because the crystals are unlikely to be strain-free /ch2,sec4.4/.

3. Heat treated samples

Heat treatment /ch6,sec3/ changed the samples' colour from a yellowish green to a light brown. Their magnetic properties also changed: the samples became anisotropic, the magnetisation curves became non-linear and the Fe^{3+} ESR

spectrum was swamped by a broad FMR line. The torque and magnetisation data gathered at each stage was used to confront models comprising combinations of fine particle effects /ch4/ together with varous particle size (or more accurately particle moment) distributions. The most successful description of the system is consistent with the ideas developed earlier /ch3/. A proportion of the iron remains in solid solution creating a paramagnetic 'sea' in which the rest of the iron, as magnesioferrite, forms a precipitate which evolves by diffusion limited Oswald ripening and has a LSW particle size distribution /ch3,sec4.2/.

3.1 Magnetisation response

The magnetisation M of the heat treated samples in a magnetic field B (when the effects of anisotropy, chemical inhomogeneity and dipolar interactions between particles /ch4,sec6/ are neglected) is

$$M = \frac{1}{\mu_0}\chi_s B + \int_0^\infty n M_s V L\left(\frac{M_s V B}{kT}\right) p(V)\,dV \qquad (1a)$$

$$L(x) = \coth(x) - 1/x \qquad (1b)$$

χ_s is the susceptibility of the paramagnetic sea of dissolved Fe^{3+}, there are n precipitate particles per unit

Rate limiting process	FIT	f	n
Surface reaction	PSD=1	1.7014	1.5
Bulk diffusion	PSD=2	1.2607	1.0
Grain boundary diffusion	PSD=3	1.1364	.75
Single volume model	PSD=0	1.0000	-

Table 1. Values of f and n for the LSW particle size distributions. $V \propto t^n$

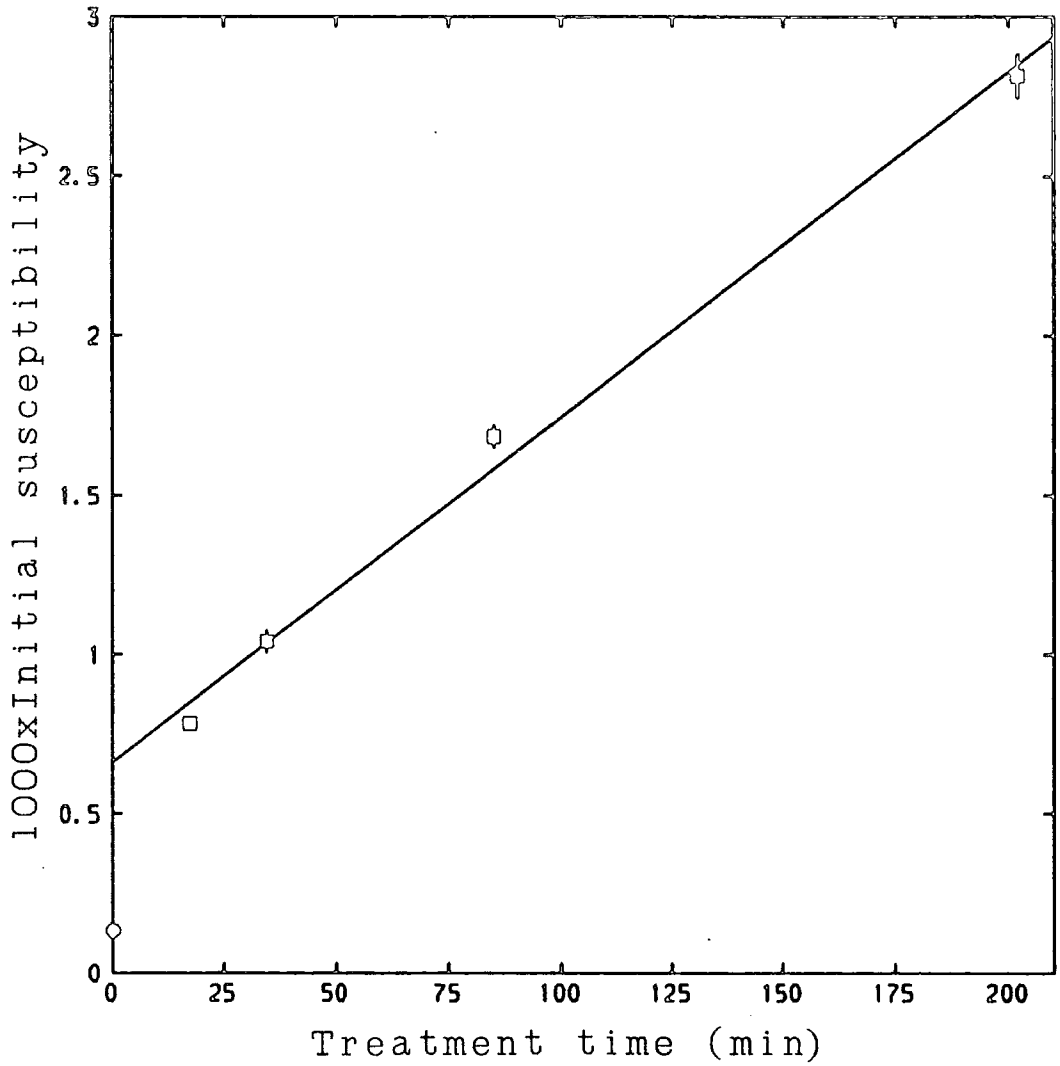

Fig 2. Initial susceptibility for various effective treatment times at 973K for sample 19850206/1a. The linear regression line excludes the as received state.

volume having a spontaneous magnetisation M_s at temperature T. V refers to the particle volumes and p(V) is the associated probability distribution. L(x) is the Langevin function. The heat treated samples possess only first order cubic anisotropy /ch7,sec3.2/ which does not affect their initial susceptibility χ_o /ch4,sec6.2/ so

$$\chi_o(T) = \mu_o \left.\frac{\partial M}{\partial B}\right|_{B=0} = \frac{C_s}{T} + \frac{\mu_o M_{sat} M_s \bar{V} f}{3kT} \qquad (2)$$

where

$$f = \frac{\overline{V^2}}{\bar{V}^2} = \frac{\int_o^\infty V^2 p(V) dV}{\left[\int_o^\infty V p(V) dV\right]^2} \quad \text{and} \quad M_{sat} = n M_s \bar{V};\ C_s = \chi_s T \qquad (3)$$

If the magnesioferrite precipitate grows by a LSW mechanism /ch3,sec4.2/ then at room temperature M_{sat} and f are constants so any change in χ_o is proportional to the change in $\bar{V}$ the mean particle volume. Values for f have been calculated numerically and are given in table 1. Figure 2 shows the room temperature susceptibility of the 19850206/1a sample, as a function of heat treatment time, estimated from the low field points of the magnetisation measurements. These are consistent with the $\bar{V} \alpha t$ (t is the treatment time) behaviour of bulk diffusion limited growth but not the $\bar{V} \alpha t^{3/2}$ of a surface reaction rate limited process. It is unlikely that the growth rate was determined by grain boundary or dislocation diffusion (in the Fe^{3+}/MgO system the precipitate is distributed exclusively within and evenly throughout the crystal grains /ch3,sec6.2/) but the possibility is not excluded by these initial susceptibility

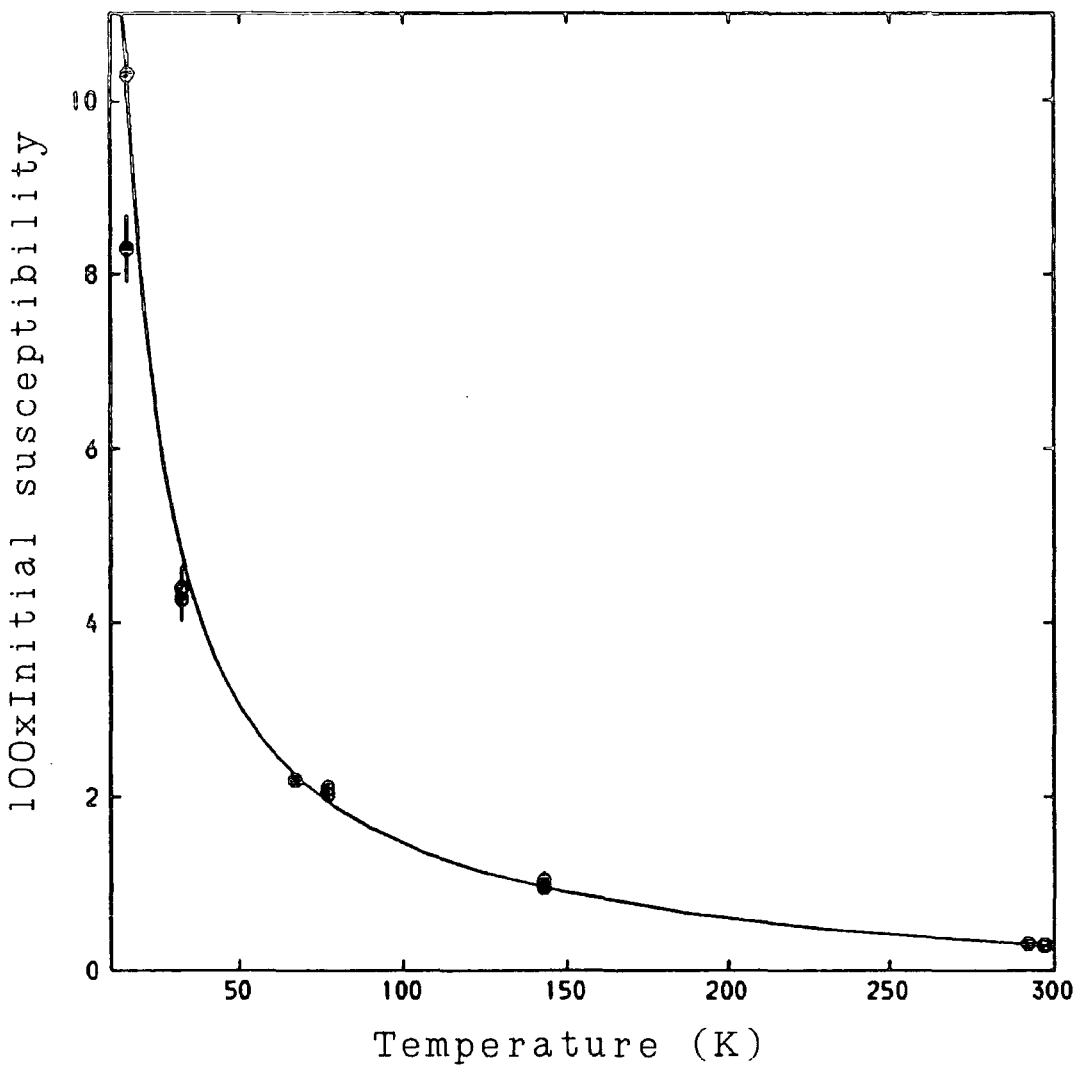

Fig 3 Initial susceptibility of sample (19850206/1a) after 202mins at 973K as function of temperature. The theoretical behaviour (solid line) is discussed in the text.

measurements.

When measurements are made at several different temperatures the temperature dependence of M_s /ch3,eqn9/ must be included explicitly

$$\chi_o(T) = \frac{C_s}{T} + \frac{n M_o^2 \overline{V^2} \mu_o \left(1 - (T/T_c)^2\right)^2}{3kT} \qquad (4)$$

where M_o is the spontaneous magnetisation of the magnesioferrite at absolute zero and T_c is its Curie temperature. $\chi_o(T)$ was estimated from measurements made between 15K and 300K after 202 minutes heat treatment (figure 3). At this stage the paramagnetic background contributes negligibly ($\sim$3%) to χ_o, the curve fitted to the measurements is equation 4 with $C_s=0$ and gives $T_c=589\pm10$K, $nM_o^2\overline{V}^2=(5.09\pm0.04)\times10^{-17}J^2T^{-2}m^{-3}$. If it is assumed that the precipitate is saturated with MgO (1.06 Mg^+ ions per molecule) /ch3,sec6.3/ the degree of inversion δ = (0.81$\pm$0.02) can be estimated from T_c /ch3,eqn8/. For MgO saturated magnesioferrite at equilibrium at 973K the expected value /ch3,eqn11/ is δ =0.78. The spontaneous magnetisation can also be deduced from T_c /ch3,eqn7/ and is $M_o=(2.1\pm0.2)\times10^5JT^{-1}m^{-3}$.

Critical examination of the magnetisation measurements reveals that the VSM's sensitivity is subject to slight fluctuations. These probably have two causes: one due to heat dissipated by the air-cooled magnet warming the pneumatic vibration isolator (18), the other due to the imperfectly stable temperature within the cryostat,

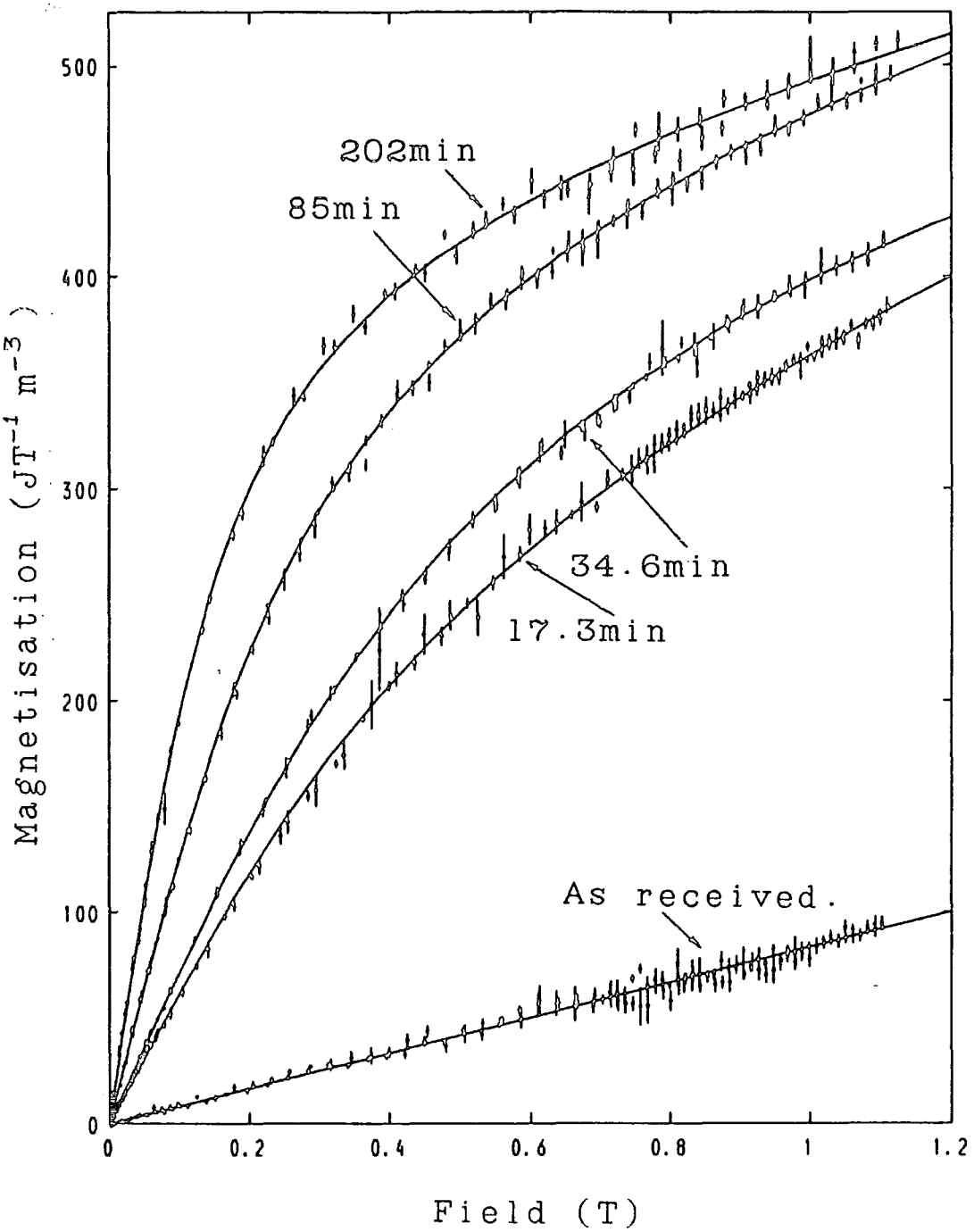

Fig 4. Room temperature magnetisation of sample 19850206/1a after various treatment times. Solid lines are equation 1 fitted to the data assuming the diffusion limited LSW distribution (PSD=2).

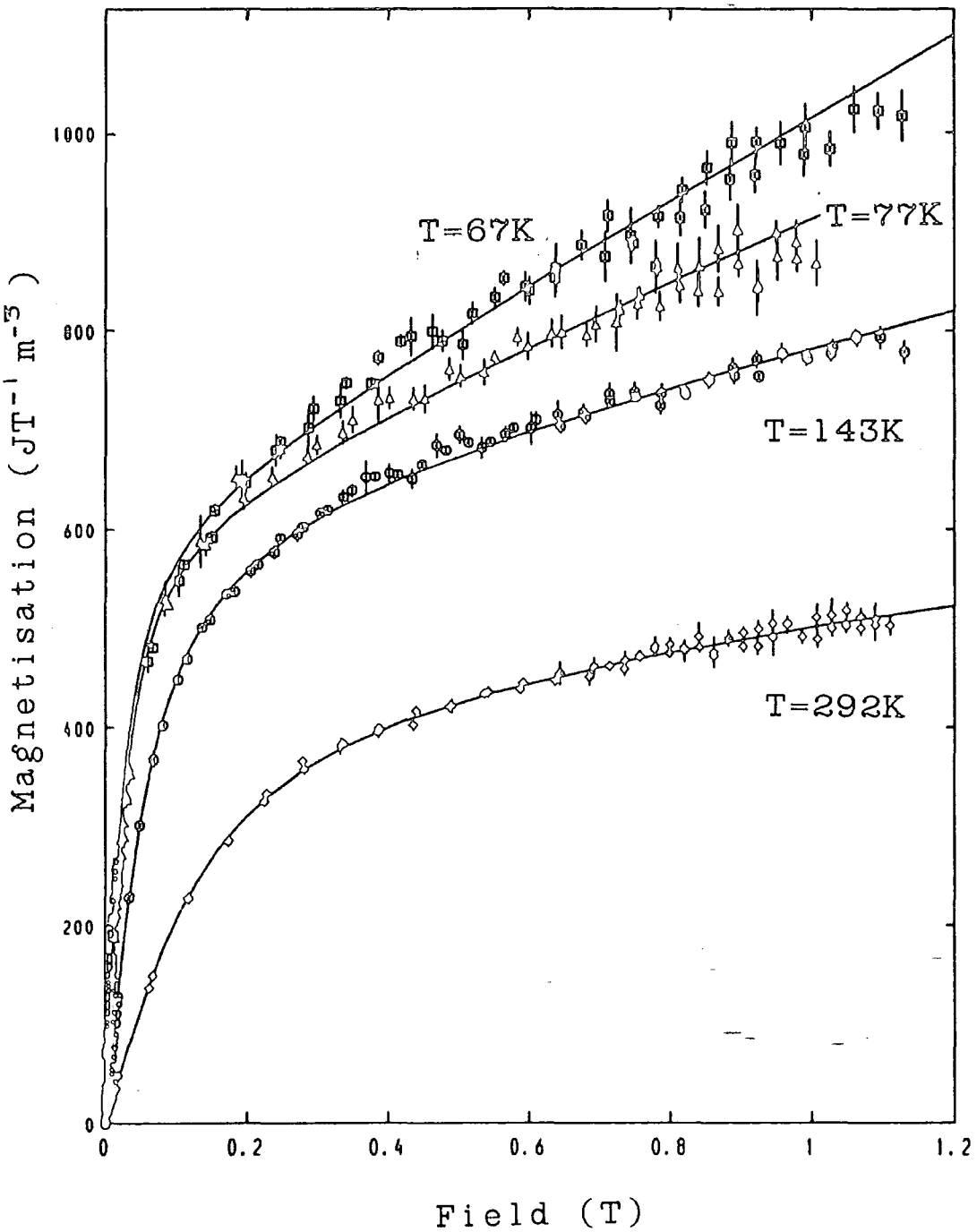

Fig 5a. Magnetisation of sample 19850206/1a after 202mins at 973K in oxygen. Solid lines are equation 1 fitted to the data assuming the diffusion limited LSW distribution (PSD=2).

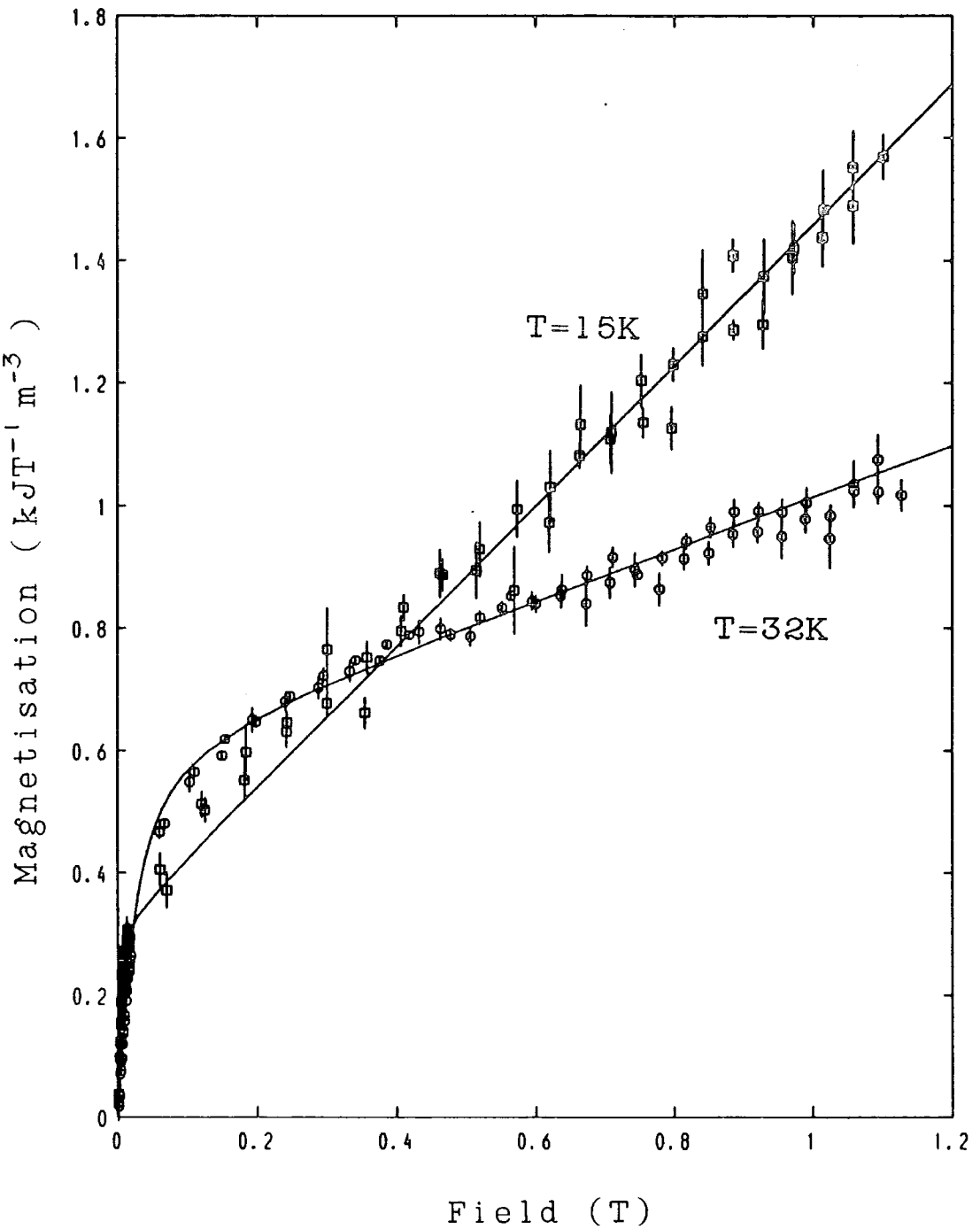
Magnetisation (kJT^{-1} m^{-3})
Field (T)
T=15K
T=32K
0
0.2
0.4
0.6
0.8
1
1.2
1.4
1.6
1.8

Fig 5b. As 5a.

especially at the lower temperatures. Consequentially the errors of successive measurements are correlated and the variances of parameters fitted to a single magnetisation curve are systematically underestimated. The problem has been ameliorated by treating positive and negative field data separately and combining estimates from all the datasets taken at a particular temperature. The model (represented by equation 1) was used to analyse the experimental magnetisation curves /ch6,sec7/. Given here are results for both a single particle volume model ("PSD=0") and the LSW diffusion limited particle size distribution ("PSD=2") /ch4,secs4.2,5/, the former results being enclosed in square brackets in the text. Figures 4 and 5 are representative examples of the 28 sets of magnetisation data examined, the fitted curves are for PSD=2. There was no significant difference between measurements made along [100] and [110] directions. The omission of dipolar interactions between particles and with the paramagnetic sea from the model (the demagnetisation terms in a mean field approximation) most seriously affects the initial susceptibility region. In the worst case, 15K measurements, this causes a 5% error in the determination of χ_o - less than the uncertainty associated with the thermometry and the cryostat's eddy-current screening at this temperature. Figure 6 shows the dependence of χ_s on temperature for the sample after the final heat treatment. A Curie Law is expected and agreement is excellent if the

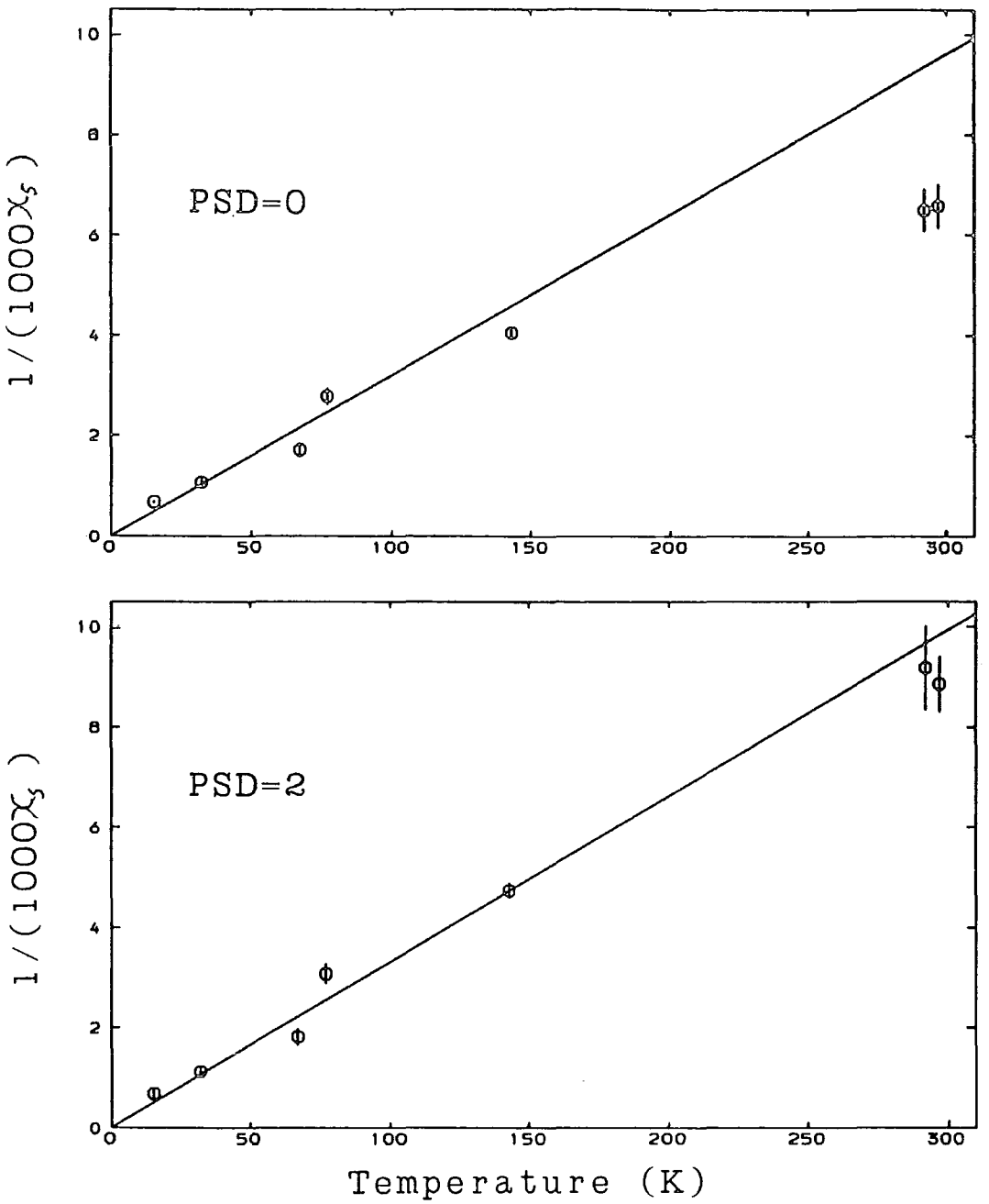

Fig 6. Background susceptibility (χ_s) of the 'paramagnetic sea' assuming a single particle size (PSD=0) and the LSW bulk diffusion limited distribution (PSD=2).

Ageing time at 973K		0	17.3	34.6	85	202	min
χ_c		10	79(8)	92(8)	168(8)	285(8)	$\times 10^{-5}$
Msat	PSD=0		249(8)	362(6)	392(4)	395(7)	$JT^{-1}m^{-3}$
χ_s			194(4)	134(6)	161(3)	152(7)	$\times 10^{-6}$
$Ms\bar{V}/kT$			5.7(6)	5.2(5)	9.3(4)	16.3(5)	T^{-1}
Msat	PSD=2		300(11)	461(11)	455(6)	434(7)	$JT^{-1}m^{-3}$
χ_s			164(4)	73(6)	112(5)	113(5)	$\times 10^{-6}$
$MS\bar{V}/kT$			4.0(5)	3.5(3)	6.6(4)	11.9(5)	T^{-1}

Table 2. Summary of room temperature (T=295K) magnetisation measurements after each period of heat treatment assuming the indicated particle size distributions. Sample 19850206/1a.

Temperature		15	32	67	77	143	292	297	K
χ_c		970(90)	433(17)	219(5)	204(5)	96(1)	31(1)	29(1)	$\times 10^{-4}$
Msat	PSD=0	294(12)	375(45)	576(21)	632(18)	611(5)	404(11)	395(7)	$JT^{-1}m^{-3}$
χ_s		14.8(3)	9.3(4)	5.8(5)	3.6(2)	2.47(7)	1.5(1)	1.5(1)	$\times 10^{-4}$
$Mo\bar{V}$		16.1(20)	12.0(16)	8.7(3)	8.2(2)	7.6(3)	9.3(6)	9.6(6)	$\times 10^{-26}JT^{-1}$
Msat	PSD=2	298(8)	405(49)	599(22)	660(19)	644(6)	447(11)	434(7)	$JT^{-1}m^{-3}$
χ_s		14.7(2)	8.9(4)	5.5(5)	3.3(2)	2.11(7)	1.1(1)	1.13(7)	$\times 10^{-4}$
$Mo\bar{V}$		12.6(20)	8.8(12)	6.7(3)	6.3(2)	5.8(3)	6.7(6)	6.6(4)	$\times 10^{-26}JT^{-1}$

Table 3. Summary of magnetisation data for sample 19850206/1a after final heat treatment.

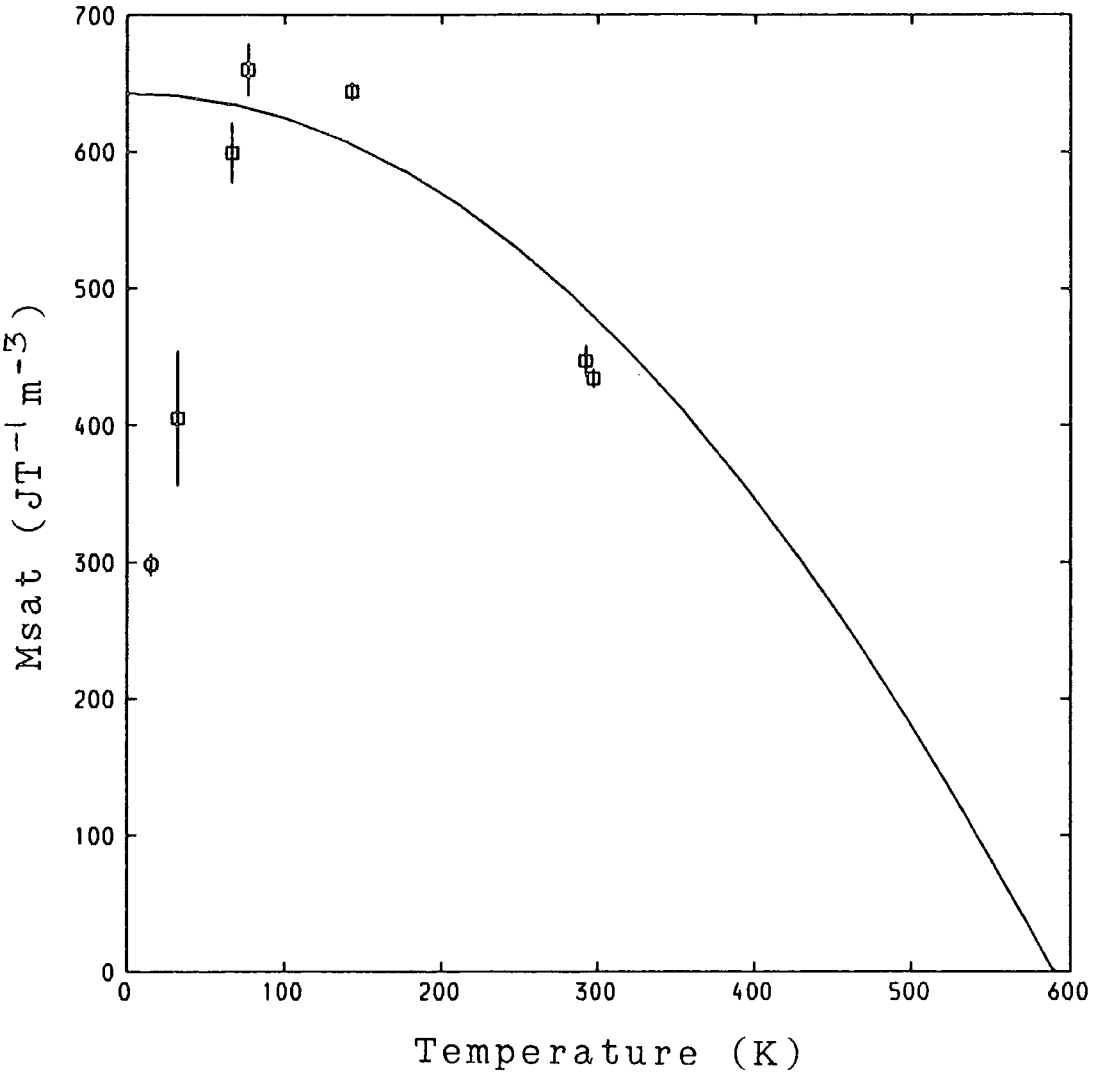

Fig 7. Saturation magnetisation estimated at various temperatures assuming the LSW diffusion limited particle size distribution.

diffusion limited PSD is used (figure 6a) with $C_s=(3.02\pm0.14)\times10^{-2}K$ [$(3.1\pm0.3)\times10^{-2}K$].

Table 2 summarises the 295K measurements made at each stage of heat treatment. A value of $C_s=3\times10^{-2}K$ implies that 1 in 164 Mg^{2+} ions are replaced by an isolated Fe^{3+} (equivalent to 8480ppm wt.) to form the paramagnetic sea. At this density ~96% of the randomly distributed Fe^{3+} would be isolated. A further 2000ppm wt. of iron is needed to form the magnesioferrite precipitate (assuming $\delta=0.81$, $x=1.06$ and $M_{sat}=450JT^{-1}m^{-3}$).

The magnetisation measurements taken after the final stage of heat treatment are summarised in table 3. The estimates of $M_o\bar{V}$, the mean particle moment at 0K, do not depend on the absolute sensitivity of the VSM. However, as the temperature falls, the paramagnetic background magnetisation increases and the estimates of $M_o\bar{V}$ become less reliable. Effects attributable to significant chemical inhomogeneity /ch4,sec3/ are not apparent. Even at 15K there was no detectable difference between measurements taken along [100] and [110] directions and no hysteresis. Combining the results at all temperatures $M_o\bar{V}=(6.4\pm0.2)\times10^{-20}JT^{-1}$ [$(8.4\pm0.3)\times10^{-20}JT^{-1}$]. The values of M_{sat} (figure 7) must be treated with caution at low temperatures: the magnetisation of the paramagnetic sea swamps that of the precipitate and the stability of the VSM's sensitivity is relatively poor. In spite of these problems the experimental results above 32K agree

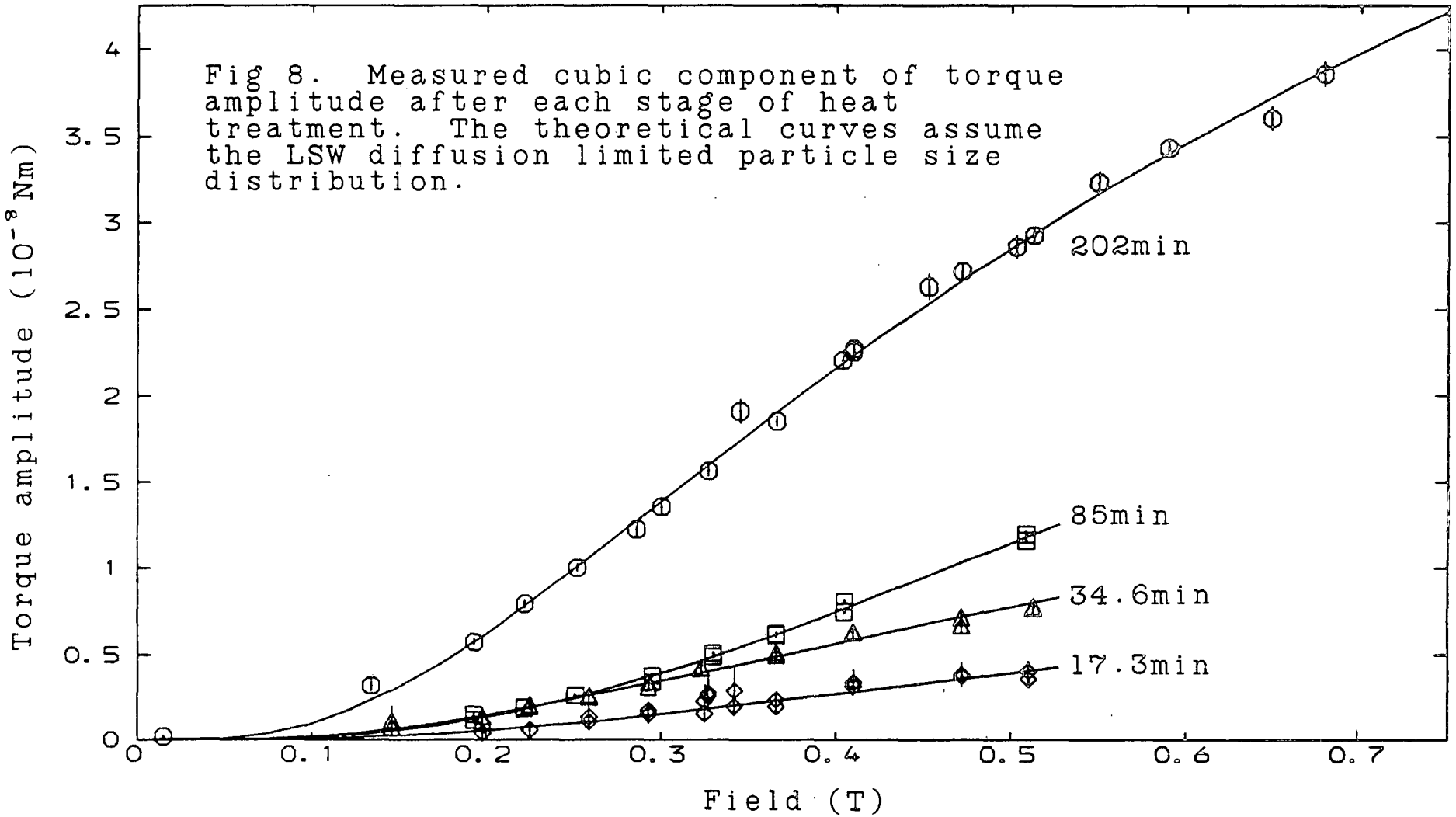
Fig 8. Measured cubic component of torque amplitude after each stage of heat treatment. The theoretical curves assume the LSW diffusion limited particle size distribution.
Torque amplitude (10^{-8} Nm)
Field (T)
0
0.5
1
1.5
2
2.5
3
3.5
4
0.1
0.2
0.3
0.4
0.5
0.6
0.7
202min
85min
34.6min
17.3min

Ageing time at 973K		17.3	34.6	85	202	min
Γ_{sat}	PSD=0	4.4(10)	8.6(10)	6.6(4)	8.4(2)	$\times 10^{-8}$Nm
$M_s\bar{V}/kT$				11.8(4)	19.1(4)	T^{-1}
K_1		-1.5(3)	-2.0(2)	-1.4(1)	-1.8(1)	$\times 10^{3}$ Jm^{-3}
Γ_{sat}	PSD=2	5.5(10)	10.9(10)	9.0(7)	10.0(2)	$\times 10^{-8}$Nm
$M_s\bar{V}/kT$				7.7(3)	13.5(3)	T^{-1}
K_1		-1.6(3)	-2.0(2)	-1.7(2)	-1.9(1)	$\times 10^{3}$ Jm

Table 4. Summary of room temperature (T=295K) torque measurements after each period of heat treatment, assuming the indicated particle size distribution. Sample 19850206/1a.

qualitatively with the expected temperature dependence /ch3,eqn9/ and the results above 32K have been used to estimate $nM_o\bar{V}=(640\pm23)JT^{-1}m^{-3}$ $[(610\pm25)JT^{-1}m^{-3}]$.

3.2 Torque response

The digitised torque curves /ch6,sec5/ were fitted by a harmonic series

$$Torque = \alpha\cos(\theta+\phi_\alpha)+\beta\cos(2\theta+\phi_\beta)+\Gamma\cos(4\theta+\phi_\Gamma) \qquad (5)$$

where θ is the angle of the magnetising field with respect to the sample. The first term is due to the slight field gradient acting on the sample moment causing "side-pull". The samples were aged in a small mgnetic field /ch6,sec3/ and the amplitude β takes into account any so caused uniaxial shape anisotropy. In fact at no stage was β found to differ significantly from zero. The cubic magnetocrystalline anisotropy of magnesioferrite gives rise to a torque amplitude Γ/ch4,sec6.2/ which saturates in sufficiently high fields when

$$\Gamma_{sat} = \frac{|K_1|n\bar{V}}{2} = \frac{|K_1|M_{sat}V'}{2M_s} \qquad (6)$$

where V' is the sample volume. ϕ_Γ is determined by the sign of the first anisotropy constant K_1. The variation of with field (figure 8) can, in principle, be used to estimate both K_1 and $M_s\bar{V}$ (table 4). In practice until the third stage of heat treatment the data was too noisy and the maximum field too low to derive both quantities so K_1 has been estimated by assuming the value of $M_s\bar{V}$ inferred from

magnetisation curves. After the third and fourth heat treatments, estimates of $M_s\bar{V}$ could be made and they are in agreement with the VSM results if the diffusion limited PSD is assumed. Combining the values from all stages $K_1=-(1.86\pm0.08)\times10^3 Jm^{-3}$ [$K_1=-(1.81\pm0.09)\times10^3 Jm^{-3}$], in the range of values found for bulk magnesioferrite which is $-(3.1\pm0.5)\times10^3 Jm^{-3}$ /ch3,sec6.3/.

3.3 Summary of static magnetic analysis

The magnetisation and torque measurements made at each stage of heat treatment are consistent wth the assumption that the samples contain (10500±300)ppm wt. of iron. When heat treated in oxygen at 973K (8500±250)ppm wt forms a saturated solution of Fe^{3+} in the MgO and (2000±200)ppm wt. Fe^{3+} is precipitated as magnesioferrite which occupies about 0.3% of the sample volume. The Curie temperature of the precipitate has been estimated from the initial susceptibility $T_c=(589\pm10)K$ and indicates a degree of inversion $\delta=(0.81\pm0.02)$ in agreement with the value expected for a bulk sample of magnesioferrite, saturated with MgO and prepared at 973K. The zero temperature spontaneous magnetisation $M_o=(2.1\pm0.1)\times10^5 JT^{-1}m^{-3}$ of the precipitate was also inferred from T_c. The magnesioferrite fine particle system appears to grow by diffusion limited Ostwald ripening, the mean particle volume depending linearly on the heat treatment time. The 973K equilibrium composition for the magnesioferrite seems to be attained after about 30

minutes of heat treatment and after about 200 minutes the mean particle volume is about $3\times10^{-25}m^3$. Estimates of the mean particle moment derived from torque measurements agree with those obtained from magnetisation curves. There is no evidence of any shape anisotropy - the anisotropy is cubic with $K_1=-(1.86\pm0.08)\times10^3 Jm^{-3}$ at room temperature and there is no significant variation with particle size. This value of K_1 is in the range of values found for bulk samples of magnesioferrite prepared at 973K.

4. FMR of magnesioferrite fine particles

The FMR spectra of heat treated Fe/MgO have a complicated appearance which depends on the sample's thermal history, orientation and temperature. Various aspects have been qualitatively described in some detail by other workers (16,19). The spectra have two components - a narrow isotropic line at g=2.00 and a much broader anisotropic "line" /ch6,fig5/.

The isotropic line is probably due to the paramagnetic sea of Fe^{3+}. Its width increases slightly with decreasing temperature (from about 3mT at 300K to about 5mT below 100K). This behaviour presumably results from the temperature dependence of the precipiate particles' magnetic moments which contribute to the line width via a dipolar interaction. The complexity of the concentration gradients in the vicinity of a particle precludes a simple quantitative verification of this suggestion. The estimated

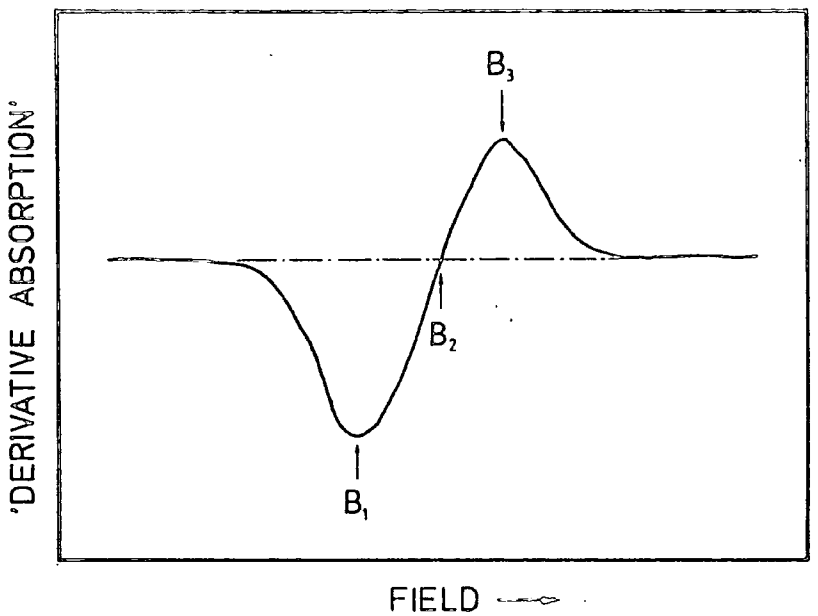

Fig 9. Definitions of the fields used to summarise the FMR spectra.

Temp. (K)	Angle (deg)	B_1 (mT)	B_2 (mT)	B_3 (mT)	Ref. 1985
100	10	307(4)	360(2)	422(4)	0728/15
100	55	284(1)	318(1)	349(1)	0728/14
150	0	309(4)	339(4)	388(4)	0728/6
150	15	307(2)	333(2)	397(2)	0728/9
150	30	310(2)	336(2)	383(2)	0728/8
150	35	310(2)	333(2)	374(2)	0728/11
150	40	305(2)	332(2)	363(2)	0728/10
150	45	303(2)	330(2)	354(2)	0728/7
150	50	298(2)	330(1)	349(2)	0728/12
150	55	296(2)	330(1)	348(2)	0728/13
150	60	296(1)	330(1)	347(1)	0728/13'
200	0	315(3)	331(1)	357(4)	0728/5
200	10	314(2)	328(2)	373(4)	0728/16
200	45	317(2)	331(1)	348(2)	0728/4
200	55	309(2)	329(2)	345(4)	0728/17

Table 5. Summary of FMR spectra of sample 19850206/1b after final heat treatment. The fields are defined in figure 9.

line width (using the Kittel-Abrahams model /ch2,sec4.6/ (16)) of the paramagnetic sea assuming it comprises 8500ppm wt. Fe^{3+} randomly distributed is $\sim$6mT in reasonable agreement with observation bearing in mind the unaccounted for influence of the precipitate.

Although the anisotropic line appears after only 17 minutes of ageing at 973K the spectra taken after the last heat treatment are most suitable for a study of the line. The same qualitative behaviour was seen at the earlier stages but the line had a lower intensity. For the purposes of comparison with theory the broad anisotropic line on each spectrum has been characterised by three values of magnetic field (figure 9). The dependence of the line shape and intensity on the sample orientation and temperature has been illustrated earlier /ch6,fig5/.

4.1 Previous experimental results

Several groups have studied the FMR spectra of heat treated Fe/MgO systems (19-25). The theory of de Biasi and Devezas has been criticised earlier /ch4,sec6.3/. In their experimental work (19-23) there was no attempt made to establish the particle size independently of the FMR results. The dimensions of samples were not given so it is not possible to judge whether the demagnetisation field ($\sim\mu_o M_{sat} \sim 0.5$mT) has a significant effect on the measured anisotropy field ($\sim$0.25mT). They ignored the variation of K_1 with temperature and invoked a "cubic shape anisotropy" to

fit the results. Inglis and others (24) have given a detailed empirical description of the evolution of the spectra as heat treatment progresses. Dubowik and Baszynski (19,23) interpreted their spectra by convolving the resonance field predicted by the theory of de Biasi and Devezas (which they misquote in their equation 2) with a particle size distribution. Although the results fitted their experimental spectra quite well the distributions used were much too broad to be compatible with the diffusive growth process.

4.2 Bulk magnesioferrite

Oguchi's result (ch 4, eqn 12) applied to a sample of magnesioferrite having no shape anisotropy, uniformly magnetised in the direction of the applied field B, predicts that resonance will occur when

$$\left[\left(\frac{h\nu}{\mu_B}\right)^2+\left(\frac{3K_1}{2M_S}\left(1-\cos 4\theta\right)\right)^2\right]=\left[gB+\frac{K_1}{4M_S}\left(5\cos 4\theta+3\right)\right]^2 \qquad (7)$$

if the field is in the (100) plane at angle θ to the [100] direction. Since $|K_1/M_S| \sim 50$mT (100K values) this theory cannot describe the experimental observations which are that, in most cases, the resonance field varies by less than 3mT over the full range of θ.

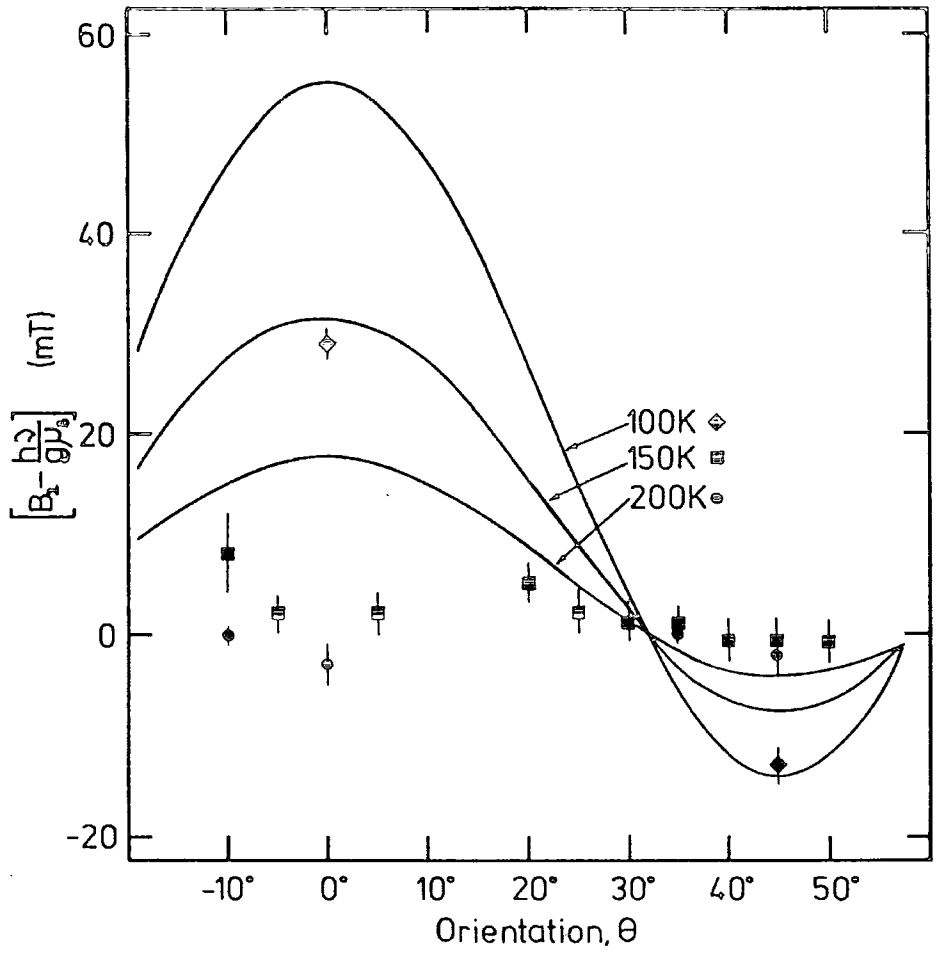

Fig 10. Comparison of the experimental results after 202min at 973K (sample 19850206/1b) with the theory of de Biasi and Devezas. B is in the (100) plane.

4.3 Theory of de Biasi and Devezas

Neither the torque measurements nor the symmetry of the FMR spectra had a detectable uniaxial component. The theory of de Biasi and Devezas (22) predicts that the apparent cubic anisotropy constant $\langle K_1 \rangle$ is given by

$$\frac{\langle K_1 \rangle}{K_1} = \frac{x^3 - 10x^2 L(x) + 35x - 105 L(x)}{x^3 L(x)} \qquad (8a)$$

$$L(x) = \coth x - 1/x \quad ; \quad x = M_s V B / kT \qquad (8b,c)$$

when all particles have the same volume V. Figure 10 compares the measured (table 5) and predicted values of $\langle K_1 \rangle$ using the values for M_s, $\bar{V}$ and K_1 obtained from the static measurements and model described earlier (ch 7, sec 3). There is no agreement between the theory and experiment.

4.4 Theory developed in this work

The theory described earlier /ch4,sec6.3/ was based on the premise that the magnetic behaviour of a fine particle can be described by a spin Hamiltonian, its terms inferred from the classical magnetic energy. When the applied static magnetic field is large enough to almost saturate an assembly of identical particles the power absorbed in an FMR experiment was found to be

$$P(B) \simeq \frac{P_0 V}{kT} (BM_s + 2K_1) \left(\frac{M_s V}{\mu_B}\right)^2 \theta_{res}^3 \exp\left(-\theta_{res}^2 (BM_s + 2K_1) V / 2kT\right) \qquad (9a)$$

$$\theta_{res}^2 = \frac{M_s}{K_1} \left(B - \frac{h\nu}{g\mu_B} + \frac{2K_1}{M_s}\right) \qquad (9b)$$

This expression has been evaluated using parameter values derived from the magnetic analysis of the Fe/MgO system

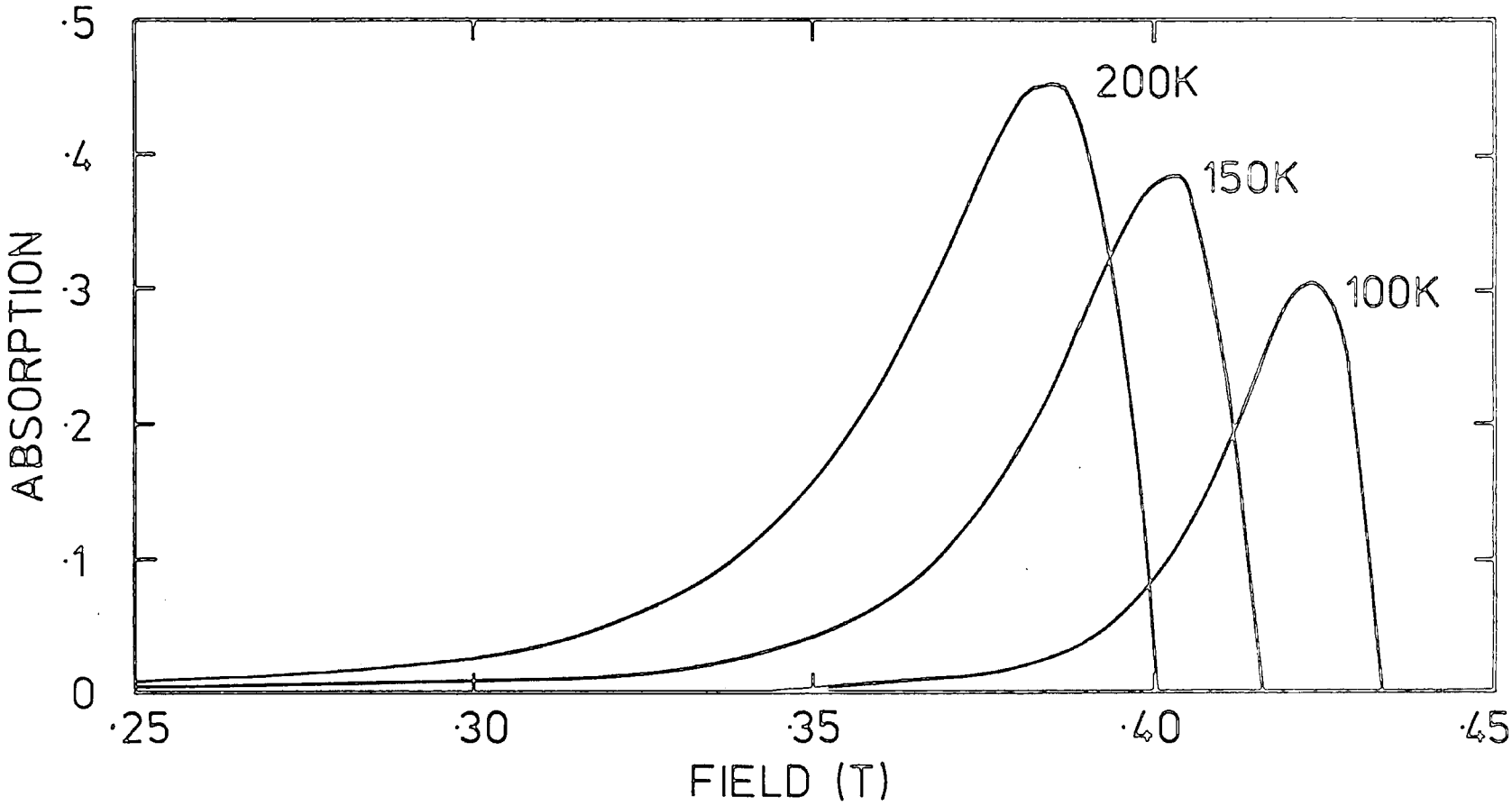

Fig 11. Theoretical FMR absorption curves predicted using the theory developed in this work and the estimates of particle properties derived from magnetisation and torque measurements. See text.

after the final heat treatment. The results (figure 11), which assume that all particles have the mean volume, are not in good agreement with the comparable experimental FMR spectra /ch6,fig 5a/; the predicted peak absorption occurs at a field only slightly less than that expected of a bulk sample, well away from the observed value of 0.331mT. The disagreement is probably caused by the large number of particles which are too small to be almost saturated by the magnetic field - the basic assumption needed to obtain the analytic approximation. Smaller particles will tend to shift the peak of the envelope closer to the isotropic g=2.00 position (0.331mT). A quantitative calculation of this effect would be difficult because the integrals necessary are extremely ill-behaved, multi-dimensional and have no closed form.

It is interesting to note that a system quite close to saturation can have a rather broad absorption envelope but otherwise the approximate version is not very helpful. Its predictions are neither so different from the experimental evidence that it can be refuted, nor in sufficient agreement to inspire confidence in its validity. Whether or not the spin Hamiltonian /ch4,eqn11/ correctly describes a fine particle at high as well as low frequencies remains an open question.

5. Summary and conclusions

The formation and growth of a superparamagnetic

precipitate of magnesioferrite in iron-doped magnesium oxide has been examined theoretically and by using experimental magnetisation, torque, ESR and FMR measurements. The torque, magnetisation and ESR results are in good agreement with the predictions. Demagnetisation tensors have been defined for, and applied to, microscopic particles of uniform magnetisation. The discussion of the particle magnetism included several new calculations of the effects of non-negligible cubic anisotropy and LSW particle size distributions on torque and magnetisation response. The theory of the FMR response of SPM systems due to de Biasi and Devezas has been criticised on theoretical grounds and found to disagree with the experiments. These are the first results published for non-metal systems which provide a satisfactory independent estimate of the precipitate size. A new theory of the FMR of a superparamagnetic particle, based on a simple spin Hamiltonian, was proposed. It has been shown that under some circumstances an analytic formula for the approximate FMR line shape can be obtained. However agreement between this approximation and the experiment is problematic. It seems likely that the disagreement is caused by the small particles in the precipitate which are not described well by the approximate formula. It would be possible, in principle, to attempt a numerical calculation to take into account the size distribution and the small presence of particles. Such a calculation would be rather difficult because of the badly behaved nature of the

integrals involved but the result is needed to establish whether the spin Hamiltonian description of a particle is valid.

It must be concluded that, until further calculations have been performed, the FMR behaviour of fine particle systems exhibiting superparamagnetism cannot be quantitatively interpreted. The analysis of the FMR spectra obtained from the magnetic fluids described in the introduction to this thesis is therefore not feasible at present.

6. References

1. Low, W. Sign of the crystalline cubic field splitting parameter a in an S state. Phys. Rev. (1957)105,792.

2. Griffiths, J.H.E. and J.W. Orton. Some weak lines in the paramagnetic resonance spectrum of impure MgO crystals. Proc. Phys. Soc. Lond. (1959)73,948.

3. Kolopus, J.L. and L.V. Holroyd. Higher order transitions of Fe^{3+} in MgO. Phys. Stat. Sol. (1965)8,711.

4. Henderson, B. and J.E. Wertz (1977) "Defects in the alkaline earth oxides" Taylor and Francis, London.

5. de Biasi, R.S. Forbidden $\Delta M_s=2$ transitions in the EPR spectrum of Fe^{3+} in MgO. Phys. Stat. Sol. (1978)B87,K29.

6. Mondine, F.A., E. Sonder and R.A. Weeks. Determination of the Fe^{2+} and Fe^{3+} concentration in MgO. J. Appl. Phys. (1977)48,3514.

7. Low, W. The paramagnetic resonance spectrum of Fe^{3+} in the cubic field of MgO. Proc. Phys. Soc. Lond.(1956)B69,1169.

8. Feher, E.R. Effect of uniaxial stresses on the paramagnetic spectra of Mn^{2+} and Fe^{3+} in MgO. Phys. Rev. (1964)136,A145.

9. Stoneham, A.M., K.A. Müller and W. Berlinger. The temperature dependence of the linewidth of iron group ions in MgO. Sol. Stat. Commun. (1972)10,1005.

10. Thorp, J.S., R.A. Vasquez, C. Adcock, and W. Hutton. Electron spin resonance linewidths of Fe^{3+} in magnesium oxide. J. Mater. Sci. (1976)11,89.

11. Sonder, E., T.G. Stratton and R.A. Weeks. Kinetics of Fe^{2+} oxiation and Fe^{3+} reduction in MgO single crystals. J. Chem. Phys. (1979)70,4603.

12. de Biasi, R.S. Evidence for clustering in Fe^{3+}-doped MgO. Magn. Lett. (1978)1,103.

13. Thorp, J.S. and M.D. Hossain ESR line broadening of Fe^{3+} in Fe/MgO at low temperatures. J. Mater. Sci. (1980) 15,2647.

14. Thorp, J.S. and M.D. Hossain. Exchange energies of iron group ions in single crystal MgO. J. Mater. Sci. Lett. (1980)15,1866.

15. Inglis, A.D. and J.S. Thorp. ESR linewidths of some iron group ions in MgO. J. Mater. Sci. Lett. (1981)16,2628.

16. Inglis, A.D. and J.S. Thorp. Clustering and electron spin resonance linewidths in Fe/MgO. J. Mater. Sci. (1981)16,1887.

17. Groves, G.W. and M.E. Fine. Solid solution and precipitation hardening in Mg-Fe-0 alloys. J. Appl. Phys. (1964)35,3587.

18. Hoon, S.R. and S.N.M. Willcock. Priv. Commun. (1986).

19. Dubowik, J. and J. Baszynski. FMR study of coherent fine magnesioferrite particles in MgO - Line shape behaviour. J. Magn. Magn. Mater. (1986)59,161.

20. de Biasi, R.S. and T.C. Devezas. Crystal anisotropy of superparamagnetic particles as measured by resonance. Phys. Letts. (1974)50A,137.

21. de Biasi, R.S. and T.C. Devezas. Ferrimagnetic resonance study of the growth rate of superparamagnetic precipitates of magnesioferrite in MgO. J. Amer. Ceram. Soc. (1976)59,55.

22. de Biasi, R.S. and T.C. Devezas. Anisotropy field of small magnetic particles as measured by resonance. J. Appl. Phys. (1978)49,2466.

23. Dubowik, J. and J. Baszynski. Superparamagnetic properties of thin films and small particles of magnesium ferrite. IEEE Trans. Magn. (1980)MAG-16,649.

24. Inglis, A.D., G.J. Russell and J.S. Thorp. Magnesioferrite formation in low-concentration Fe/MgO single crystals. J. Mater. Sci. (1982)17,2939.

25. de Biasi, R.S. and T.C. Devezas. Shape anisotropy of ultrafine magnesium ferrite precipitates. J. Magn. Magn. Mater. (1983)35,121.

Acknowledgements

I would like to thank the following people for the help and friendship which I've enjoyed during the course of this work which was supported by a University of Durham Research Studentship:

Professors A.W. Wolfendale and G.C. Roberts granted the use of the facilities of the Departments of Physics and Applied Physics. Drs. Desmond Evans and John Thorp supervised the project and were an indefatigable source of ideas and good advice. Stan Jobson, Collin Savage, Pauline Russell and the staff of the Teaching Workshops in each department provided expert technical assistance. The work would have been impossible without the help of Drs. David Lambrick and Steven Hoon and the collective wisdom and facilities of the High Frequency Measurements and Solid State groups with whom it is a privilege to have been associated. Discussions with Neil Everall, Malcolm Hawton (the 'threading' algorithm), Peter Lux, Richard Myers, Dr. David Paige, Dr. Brian Tanner and Dr. Simon Willcock have proved invaluable. I am unlikely ever to forget the care and attention of Dr. Pattman and his staff at Newcastle General Hospital or the support of the many friends, mainly associated with the Graduate Society and DSU, I've made during my stay in Durham. Finally I'd like to apologise to everybody I've not mentioned and thank Margaret Chipchase for typing this thesis.

Appendix 1

Calibration of VSM

The VSM was calibrated immediately before and after taking the data for each magnetisation curve. Any significant difference between the two reference signals resulted in the entire set of data being disgarded and retaken. The reference sample used was a 4N purity nickel single crystal, mass 9.04×10^{-5}kg, in the form of an ellipsoid with its long (5.8mm) axis coincident with the [111] direction (1). Its short axes were approximately 1.8mm. The magnetising field (1.07T) was applied along the [111] direction. With the demagnetisation factor of 0.12 this resulted in an internal field 1.00T. The specific magnetisation at temperature T was then assumed to be (2-4)

$$M(T)=58.69(1-aT^{3/2}-bT^{5/2}) \quad [JT^{-1}kg^{-1}]$$

$$a=6.63\times10^{-6}K^{-3/2} \quad b=1.85\times10^{-8}K^{-5/2}$$

For example $M(294K)=55.12JT^{-1}kg^{-1}$ in agreement with Graham's recommended value of $55.25(20)JT^{-1}kg^{-1}$ (5).

References

1. Willcock, S.N.M. Ph.D. Thesis (1986), University of Durham.
2. Pauthenet, R. Spin-waves in nickel, iron, and yttrium-iron garnet. J. Appl. Phys. (1983)53,2029.
3. Pauthenet, R. Experimental verification of spin-wave theory in high fields. J. Appl. Phys. (1983)53,8187.
4. Lambrick, D.B. Ph.D. Thesis (1986), University of Durham.
5. Graham Jr., C.D. Iron and nickel as magnetization standards. J. Appl. Phys. (1982)53,2032.

Appendix 2

Additional FMR spectra

The following pages are copies of some of the FMR spectra taken after the first three stages of heat treatment of sample 19850206/1b. The field calibration (in MHz) refers to the proton resonance of glycerol. "MA" is proportional to the 100kHz modulation amplitude and "LEAK" is the detector bias current. "SL" is proportional to the gain of the spectrometer's signal channel and "TC" is the integration time constant for its the phase sensitive detector.

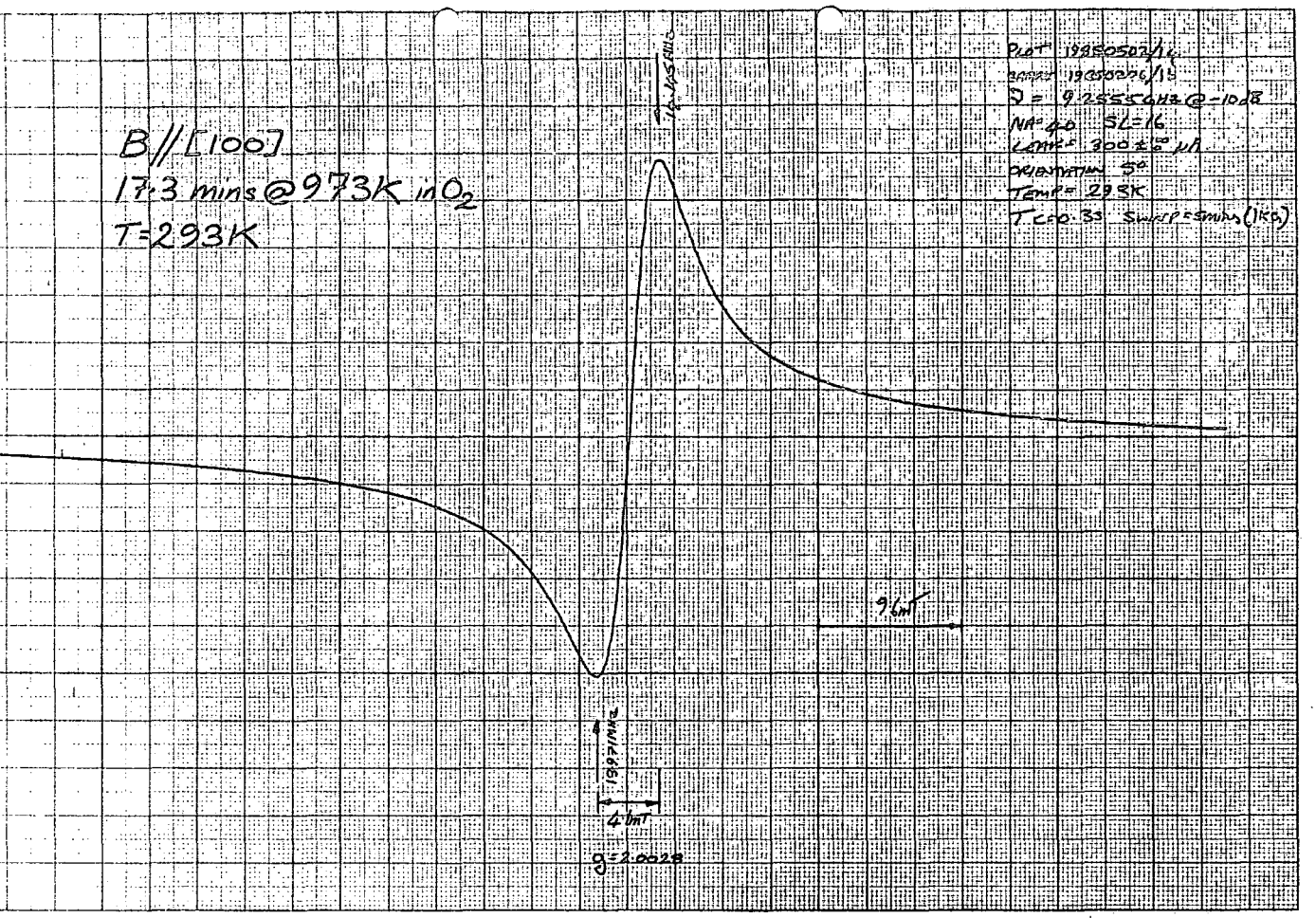
B//[100]
17.3 mins @ 973K in O_2
T=293K
PLOT 19850502/16
SAMPLE 19850206/16
ν = 9.25556 GHz @ -10dB
NA=40 SL=16
LAMP= 300±10 μA
ORIENTATION 50°
TEMP= 293K
TC=0.33 SWEEP=5MINS (1KG)
9.6mT
4.0mT
g=2.0028

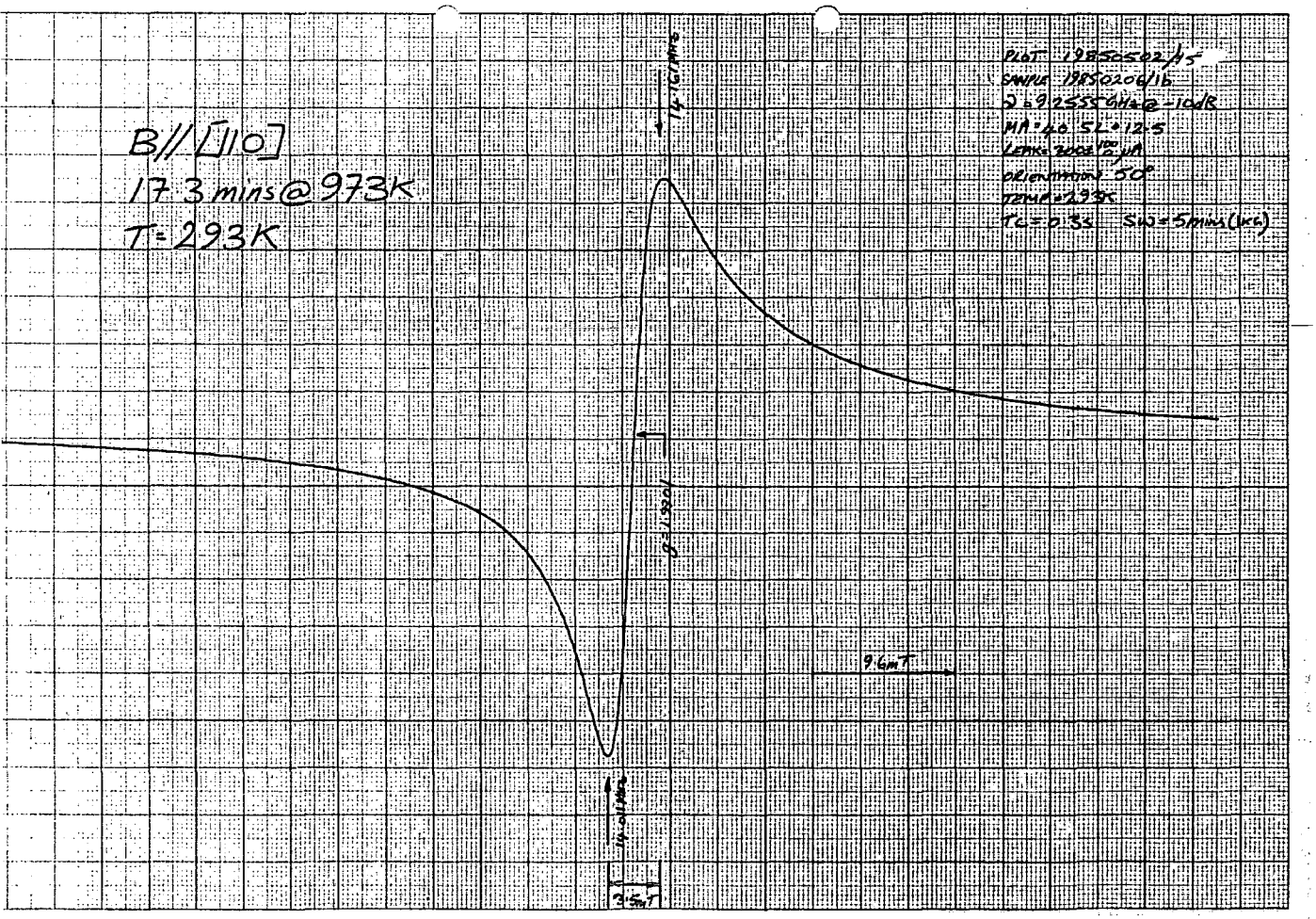
B//[110]
17.3 mins @ 973K
T=293K
PLOT 19850502/15
SAMPLE 19850206/16
ν = 9.25556 GHz @ -10dB
NA=40 SL=12.5
LAMP= 300±10 μA
ORIENTATION 50°
TEMP=293K
TC=0.33 SWP=5MINS (1KG)
9.6mT
3.5mT

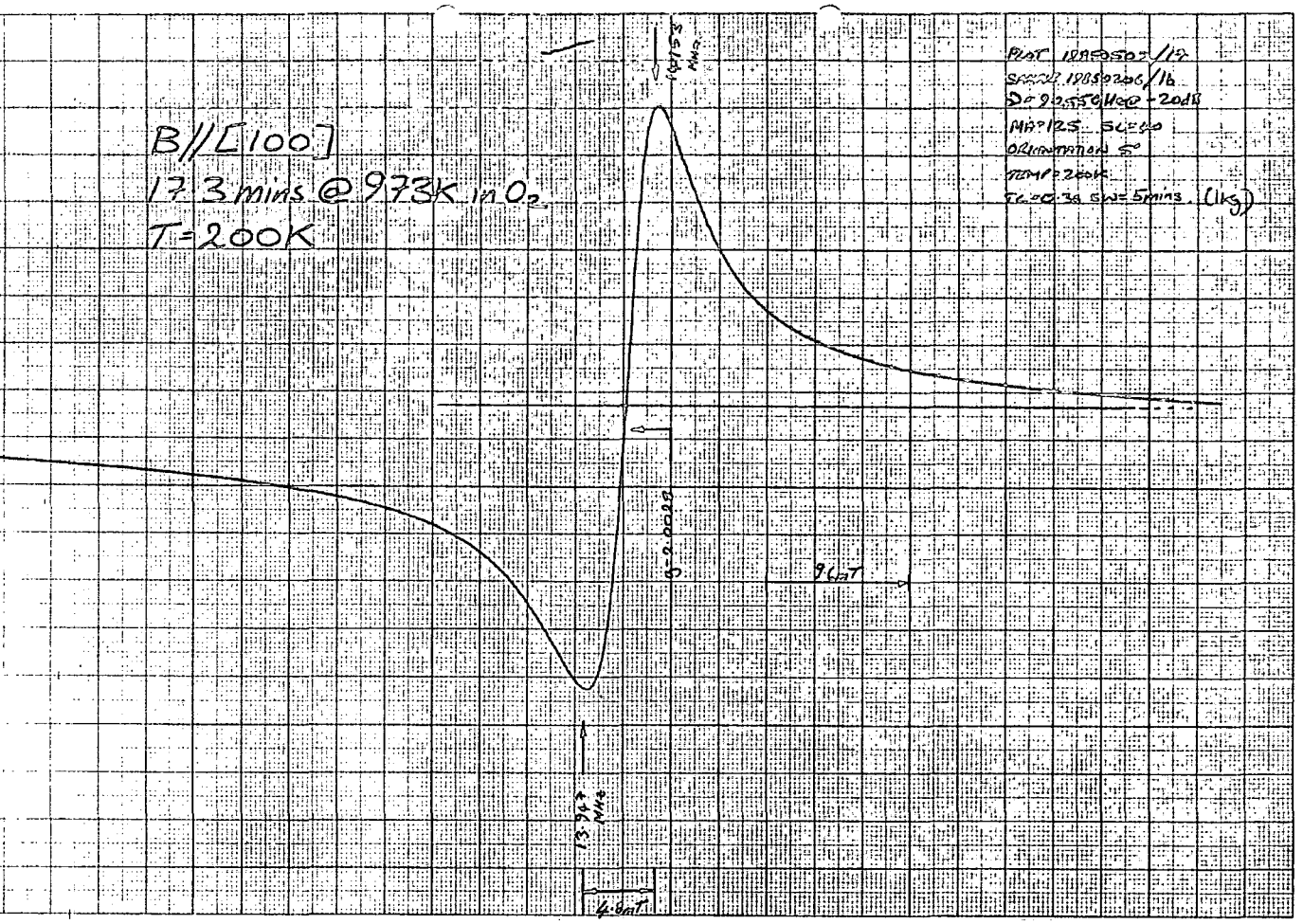
B//[100]
17.3 mins @ 973K in O_2
T = 200K
PLOT 19850502/19
SAMPLE 19850206/1b
DE 9.25566 Hz @ -20dB
MA=125 SC=50
ORIENTATION 5°
TEMP=200K
TC=0.3s SWP=5mins. (1kG)
5.1mT
5mT
13.9mT
4.8mT
9.6mT

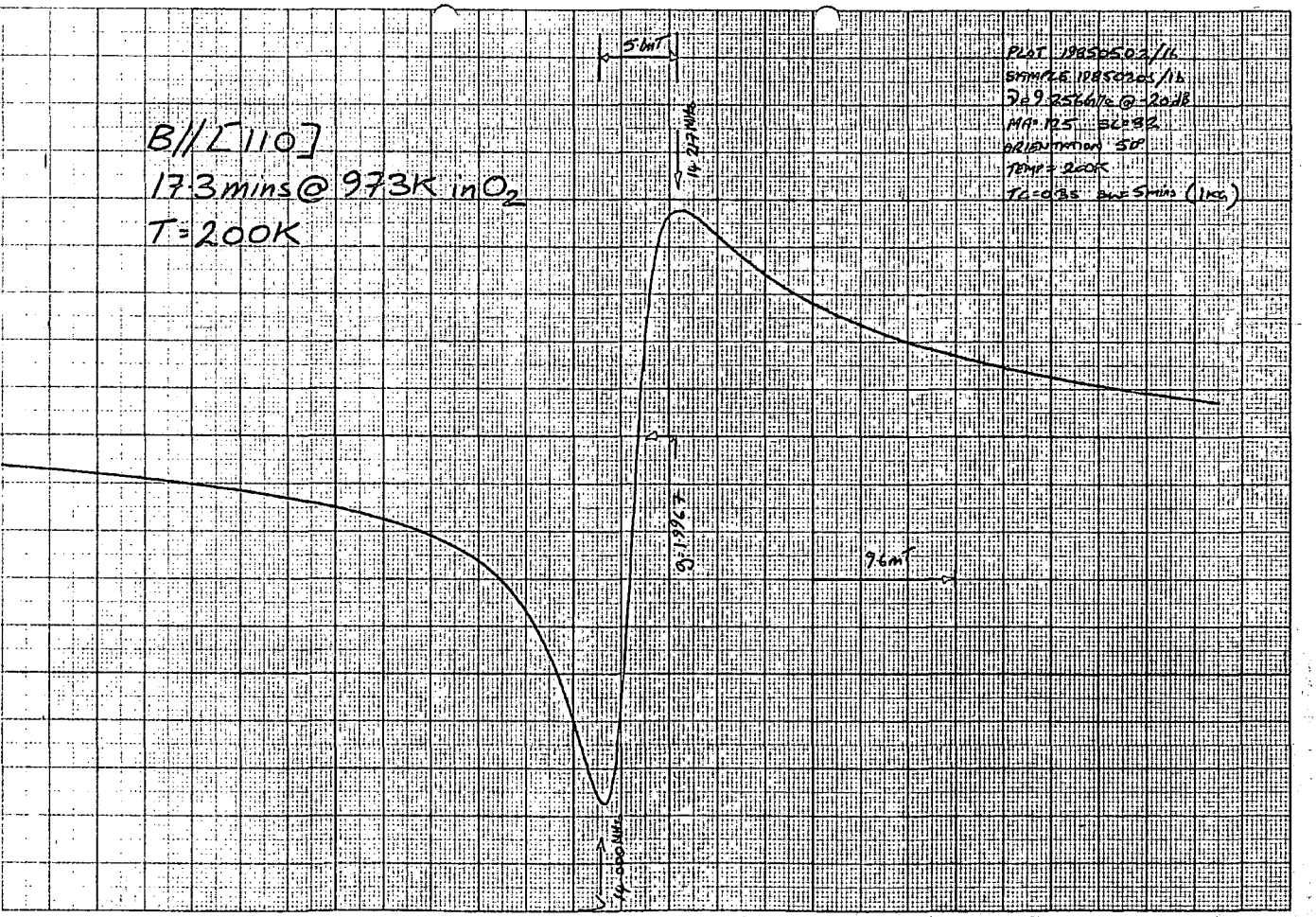
B//[110]
17.3 mins @ 973K in O_2
T = 200K
PLOT 19850502/16
SAMPLE 19850206/1b
DE 9.25566 Hz @ -20dB
MA=125 SC=50
ORIENTATION 50
TEMP=200K
TC=0.3s SWP=5mins (1kG)
5.6mT
5mT
14.2mT
9.6mT

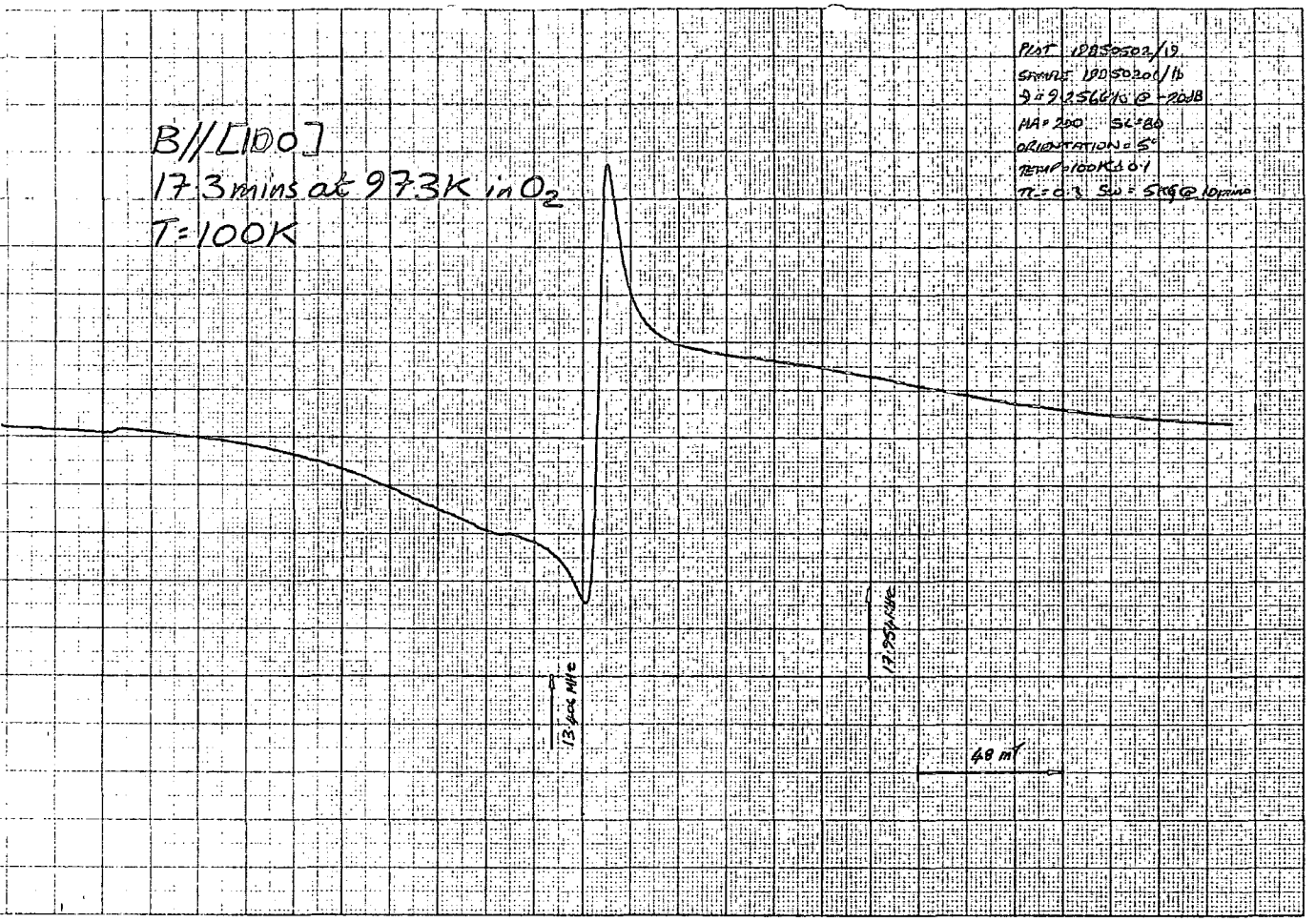
B//[100]
17·3mins at 973K in O_2
T=100K
PLOT 19850502/19
SAMPLE 19850206/1b
9=2.2566/6 @ -20dB
MA=200 SL=80
ORIENTATION=5°
TEMP=100K±0.1
TC=0.3 Sw=5KG@10mins
13.56MHz
17.05MHz
48 mT

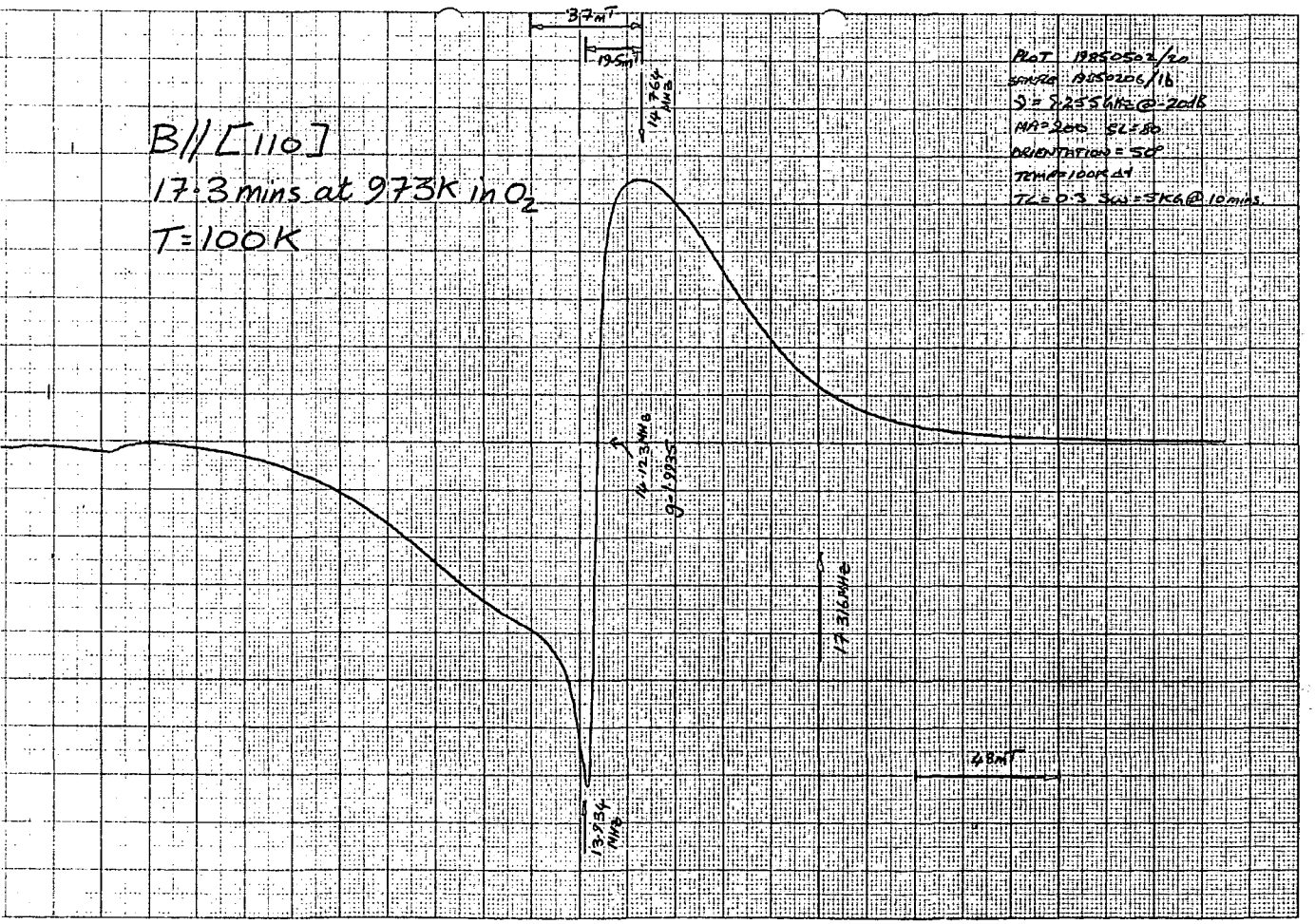
B//[110]
17·3mins at 973K in O_2
T=100K
37mT
19.5mT
14.764 MHz
PLOT 19850502/20
SAMPLE 19850206/1b
9=2.2566@-20dB
MA=200 SL=80
ORIENTATION=50°
TEMP=100K±1
TC=0.3 Sw=5KG@10mins
14.123MHz
g=1.9935
17.316MHz
13.954 MHz
48mT

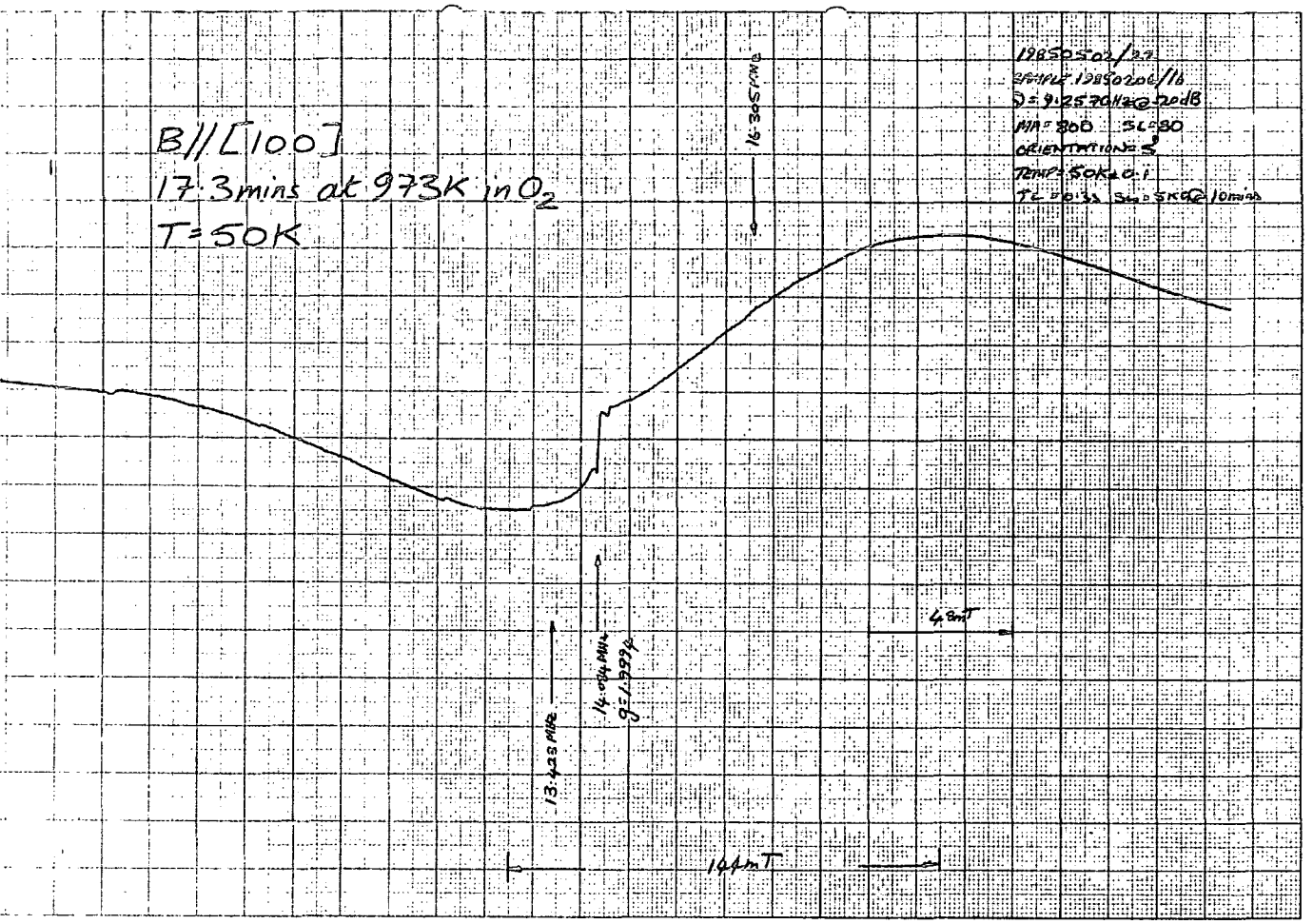
B // [100]
17·3 mins at 973K in O_2
T = 50K
19850502/22
SAMPLE 19850206/1b
9 = 9.2570 GHz @ -20dB
MA = 800 SL = 80
ORIENTATION = 5°
TEMP = 50K ± 0.1
TC = 0.33 Sw = 5KG @ 10 mins
16.305 MHz
13.423 MHz
14.094 MHz
g = 1.999
48mT
141mT

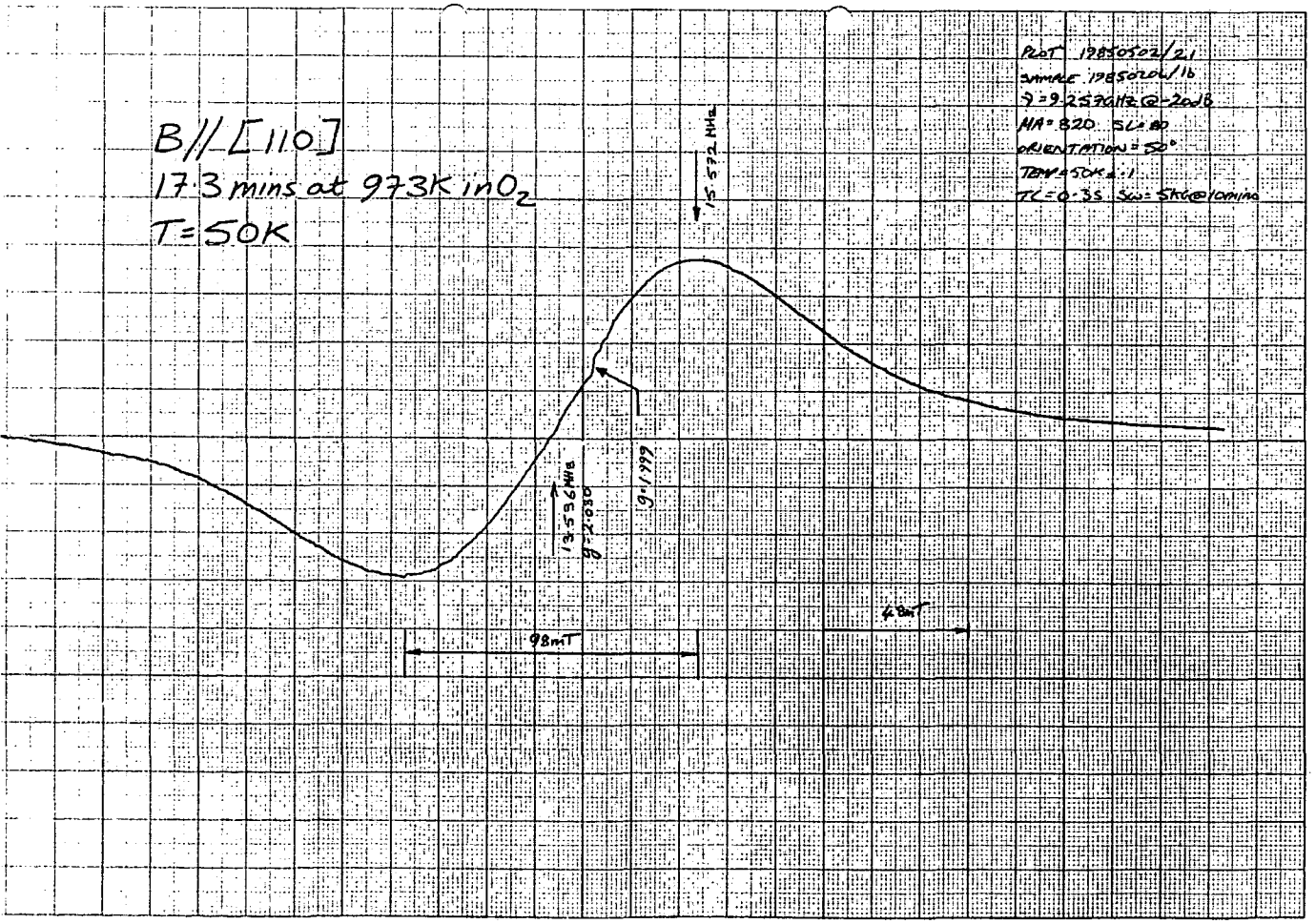
B // [110]
17·3 mins at 973K in O_2
T = 50K
PLOT 19850502/21
SAMPLE 19850206/1b
9 = 9.2570 GHz @ -20dB
MA = 820 SL = 80
ORIENTATION = 50°
TEMP = 50K ± 1
TC = 0.33 Sw = 5KG @ 10 mins
15.572 MHz
13.536 MHz
g = 2.030
g = 1.999
48mT
98mT

B//[100]
34·6 mins at 973K in O_2
T = 293K

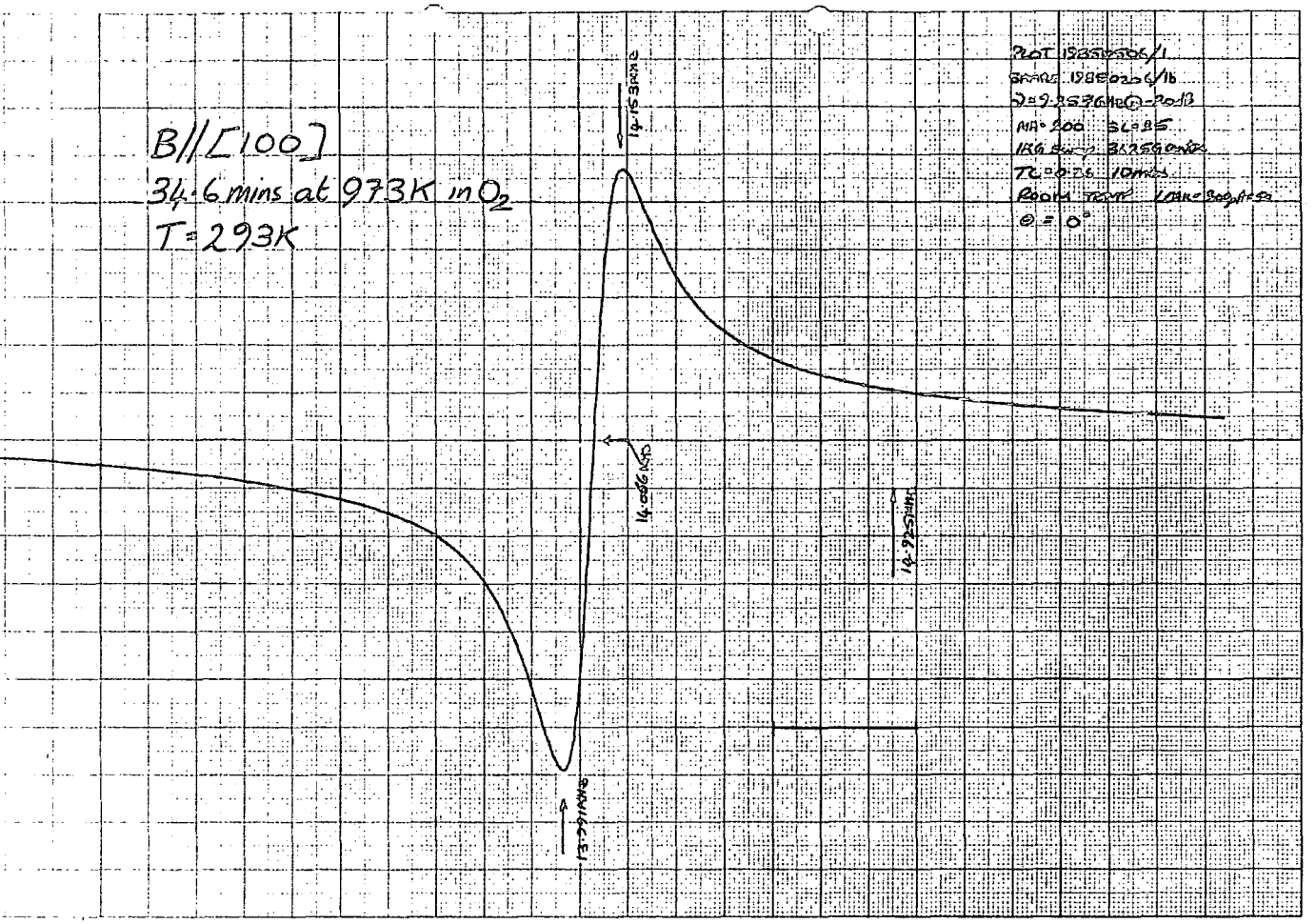

B//[110]
34·6 mins @ 973K in O_2
T = 293K

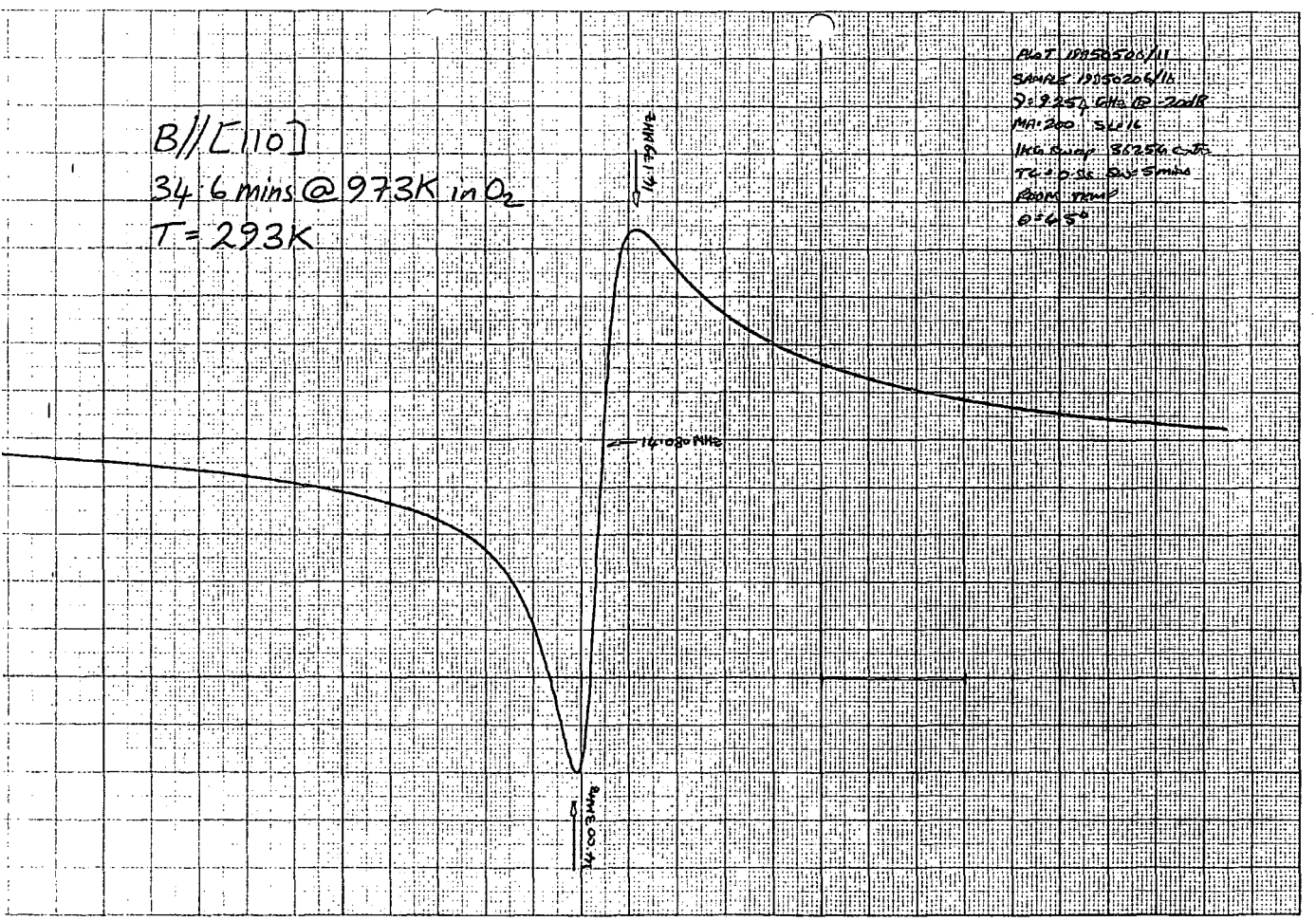

B//[100]
34.6mins @ 973K in O_2
T = 200K

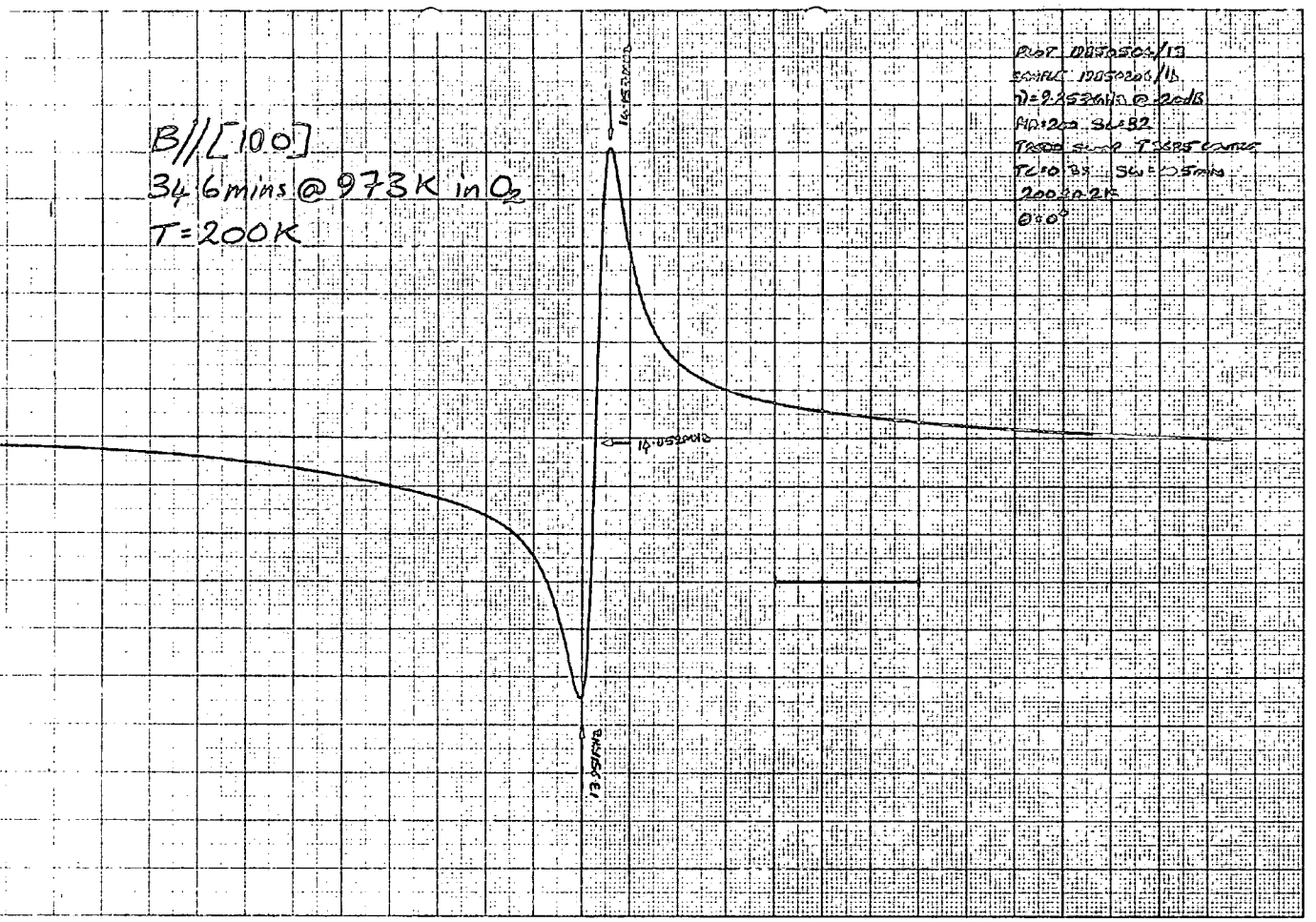

B//[110]
34.6mins @ 973K in O_2
T = 200K

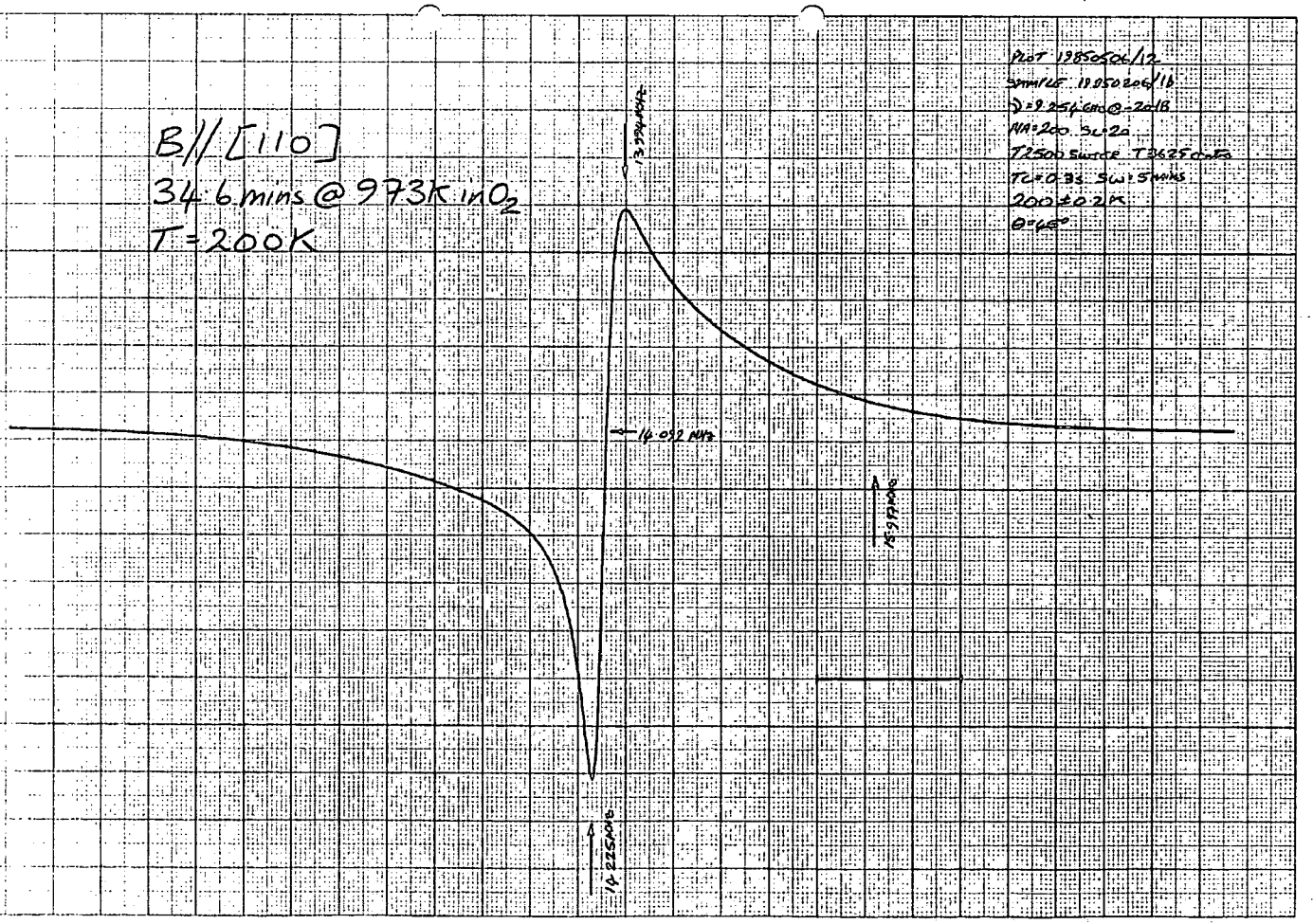

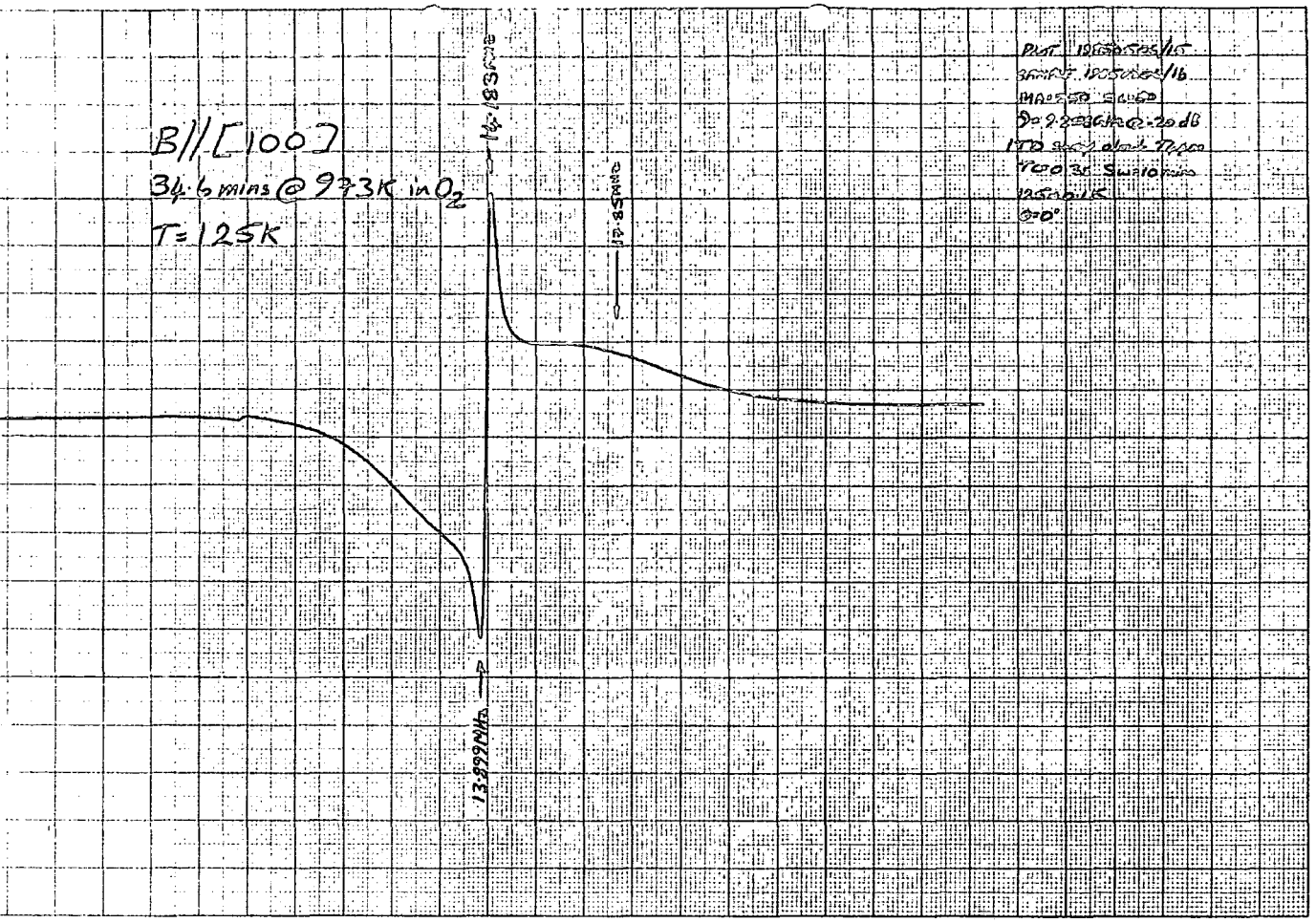
B//[100]
34.6 mins @ 973K in O_2
T = 125K
14.183GHz
8.5mins
13.999GHz

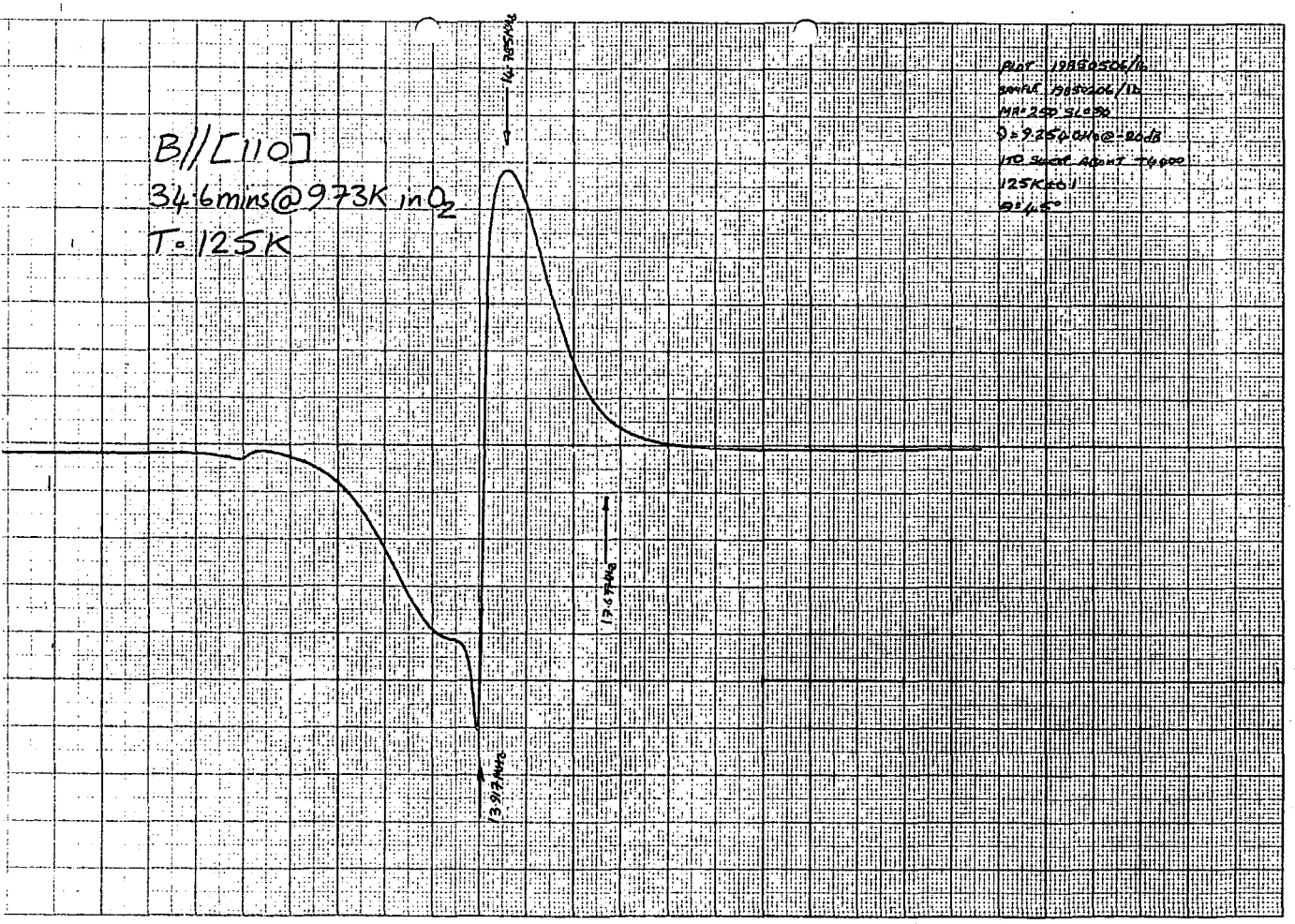
B//[110]
34.6mins@973K in O_2
T. 125K
14.325GHz
13.5mins
13.973GHz

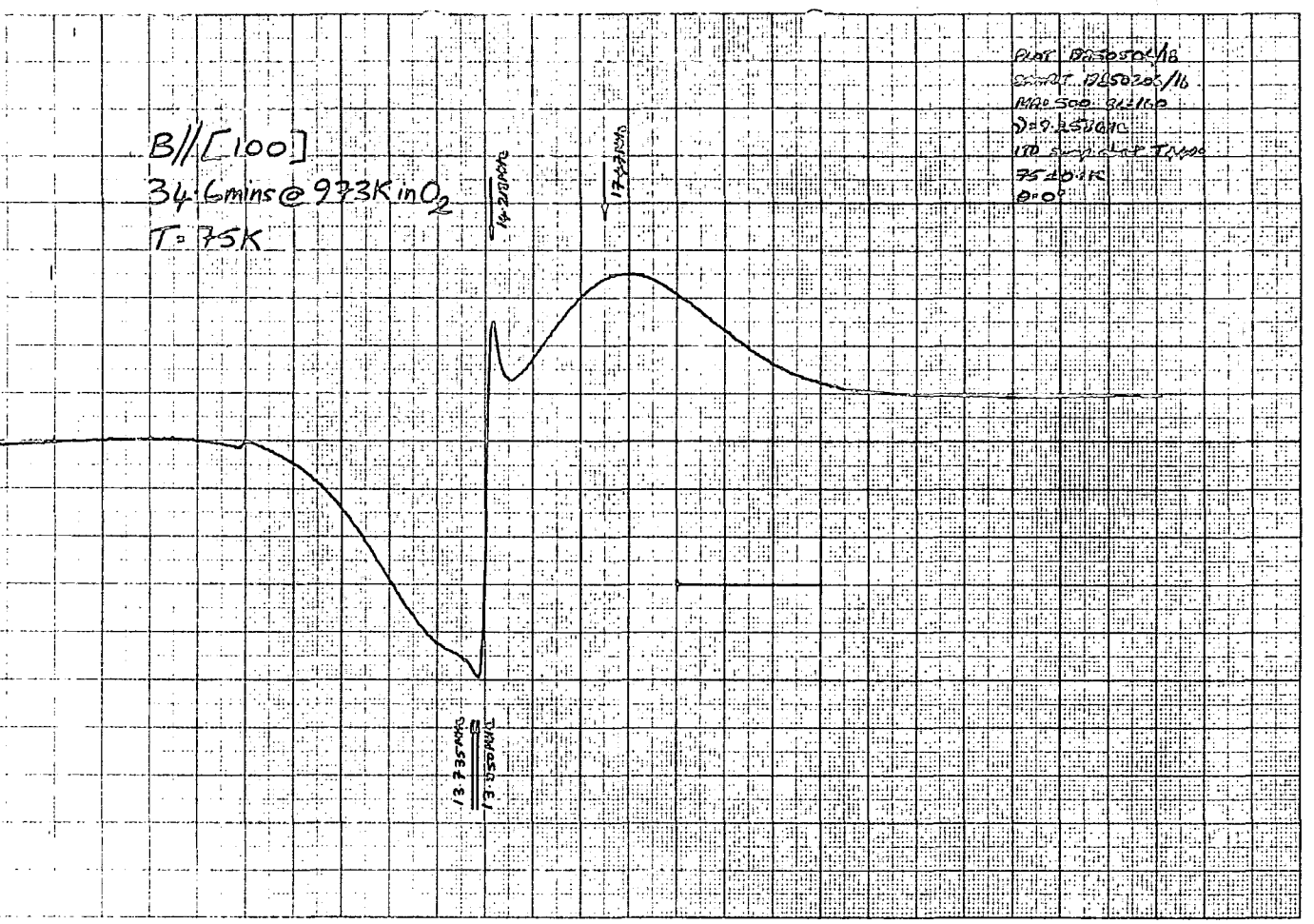
B//[100]
34.6mins@973K in O_2
T=75K
PLOT 19850506/18
SAMPLE 19850206/16
MA=500 SL=160
ν=9.255GHz
ITO SUBSTRATE
75±0.1K
θ=0°

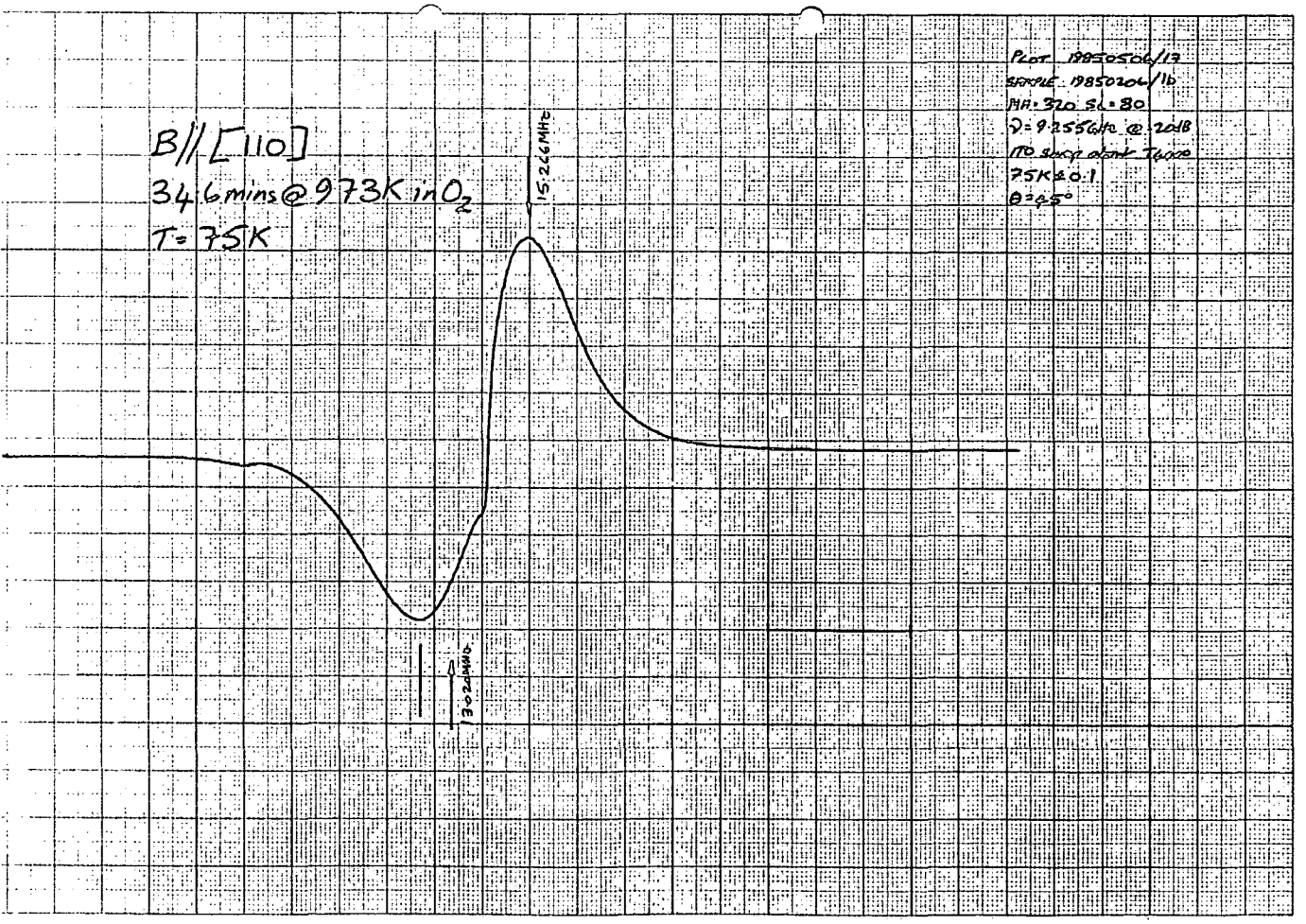
B//[110]
34.6mins@973K in O_2
T=75K
PLOT 19850506/17
SAMPLE 19850206/16
MA=320 SL=80
ν=9.255GHz @ 2dB
ITO SUBSTRATE
75K±0.1
θ=45°

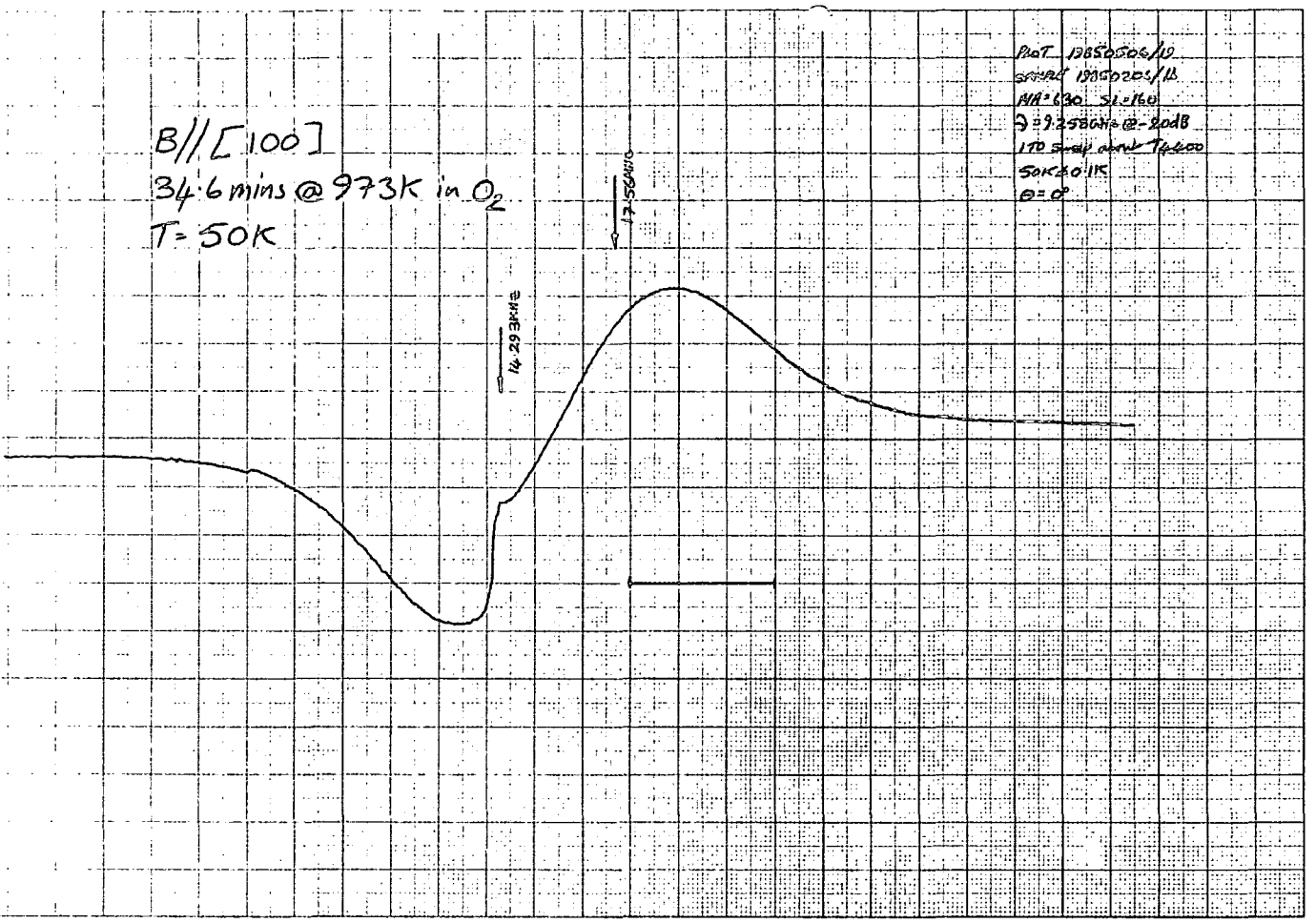
B // [100]
34·6 mins @ 973K in O_2
T = 50K
PLOT 19850506/19
SAMPLE 19850205/1b
HA=630 SL=160
ν = 9.2580GHz @ -20dB
ITC Sweep about T4200
50K ± 0.1K
θ = 0°
17.56MHz
14.29MHz

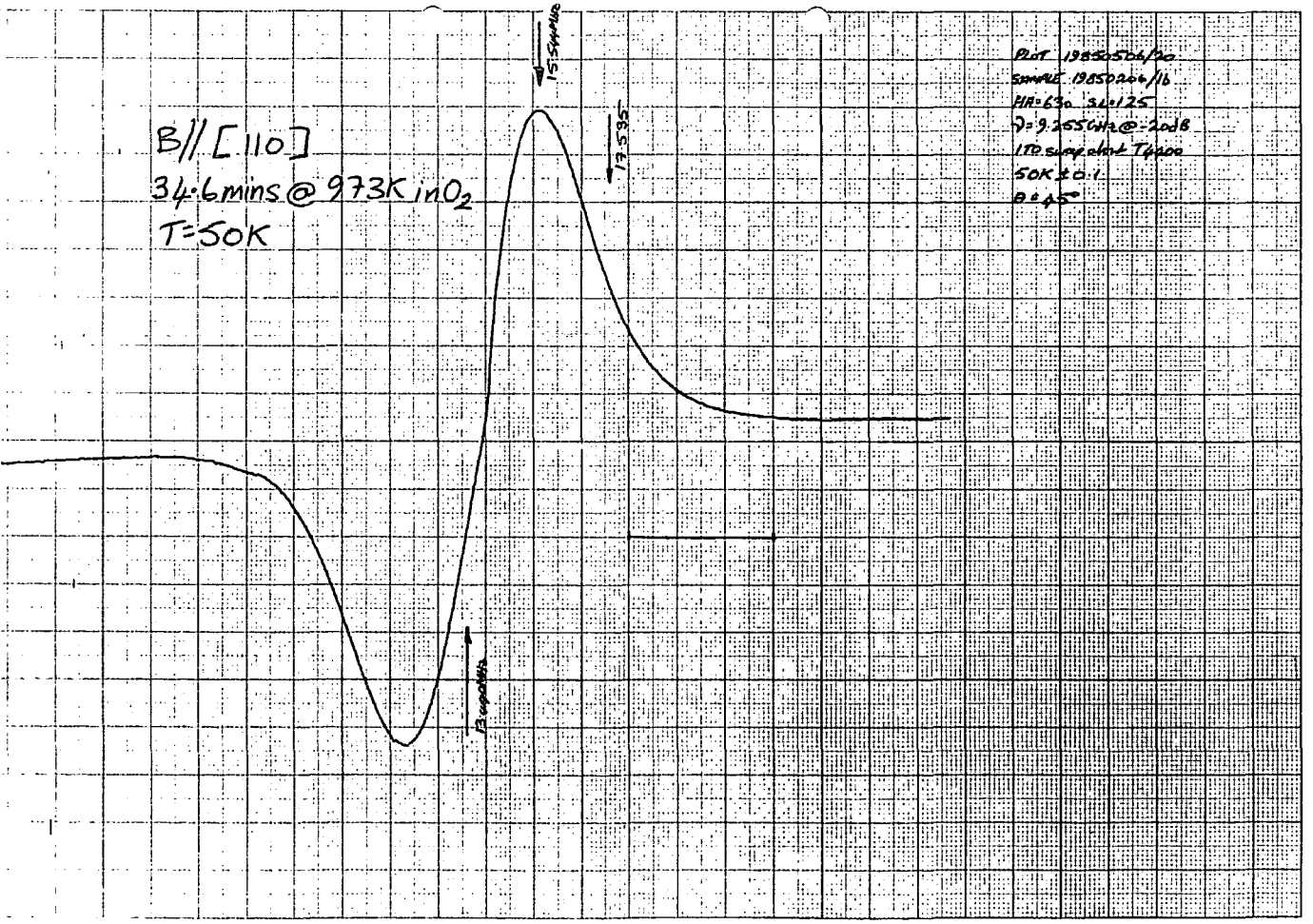
B // [110]
34·6 mins @ 973K in O_2
T = 50K
PLOT 19850506/20
SAMPLE 19850206/1b
HA=630 SL=125
ν = 9.255GHz @ -20dB
ITC sweep about T4200
50K ± 0.1
θ = 45°
15.54MHz
17.53MHz
Impurities

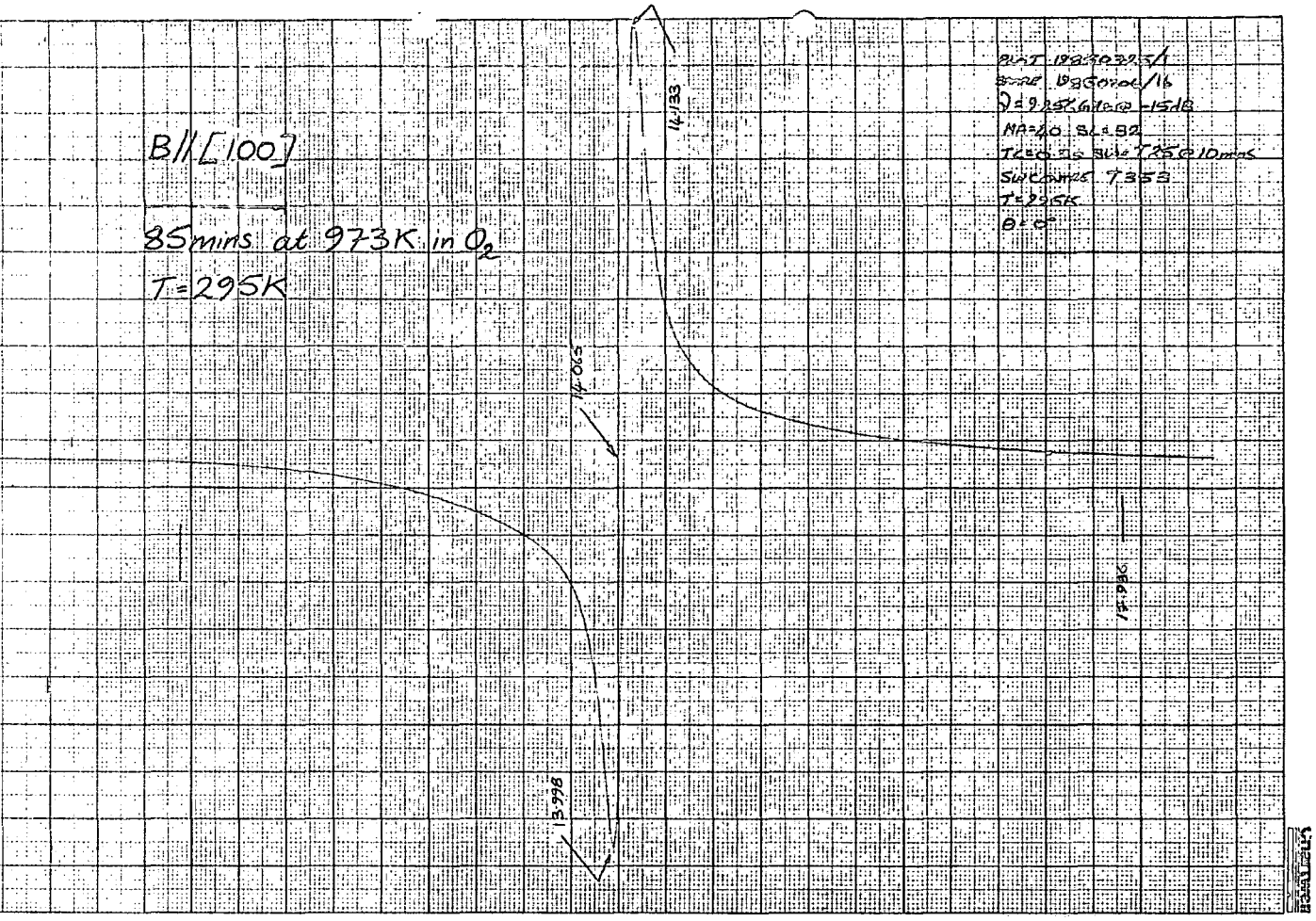
B//[100]
85 mins at 973K in O_2
T=295K
14.133
14.065
13.998
1.936

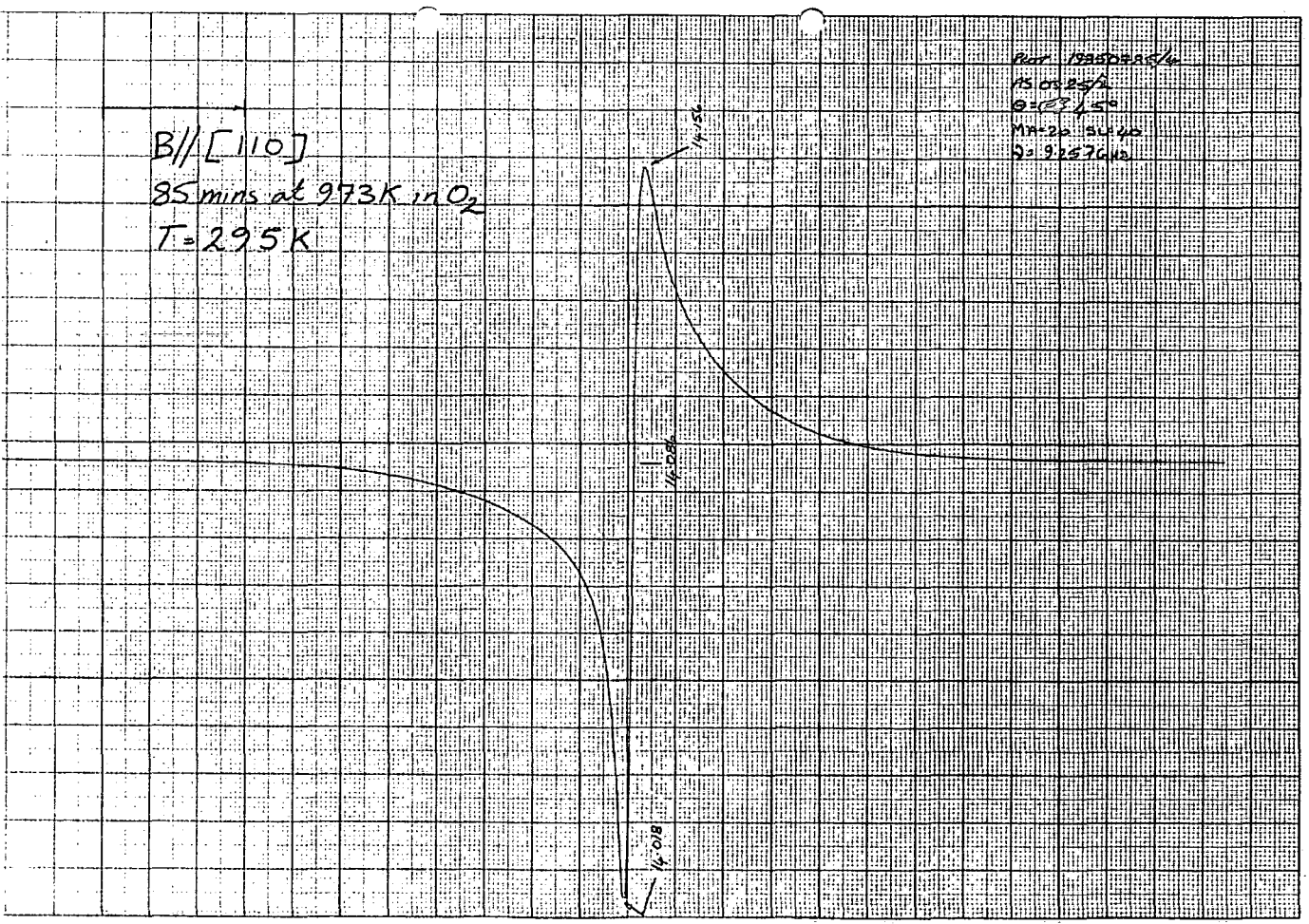
B//[110]
85 mins at 973K in O_2
T=295K
14.155
14.088
14.018

B//[100]
85mins at 973K in O_2
T=200K

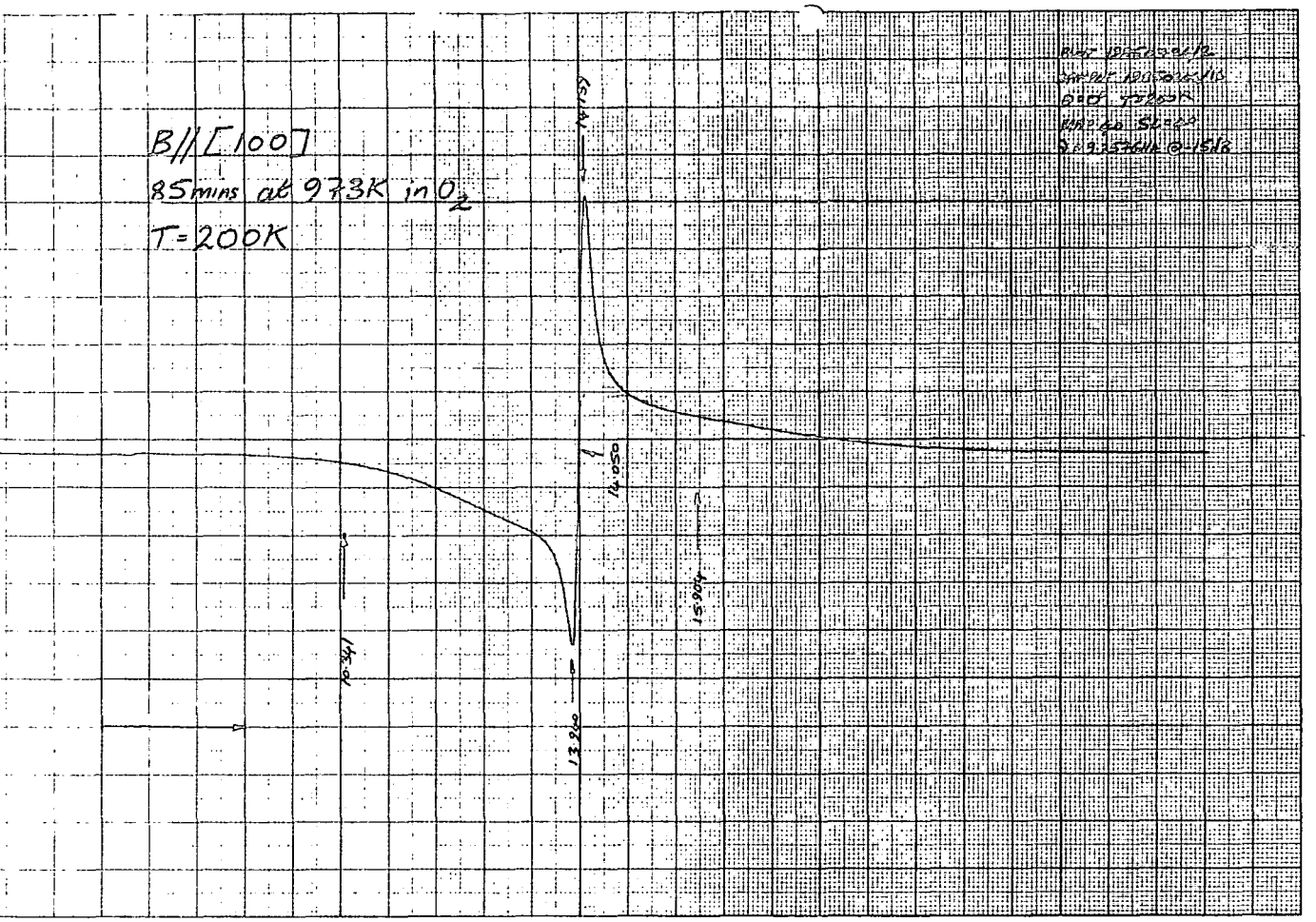

B//[110]
85mins at 973K in O_2
T=200K

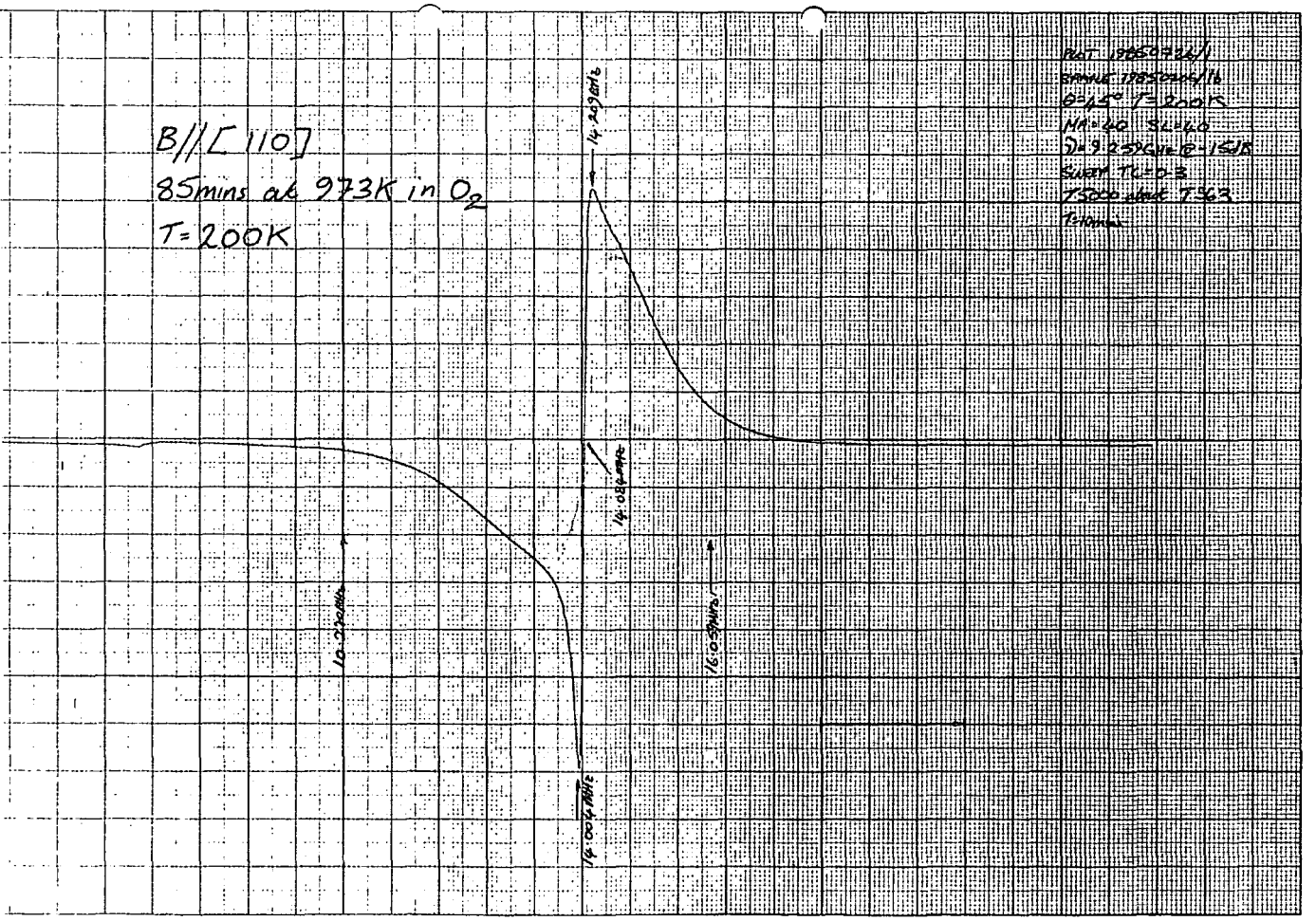

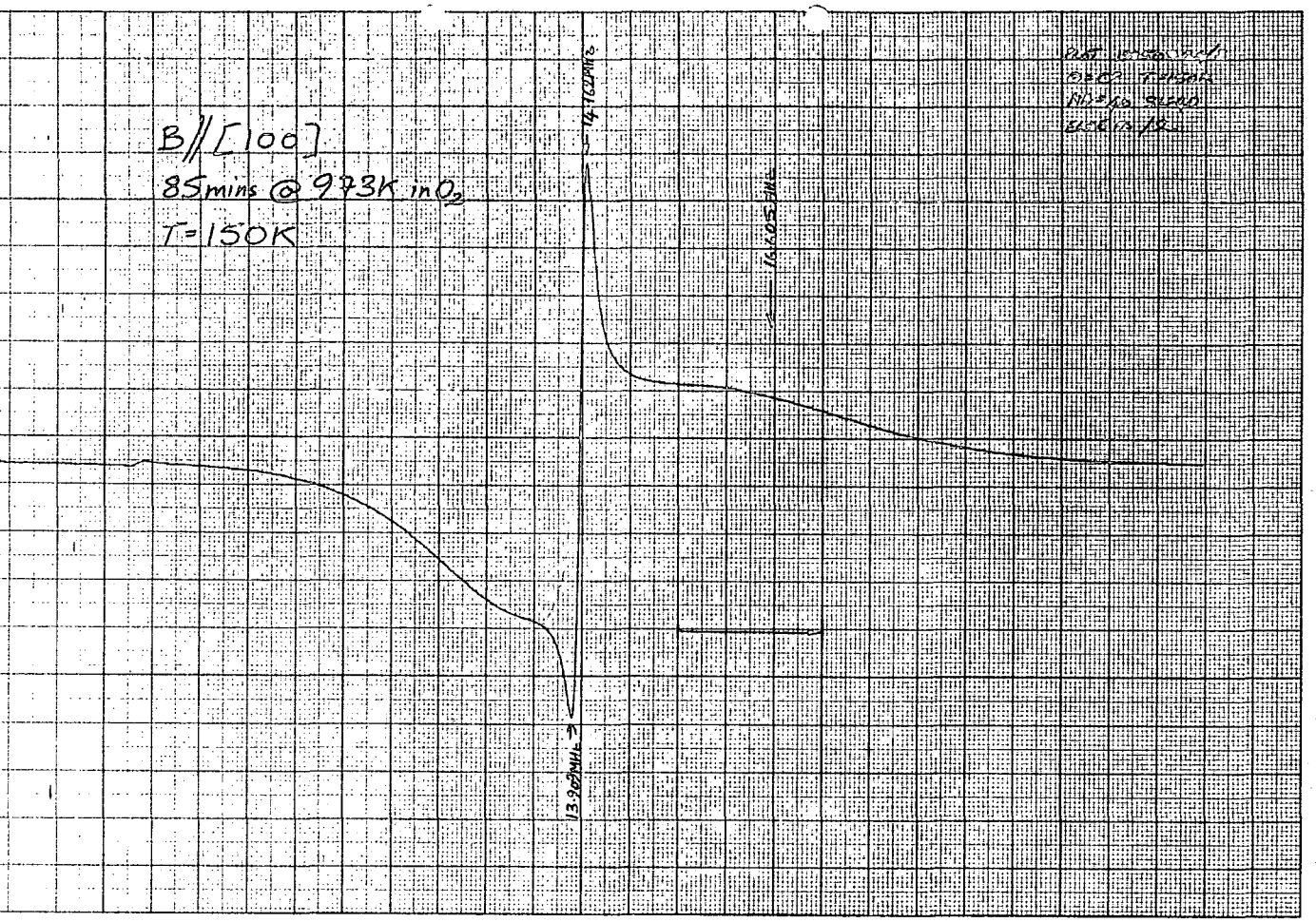
B // [100]
85mins @ 973K in O_2
T = 150K
14.162MHz
14.105MHz
13.980MHz

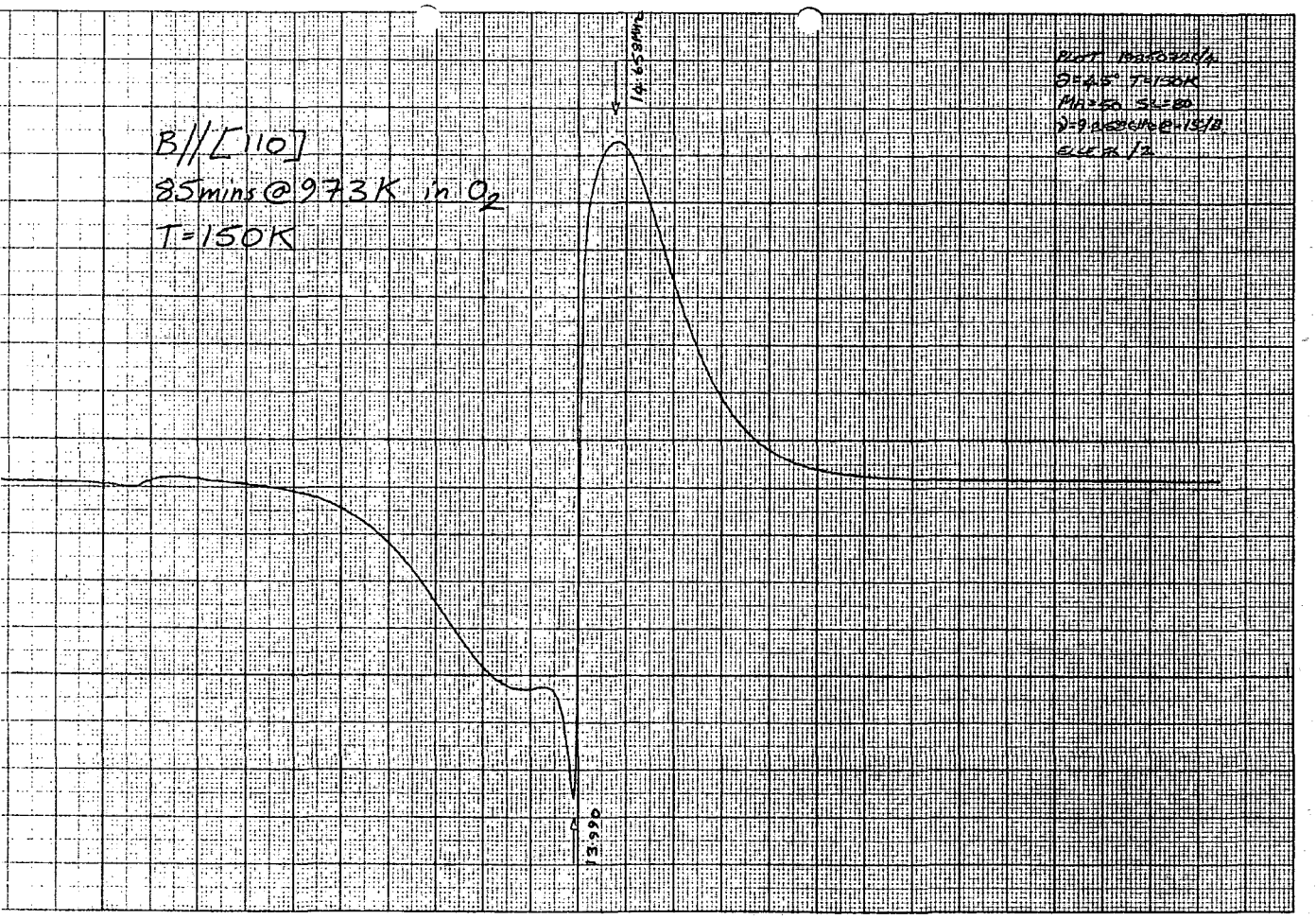
B // [110]
85mins @ 973K in O_2
T = 150K
14.455MHz
13.990

B // [100]
85 mins @ 973K in O_2
T = 100K

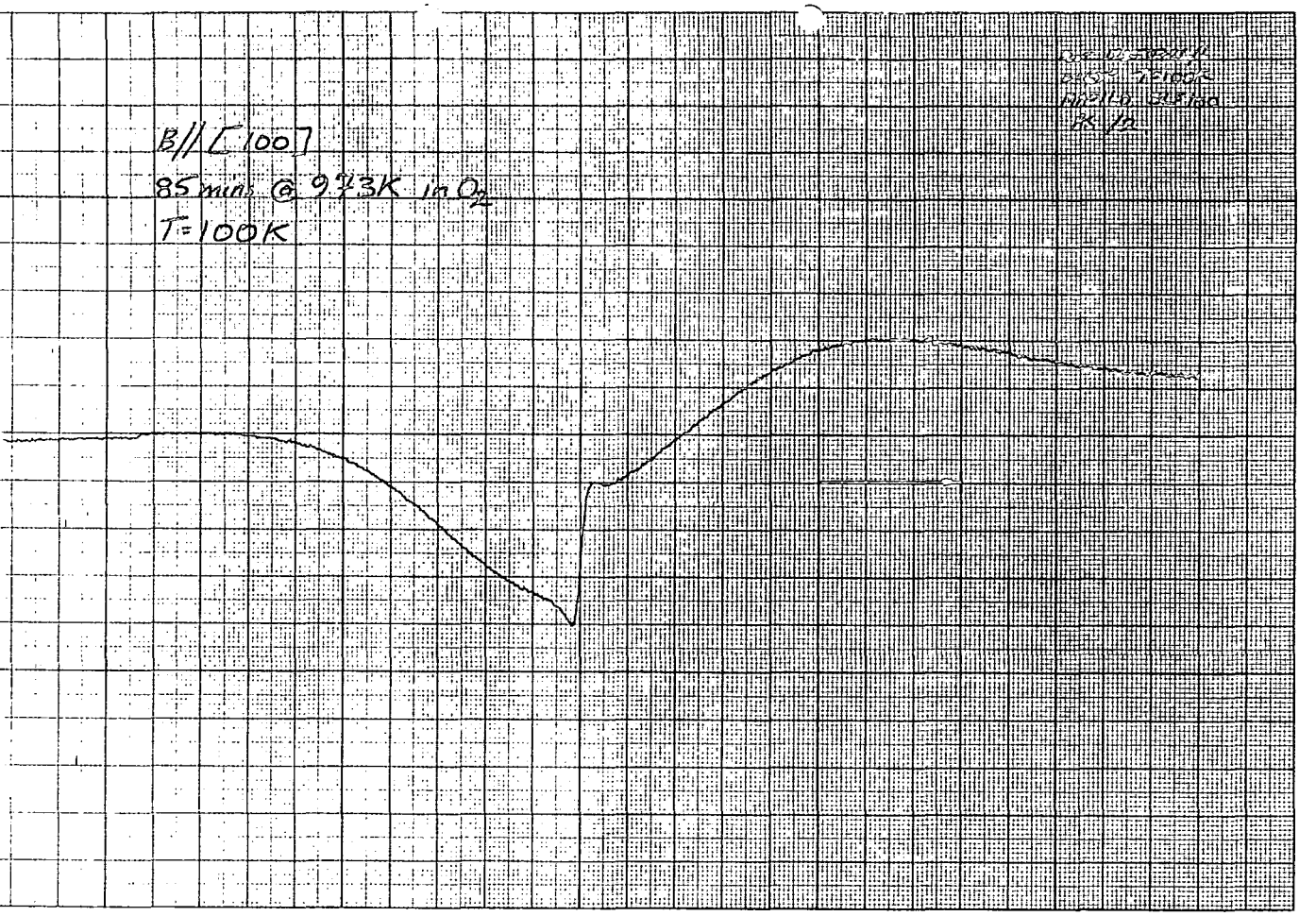

B // [110]
85 mins @ 973K in O_2
T = 100K